Energetics of Catalytic Intermediates on Nickel(111) by Calorimetry: Empirical Trends and Benchmarks for Quantum Theory

Spencer J. Carey

A dissertation

submitted in partial fulfillment of the

requirements for the degree of

Doctor of Philosophy

University of Washington

2018

Reading Committee:

Charles T. Campbell, Chair

Eric Stuve

Daniel Gamelin

Bo Zhang

Program Authorized to Offer Degree:

Chemistry

University of Washington

Abstract

Energetics of Catalytic Intermediates on Nickel(111) by Calorimetry: Empirical Trends and Benchmarks for Quantum Theory

Spencer J. Carey

Chair of the Supervisory Committee:
Professor Charles T. Campbell
Chemistry

Our society depends on the use of catalysts for the manufacture of 90% of chemical industry products, for the mass production of fertilizers that grow our food supply, for the synthesis of the fuels that drive our transportation systems, and for the purification of pollutants, such as those produced by car engines. With this utility comes a huge investment of effort to understand the fundamental science behind catalysts and to improve their efficiency, durability, and selectivity. It is also important to be able to design new catalysts for changing feedstocks (e.g., replacement of coal and petroleum with methane, biomass and other renewables). In the last fifty years, new methods to study catalytic processes have been developed, which in turn resulted in an explosion of research studies that address the fundamental questions in the catalysis field. Quantum mechanical calculations using Density Functional Theory (DFT) are

one such technique that has become invaluable in studying catalysts. This method allows for the efficient and inexpensive prediction of catalyst mechanisms and kinetics, structure-function relationships, and even in screening for new, more effective catalysts. However, the accuracy of these predictions depends upon reliable energetic information of adsorbed catalytic reaction intermediates, such as their heats of formation and bond enthalpies to the surface. The energies of adsorbed intermediates and transition states on surfaces are the key factors that determine the effectiveness of any given catalyst. The results of this dissertation show that the energy accuracy of these DFT methods is far less than desirable, and it provides many experimental benchmark energies that will be useful for the development of more accurate DFT functionals.

This dissertation is part of a decades-long effort by our research group to compile a large database that contains the heats of formation of many adsorbates on different model catalyst surfaces. This database aims to provide valuable benchmarks that theorists can use to improve DFT functionals. To expand this database, our research group uses Single-Crystal Adsorption Calorimetry (SCAC), the only method able to directly measure the binding energies of adsorbates to model surfaces. My research is focused on expanding the adsorbate bond energy database in the areas that it is lacking. Specifically, previous to this dissertation, this database only included adsorbed molecular fragments on one metal surface, Pt(111) and only included aromatic molecules on one non-noble metal surface, again Pt(111). We have extended both of these classes of adsorbates to their energies on the Ni(111) surface, with comparisons between the energies on Pt(111) versus Ni(111) which help explain some of the differences in catalytic properties of Pt versus Ni.

In this thesis, SCAC is used to study the molecular adsorption of phenol and benzene on both Pt(111) and Ni(111). Both benzene and phenol are aromatic, and their energetics are

heavily influenced by van der Waal forces. SCAC is also used to study the dissociative adsorption of methyl iodide on Ni(111) to produce adsorbed methyl and iodine adatoms and the dissociative adsorption of methanol on O-precovered Ni(111) to produce adsorbed methoxy and hydroxyl. Adsorbed methyl and methoxy are important molecular fragments that are catalytic intermediates in several industrial processes. Finally, a new equation is derived that relates the sigma bond enthalpies of several molecular fragments to both Ni(111) and Pt(111). This trend allows predictions of the sigma bond enthalpies of other small molecular fragments to transition metal surfaces.

TABLE OF CONTENTS

LIST OF FIGURES

LIST OF TABLES

ACKNOWLEDGEMENTS

I would like to first thank Dr. Christopher Wolcott for spending many hours training me and laying the foundations for my future successes. I would like to thank Dr. Keeper Sharkey, my general chemistry TA from the University of Arizona, who first inspired my fascination with chemistry. I would like to thank Dr. Hajo Freund and Dr. Swetlana Schauermann for the opportunity to work at the Fritz Haber Institute in Berlin, Germany for four months. It was an incredible experience and I learned a great deal. I would like to thank all of committee members, including Dr. Stuve, Dr. Zhang, Dr. Vaughan, and Dr. Gamelin for mentoring me throughout my graduate school career. I would like to thank Lon Buck, Bill Beaty, and Roy Olund in the UW Chemistry Electronic Shop. You have saved me a tremendous amount of time and headache quickly solving all of my electronics related problems with which I would otherwise still be struggling. I would like to thank Eric Strakbein, Brian Wadey, Ed McArthur, and Brian Holm from the UW Chemistry Machine Shop. You were invaluable in making repairs and improvements to our homemade instrument. I would like to thank Jim Gladden who was immensely helpful modifying and making dramatic improvements to the mess of a code that we use to work up our data. I would like to thank all my friends and family, especially my parents, Margot and Michael, my sister, Cayelan, and fiancée, Allie, for all their support through my graduate studies. I would like to thank everyone who has helped me collect the data presented here, especially Dr. Wei Zhao, with whom I have collaborated with most of my graduate school career. I would like to thank everyone in the Campbell group, both current members and past,

for all their assistance and support they gave every day. Finally, and most importantly, I would like to thank Charlie Campbell, whose mentorship and support was incredible and has made my graduate school experience truly wonderful. I am indebted to all of you.

Chapter 1. INTRODUCTION

The development of heterogeneous catalysis is essential in supporting the existence of modern society. Approximately, 90% of chemical industry products depend on catalysts for their manufacture. They are responsible for the mass production of fertilizers, which has provided food for the massive population growth that has occurred in the last 200 years. Catalysts play a critical role in the production of fuels that drive our transportation systems. Pollution is substantially mitigated by catalysts, in particular by preventing the formation of wasteful, unwanted byproducts. Catalysts also provide end-of-pipe solutions to reduce pollution, such as the catalytic converter, which removes carbon monoxide, nitrous oxides, and other toxic pollutants from car exhaust, thereby dramatically improving air quality.[1,2] With the significant role catalysis plays in our lives comes a huge investment of effort to understand the underlying science behind catalysts and to improve catalytic efficiency, durability, and selectivity.

The late transition metal catalysts that are commonly used in industry are highly complex, often including several different crystal faces of both the metal nanoparticles and the support materials on which they are dispersed, or even amorphous materials, dopants, and sometimes (after use) poisons. Particle size effects and interactions of the metal with catalyst support structures can also be important. To simplify the structure for better understanding, there are several different approaches to improve our knowledge of these systems. One approach in our laboratory is to study model catalysts, specifically single crystals. These surfaces are the simplest model catalysts as they are a material whose crystal lattice throughout the entire sample is continuous. This allows us to study one crystal face of a metal, such as Ni(111) or Pt(111). By understanding the interactions and chemistry of these single crystal surfaces on a molecular

level, we can learn about the fundamental nature of the interactions with adsorbed intermediates of the metal surfaces taking place on the more complicated catalysts.

One method to study catalytic surfaces that has grown powerful and increasingly popular over the last twenty years is to use theoretical models. Density Functional Theory (DFT), a popular computational quantum mechanical modelling technique, methods have proved invaluable in elucidating catalyst mechanisms, structure-function relationships in catalysis, and even in screening for new, more effective catalysts. Indeed, the groups of Nørskov, Mavrikakis, Greeley and others have successfully used DFT methods to guide discovery of better catalysts.[3,4,13,5–12] Furthermore, DFT has the clear advantage of providing results quickly with a lower cost than what is associated with experimental methods. DFT will certainly play a significant role in the future development of catalytic processes. However, these theoretical calculations must accurately estimate elementary-step reaction energies to predict catalytic efficiency. An error of 20 kJ/mol in the rate limiting step of a 400 °C reaction translates into a reaction rate difference of 400 times. With this high bar for accurate calculations, it is critical to know the overall accuracy and limitations of DFT.

In order to test the accuracy of DFT methods, our research group compiled a database containing 39 experimentally determined adsorption energies.[14] This database was updated in 2016 to contain 81 energies.[15] These results were compared to the theoretically calculated adsorption energies from six popular DFT methods. Their respective errors are shown in Figure 1.1, with small adsorbates (atoms and diatomics) being represented in Figure 1.1A and larger adsorbates with larger contributions from van der Waals forces in Figure 1.1B. The average energy of the molecular fragments in Figure 1.1A is -127 kJ/mol and in Figure 1.1B is -66 kJ/mol. Several functionals calculate type A adsorbates with a mean absolute error near 20

kJ/mol (or ~15 %). However, these same functionals result in much more significant errors for type B adsorbates with large contributions from van der Waals, 30-60 kJ/mol, i.e., 40-90%.

Clearly, these DFT methods could be improved and indeed much work has been performed to reduce these errors. The benchmarks provided by the work in this database allow theorists to make improvements to their methods. For instance, work to improve DFT models of vdW forces has greatly intensified in the last ten years.[16–22] In order to further guide the improvement of DFT, we must provide experimentally determined energetic benchmarks such as those given in this database. Unfortunately, this database is limited in scope and could be greatly improved. All of the molecular fragments in the experimental databases mentioned above that have been reported on multiple metal surfaces were only atomic adsorbates (H, O, N, F, Cl, I). All the larger fragments that had been reported were only done on a single metal surface, Pt(111).[14] Furthermore, no adsorption energies had been reported for any aromatic adsorbates on non-noble metals except Pt(111).[15] DFT cannot continue to improve without a larger, more diverse database of experimental adsorption energies on other metal surfaces besides Pt(111). This dissertation reports many adsorption energies on the Ni(111) surface. Nickel is also a very common catalyst metal like Pt, and the (111) surface is its most stable and most widely studied surface.

Many of the experimental adsorption energies systems in the above-mentioned databases were measured with temperature programmed desorption (TPD) and equilibrium adsorption isotherm experiments, which can measure adsorption energies, but only under special circumstances.[23] Specifically, these two methods require reversible adsorption and therefore cannot study more complicated adsorption systems such as if the target molecule or molecular fragment dissociates or decomposes upon heating.

Our group is unique in the use Single Crystal Adsorption Calorimetry (SCAC) to measure these energetic benchmarks. In 1991, Sir King's group developed SCAC,[24] presently the only method to directly measure the binding energies of adsorbates to model surfaces. This allows us to study and measure the energetics of systems that TPD and equilibrium adsorption isotherms cannot, specifically systems where adsorption is not fully reversible. This includes almost all dissociative adsorption reactions (necessary to study the energies of adsorbed molecular fragments) and the adsorption of aromatic molecules on all transition metals except Cu, Ag, and Au. Dr. Campbell's group later improved upon King's instrument by introducing a new heat detector that uses a pyroelectric β-polyvinylidene fluoride (PVDF) ribbon that is gently pressed into the back of the sample.[25] More information on this instrumentation will be detailed in Chapter 2.

With this more versatile calorimetry method, our goal is to expand this database by studying molecular fragments on surfaces beyond Pt(111) and to study additional aromatic molecules to provide additional energetic benchmarks for systems with large contributions from van der Waals forces. In this dissertation, new research is presented that 1) adds a significant number of molecular fragment bond energies on transition metal surfaces to the database that go beyond Pt(111), specifically on Ni(111), 2) adds a significant number of aromatic molecular adsorption energies with high contributions from van der Waals forces on both Pt(111) and Ni(111), and 3) develops a new method to predict sigma bond energies of molecular fragments on top sites.

Most of the research in this dissertation was performed on Ni(111). This surface was specifically chosen in order to provide the most valuable benchmarks for computational studies in catalysis that go beyond Pt(111). Table 1.1 summarizes calculations performed by

Mavrikakis's group using the PW91 functional.[26–28] These calculations were performed on 13 different late transition metal surfaces. Based on these results, our group determined that the most interesting and useful surfaces were Pt(111), Ni(111), and Cu(111) for two reasons. First, these three surfaces are commonly used catalysts and are frequently found in industrial operations. Second, the predicted bonding energies of these metals to different types of molecular fragments are the most varied. Pt(111) binds to CH_x species the strongest compared to Ni or Cu (although this particular calculation will be shown to be inaccurate in Chapter 5), but binds the weakest to oxygen species. In addition, Cu(111) forms the strongest bonds to oxygen species but binds much weaker to carbon. Other metals that were tested were found to have similar behavior to Pt, Ni, or Cu. For instance, Pd(111) is expected to bind similarly to Pt(111); DFT predicts that Rh(111) behaves similar to Ni(111). Over the last ten years, the our calorimeter has focused on measuring these adsorption energies on Pt(111).[29–33] Presently, we look to continue our work on Ni(111) with future graduate students focusing on Cu(111).

Beyond its value to DFT research groups, Ni catalysts play a large role in industry. Nickel is one of the most common catalysts used for hydrogenation reactions, which are very useful for the production of chemical products, pharmaceuticals, and monomers used in polymer synthesis. Ni catalysts are specifically used for the hydrogenation reactions, including those involving benzene, alkenes, pinene, sulpholene, nitrobenzenes, nitrotoulenes, and resins.[2] Nickel supported on alumina is also the standard catalyst used for methanation of CO and CO_2, e.g., from synthesis gas. Ni is also the preferred catalyst for steam reforming of methane because of its high activity, wide availability, and low cost.[2]

My dissertation research using SCAC has resulted in 7 published papers, with 2 more papers in preparation or under review. A list of these publications is provided below:

1. Zhao, W.; Bajdich, M.; **Carey, S. J.**; Vojvodic, A.; Noerskov, J. K.; Campbell, C. T. Water dissociative adsorption on NiO(111): energetics and structure of the hydroxylated surface, *ACS Catalysis* (2016) 6(11), 7377-7384.
2. **Carey, S. J.**; Zhao, W.; Campbell, C. T. Energetics of adsorbed methyl and methyl iodide on Ni(111) by calorimetry: comparison to Pt(111) and implications for catalysis, *ACS Catalysis* (2017), 7(2), 1286-1294.
3. Zhao, W.; **Carey, S. J.**; Morgan, S. E.; Campbell, C. T. Energetics of adsorbed formate and formic acid on Ni(111) by calorimetry, *Journal of Catalysis* (2017), 352, 300-304.
4. Zhao, W.; **Carey, S. J.**; Mao, Z.; Campbell, C. T. Adsorbed hydroxyl and water on Ni(111): heats of formation by calorimetry. *ACS Catalysis* (2018), 8(2), 1485-1489.
5. **Carey, S. J.**; Zhao, W.; Campbell, C. T. Energetics of adsorbed benzene on Ni(111) and Pt(111) by calorimetry. *Surface Science* (2018). In press. (DOI:10.1016/j.susc.2018.02.014).
6. Zaki, E.; Mirabella; F., Ivars, F.; Seifert, J.; **Carey, S. J.**; Li, X.; Paier, J.; Sauer, J., Shaikhutdinov, S.; Freund, H.-J.; Water adsorption on Fe_3O_4(111): dissociation and network formation (Accepted at *Physical Chemistry Chemical Physics*).
7. **Carey, S. J.**; Mao, Z.; Zhao, W.; Campbell, C. T. Energetics of adsorbed phenol on Ni(111) and Pt(111) by calorimetry. (DOI: 10.1021/acs.jpcc.8b03155).
8. **Carey, S. J.**; Zhao, W.; Zhang, W.; Mao, Z.; Harman E.; Baumann, A.-K.; Campbell, C. T. Energetics of adsorbed methoxy and methanol on Ni(111) by calorimetry. (In Preparation)

9. **Carey, S. J.**; Zhao, W.; Campbell, C. T. Trends of molecular fragments on metal surfaces. (In Preparation)

This dissertation will continue in Chapter 2 with a description of the calorimeter and methods that were used to collect all data in subsequent chapters and the experimental methods. Chapters 3-6 will detail energetics of different adsorbed catalytic intermediates that were measured with calorimetry. Specifically, I will discuss the adsorption energetics on both Pt(111) and Ni(111) of benzene and phenol in Chapters 3 and 4, respectively. The energetics of these molecules are heavily influenced by van der Waals forces and provide important contributions to the aforementioned adsorption energy database. In Chapter 5, I will discuss the energetics of methyl on the Ni(111) surface. Methyl is known to be a key intermediate in energy-related catalysis over transition metals, including combustion, partial oxidation, steam re-forming and dry reforming of methane, methanation, Fischer−Tropsch, steam reforming, and combustion of various other hydrocarbons and oxygenates, methanol decomposition, and several fuel cell reactions. In Chapter 6, I will discuss the energetics of adsorbed methoxy on the Ni(111) surface. Methoxy is the simplest alkoxide and is a key intermediate for catalytic combustion, selective oxidation, and steam reforming. Finally, in Chapter 7, I will detail a new equation that allows us to relate the sigma bond energies of several molecular fragments on several different metal surfaces with a linear trend that possesses a slope of 1. This trend will allow us to make predictions of the sigma bond energies of other molecular fragments.

1.1 TABLES AND FIGURES

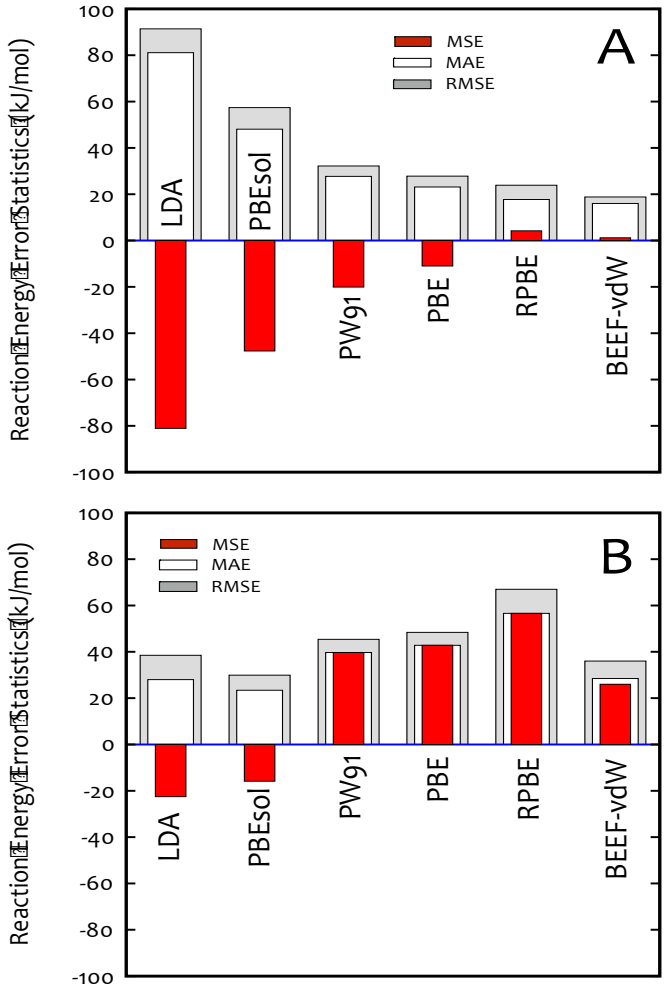

Figure 1.1 Comparison of the accuracy of six different DFT functionals relative to 39 experimentally determined adsorption energies. (A) compares chemisorbed systems with negligible van der Waals forces and (B) compares systems with large van der Waals forces contributions to the adsorption energy. The red, white, and grey bars represent the mean standard error, the mean absolute error, and the weighted root mean squared error, respectively, all *per molecular fragment* produced in the adsorption reaction.

Table 1.1. Bond energies (in kJ/mol) of several molecular fragments adsorbed to the Pt(111), Cu(111), and Ni(111) surface calculated using the PW91 functional.[26–28]

Species	Pt(111)	Cu(111)	Ni(111)
-H	-265	-231	-279
-OH	-206	-274	-289
-O	-373	-414	-495
-CO	-185	-82	-198
$-CH_3$	-197	-121	-178
$-CH_2$	-381	-268	-371
-CH	-620	-446	-600
-C	-651	-429	-633

Chapter 2. EXPERIMENTAL INSTRUMENTATION AND METHODS

Single crystal adsorption calorimetry (SCAC) is an ultrahigh vacuum (base pressure $<2 \times 10^{-10}$ mbar) surface science instrument. The SCAC used for all the experiments performed in this work is equipped with X-ray photoelectron spectroscopy (XPS), Auger electron spectroscopy (AES), low-energy ion scattering spectroscopy (LEIS), and low-energy electron diffraction (LEED). An example of a single crystal adsorption calorimeter is shown in Figure 2.1. This apparatus and its procedures for SCAC have been discussed extensively previously.[34,35] In this chapter, I will briefly discuss the sample preparations, instrumentation, and methods.

The sample used was a 1 μm thick metal (Ni(111) or Pt(111)) single-crystal foil, supplied by Jacques Chevallier at Aarhus University in Denmark. The sample surface was cleaned by 1.25 kV Ar^+ ion sputtering to remove sulfur and other contaminants, annealing at 673 K in 1×10^{-7} mbar O_2(g) for 1 min to remove any surface carbon, and then annealing at 1050 K to remove oxygen. This treatment was repeated until impurities were below the detection limit of AES and XPS, and the surface gave a very sharp LEED pattern. Before calorimetry, the clean sample was brought to thermal equilibrium with the calorimeter and then flash-heated to 1050 K (<2 s) to ensure a clean surface. The sample was then brought back into contact with the pyroelectric detector and thermal equilibrium was re-established (less than 5 min), after which the experiment was performed. An interior view of the calorimeter and these components are shown in Figure 2.2.

Calorimetry was performed by exposing the surface to a pulsed molecular beam of molecular gas (such as methyl iodide, methanol, benzene, or phenol). Each pulse was 102 ms

long and was repeated every 3-5 s. The organic molecules used to create the molecular beam were outgassed by several freeze−pump−thaw cycles after being put into its reservoir on the vacuum chamber. Its purity was checked with a mass spectrometer. The beam was created by expanding ~2.0 mbar of molecules through a microchannel array at 300 ± 5 K (defining the gas temperature) and then collimated through a series of five liquid nitrogen-cooled orifices as described previously.[34] Coverages are reported in monolayers (ML) and are defined as the number of molecules that adsorb to the surface irreversibly, normalized by the number of surface atoms (1.86×10^{19} atoms/m^2 for Ni(111) and 1.50×10^{19} atoms/m^2 for Pt(111)). The beam spot size on the surface was previously determined to be 4.36 mm in diameter.[34] In a given experiment, the dose per pulse was highly precise (<1% pulse-to-pulse variation, determined by the reproducibility of the chopper's beam-open time). A more detailed description of the experimental principles and implementation of the molecular beam can be found elsewhere.[29,34] The flux of molecules from the molecular beam is measured by impinging the beam onto a liquid-nitrogen-cooled quartz crystal microbalance (QCM), precovered with molecular multilayers. Calibration of the QCM has been described previously.[34]

The heat released from the adsorption of one molecular pulse is measured with a pyroelectric polymer ribbon gently pressed against the back side of the sample.[25,35] The sensitivity of the pyroelectric detector was calibrated after each experiment by depositing a known amount of energy into the sample by use of a HeNe (632.8 nm) laser. The absolute accuracy of the calorimetric heats is estimated to be better than 4% (i.e., any systematic errors are less than 4%) for systems like those studied here, which have sticking probabilities above 0.8. This is based on comparisons to literature values for standard enthalpies of sublimation of the bulk solid when solids with known enthalpies are formed, specifically multilayers of

adsorbed cyclohexene,[29] methanol,[30] methyl iodide,[31] and water[32] on Pt(111). For these molecules, the differences between the measured value and the estimated heat of sublimation based on the literature values (after correction for temperature differences using literature values for heat capacities) were −5.6%, −3.3%, <1%, and −5.1%, respectively. Note these differences from bulk sublimation values may be due to errors in the literature values or the possibility that we were not producing exactly the most stable phase at these low temperatures (possibly explaining the fact that our heats are lower than the literature values in the two cases where they differ most). However, these differences are all within the error bars (at 95% confidence) of the two values being compared, and therefore they do not differ in any statistically significant way. Relative measurements (for example, differences in heat with changes in coverage or temperature) can be much more accurate. The precision of energy calibration can be improved by averaging multiple runs.

Sticking probabilities were measured simultaneously with calorimetric measurements, via the King and Wells method.[36] A mass spectrometer, without line-of-sight to the sample, measured the background pressure increase of methanol, CH_3OH (g) (m/z = 31), or methyl iodide, CH_3I (g) (m/z = 142), in the chamber. A gold flag was positioned in front of the sample and used to determine the mass spectrometry signal corresponding to full reflection of molecules. The sticking probability is calculated by integrating the mass spectrometer signal measured from the increase in molecular partial pressure above background when the molecular beam is pulsed onto the sample surface in comparison with the increase in methanol partial pressure resulting when pulsed onto the inert gold flag. We report two types of sticking probabilities, long-term and short-term.[29] The long-term sticking probability, S_∞, is the probability that a gas molecule strikes the Ni(111) surface, sticks, and remains until the next gas pulse starts ∼3 s later. This

measurement is used to calculate the adsorbate coverage remaining at the start of the next gas pulse. The short-term sticking probability, $S_{102\ ms}$, is the probability that a gas molecule strikes the metal surface, sticks, and remains at least throughout the time frame of our heat measurement (i.e., the first 102 ms). This is used to calculate the moles of gas-phase reactant that contribute to the measured heat of adsorption, so we can report that value in kilojoules per mole adsorbed. When there is no desorption between pulses, the two sticking probabilities are the same.

The calorimeter and sample are cooled by a large thermal reservoir, but one cannot mount a thermocouple directly on the ultrathin single crystal used for calorimetry nor on the sample platen to which it is mounted (because this whole platen is removed from its manipulator and mounted on the thermal reservoir during calorimetry to achieve better signal stability). Therefore, the sample temperature was monitored by two alumel/chromel thermocouples spot-welded to the two closest locations, one spot-welded to the holder of the pyroelectric detector and another to the thermal reservoir. We took the average of these two temperature readings as the sample temperature here. For the sample temperatures used here, the readings of these two thermocouples differed by ~10 K on average.

2.1 FIGURES

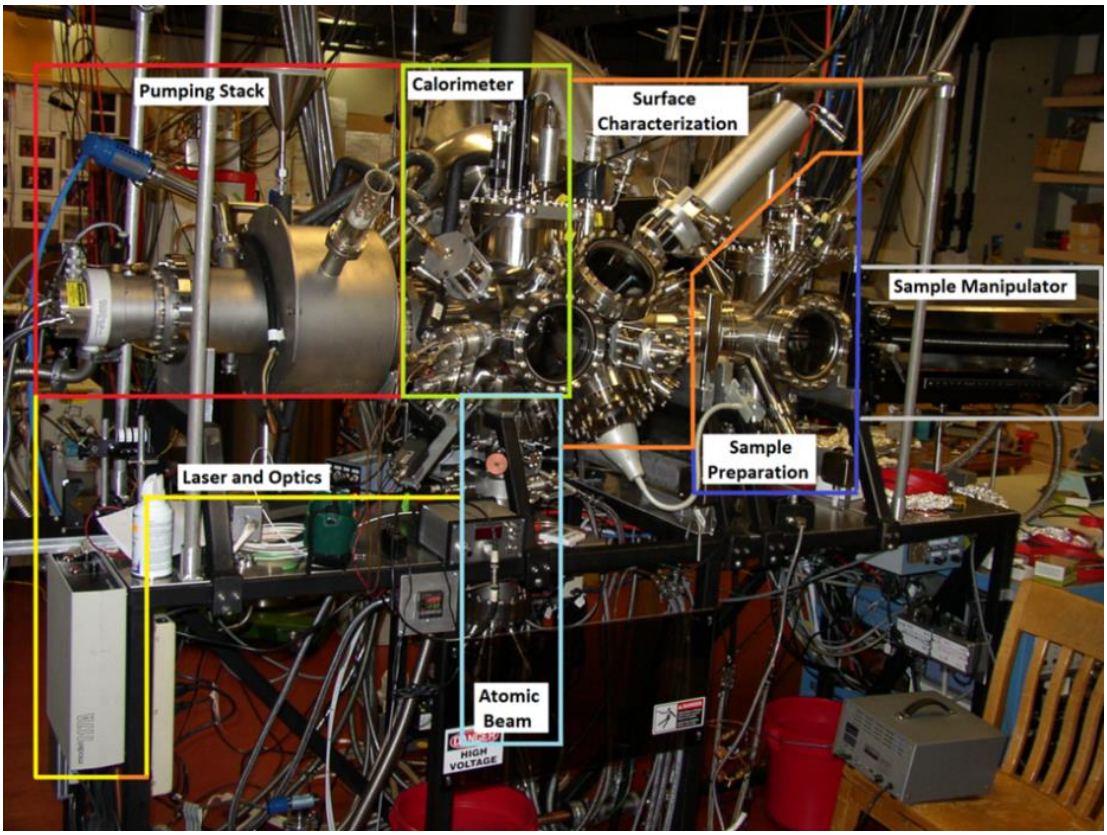

Figure 2.1. External view of a single crystal adsorption calorimeter. The major components are labelled.

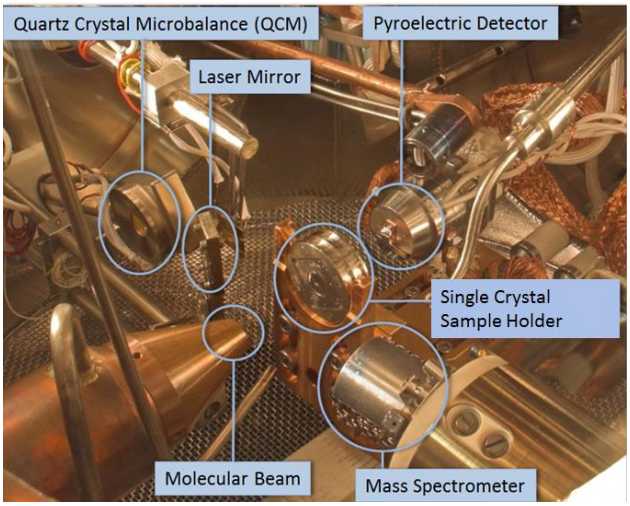

Figure 2.2. Photograph of the interior of the SCAC. Several of the components related to calorimetry are labelled.

Chapter 3. ENERGETICS OF ADSORBED BENZENE ON NI(111) AND PT(111) BY CALORIMETRY

This chapter reprinted with permission from: S.J. Carey, W. Zhao, and C.T. Campbell, Energetics of Adsorbed Benzene on Ni(111) and Pt(111) by Calorimetry, Surface Science (2018), Article ASAP, DOI: 10.1016/j.susc.2018.02.014

Chapter Abstract

The heat of adsorption and sticking probability of benzene were measured on Ni(111) and Pt(111) at 90 K using single crystal adsorption calorimetry (SCAC). Benzene adsorbs molecularly with a heat of 208 kJ/mol on terrace sites in the low-coverage limit on Ni(111) and has a standard enthalpy of formation (ΔH_f^0) of C_6H_6(ad) of -251 kJ/mol at a coverage of 1/9 ML. These results are compared to calorimetric results on Pt(111), where the standard enthalpy of formation (ΔH_f^0) of C_6H_6(ad) was found to be -244 kJ/mol at a coverage of 1/9 ML. The slightly stronger bonding to Ni is attributed to stronger C-Ni covalent bonding partially compensated by weaker van der Waals (vdW) attractions to Ni compared to Pt. The measured energetics for benzene are compared to Density Functional Theory (DFT) calculations from previous literature, showing that functionals that do not contain corrections for vdW interactions badly underestimate the bond energies of benzene to both Ni(111) and Pt(111), while many of those that correct for vdW interactions are much more accurate.

3.1 INTRODUCTION

Solid nickel catalysts are used industrially for a wide variety of reactions involving benzene and substituted benzenes, and promise many future applications involving substituted

benzenes, such as in biomass conversion. Nickel catalysts are also important in many reactions involving larger aromatic molecules. Thus, the interaction of benzene with nickel surfaces is of fundamental importance in catalysis research. However, no one has ever measured the heat of adsorption of benzene or any other aromatic molecule on well-defined sites on any nickel surface. Here we report calorimetric measurements of the heat of adsorption of benzene on Ni(111) and Pt(111) as a detailed function of coverage, and compare to our group's earlier results for Pt(111)[37] and the results of estimations of these energetics using density functional theory (DFT)[38,39], which tend to underestimate benzene's heat of adsorption. These results make Ni(111) and Pt(111) the only two transition metal surfaces for which the heat of benzene adsorption has been measured, except on the noble metals (Cu, Ag and Au)[15], where heats have been measured by temperature programmed desorption (TPD). (At coverages below half of saturation, benzene dissociates completely during TPD on all transition metal surfaces except noble metals, rendering TPD inapplicable for determining heats of adsorption.)

Benzene adsorption to metals like Pt(111) and Ni(111) is thought to involve strong van der Waal attractions, which are more difficult to model with theoretical methods such as DFT.[14,16,17,38] The adsorption energies for benzene on Ni(111) and Pt(111) thus provides important new benchmarks for testing the energy accuracy of new DFT methods that are being designed to better model these types of interactions. The important role of van der Waals interactions in adsorption has recently been reviewed.[40,41] The results here help confirm the much stronger van der Waals attractions to Pt surfaces than to Ni predicted theoretically.

Benzene adsorption on Ni(111) under ultrahigh vacuum (UHV) conditions has been extensively studied by vibrational spectroscopy[42], TPD[43], X-ray Photoelectron Spectroscopy[44,45], Angle-Resolved Ultraviolet Photoelectron Spectroscopy (ARUPS)[46], and LEED[43,45]. Dosing

benzene onto a Ni(111) surface from 125-180 K results in the first layer of benzene lying flat, parallel to the nickel surface, interacting through its π electron system.[42,44,45] Heating multilayers of benzene to 180-220 K, causes the benzene to change adsorption state, resulting in a ($\sqrt{7}$ x $\sqrt{7}$) R19.1° LEED pattern with a coverage of 1/7 ML.[45] At low temperatures, benzene is expected to form multilayers on the surface. Three multilayer desorption TPD peaks have been measured at relatively low coverage (154 K, 136 K, and 146 K), corresponding to the first physisorbed layer that is likely parallel to the surface on top of the chemisorbed layer, a transition layer, and bulk benzene (solid).[43] The 146 K peak is not observed until a 1.8L exposure, and its peak temperature rapidly shifts to higher temperatures with increasing coverage. The 136 K peak disappears at higher exposures (>2.4L benzene).[43]

Benzene on Pt(111) has also been extensively studied using traditional UHV methods[42,47–54], including single crystal adsorption calorimetry[37]. Benzene forms a disordered layer, lying parallel to the platinum surface.[42,47] STM images have shown that benzene will adsorb on multiple adsorption sites, with bridge sites being the most energetically favored. If benzene is dosed at room temperature and the sample is then cooled to 4 K, benzene adsorbs in a 1:2:3 ratio to top, hollow, and bridge sites, respectively. However, if benzene is adsorbed onto a Pt(111) surface directly at 4 K, bridge sites are predominantly observed with only small fractions of top and hollow sites observed.[48] Other studies have found further evidence for hollow site adsorption, including HREELS[42,55] and ARUPS[50], and evidence for bridge site adsorption, including LEED studies[51,52]. Virtually all theoretical studies calculate that benzene is more stable on bridge sites, although hcp hollow sites are often not much less energetically favorable.[16,17,64,56–63] Benzene saturates the Pt(111) surface with a coverage of ~0.15 ML and will form multilayers at low temperatures, which desorb in TPD studies at ~195 K.[53,54] The heat

of adsorption of benzene on Pt(111) at 300 K was measured versus coverage by SCAC.[37] Here, we reproduce those measurements at lower temperature for more direct comparison to the new results here for Ni(111).

3.2 EXPERIMENTAL

Experiments were performed in a UHV chamber (base pressure $<2 \times 10^{-10}$ mbar) equipped with X-ray photoelectron spectroscopy (XPS), Auger electron spectroscopy (AES), low-energy ion scattering spectroscopy (LEIS), low-energy electron diffraction (LEED), and SCAC. The samples used were 1 μm thick Ni(111) and Pt(111) single-crystal foils, supplied by Jacques Chevallier at Aarhus University in Denmark. The sample surface was cleaned by Ar^+ ion sputtering and annealing to remove contaminants. This treatment was repeated until impurities were below the detection limit of XPS, and the surface gave a sharp (111) LEED pattern. Detailed descriptions of the apparatus, molecular beam, sticking probability, heat measurements, and other procedures for SCAC may be found elsewhere.[29,34,35,65]

Briefly, calorimetry was performed by holding the clean Ni(111) or Pt(111) single crystal at a given temperature and exposing it to a pulsed molecular beam of benzene. The heat of adsorption was measured with a pyroelectric detector pressed against the backside of the sample.[25,35] The sensitivity of the pyroelectric detector was calibrated after each experiment by depositing a known amount of energy into the sample by use of a HeNe (632.8 nm) laser. The sticking probability was measured simultaneously with the heat of adsorption using a quadrupole mass spectrometer as described previously.[36] We report two types of sticking probabilities, long-term and short-term.[29] The long-term sticking probability, S_∞, is the probability that a gas molecule strikes the surface, sticks, and remains until the next gas pulse starts ~3 s later. This

measurement is used to calculate the adsorbate coverage remaining at the start of the next gas pulse. The short-term sticking probability, $S_{102\ ms}$, is the probability that a gas molecule strikes the surface, sticks, and remains at least throughout the time frame of our heat measurement (i.e., the first 102 ms). This is used to calculate the moles of gas-phase reactant that contribute to the measured heat of adsorption, so we can report that value in kilojoules per mole adsorbed.

The molecular beam was created by expanding ~2.1 mbar of benzene (Millipore Sigma, >99.7%) through a microchannel array held at 300 ± 5 K (defining the gas temperature) and then collimated through a series of five liquid nitrogen-cooled orifices. A chopper converts the beam into pulses that are 102 ms long and repeat every 3 s. Coverages are reported in monolayers (ML) and are defined as the number of benzene molecules that adsorb to the surface irreversibly, normalized by the number of metal surface atoms in the Ni(111) surface (1.86×10^{19} Ni atoms/m^2) or Pt(111) surface (1.50×10^{19} Pt atoms/m^2). A typical benzene dose was ~0.002-0.005 ML per pulse with a beam spot size previously determined to be 4.36 mm in diameter.[34]

3.3 RESULTS

Sticking Probability. As described previously[29] and above, we measured two types of sticking probabilities: the short-term sticking probability, $S_{102\ ms}$, and the long-term sticking probability, S_∞. Figure 3.1 shows the average short-term and long-term sticking probabilities measured as a function of coverage on both Ni(111) and Pt(111). At this low temperature, benzene's sticking probability is near unity for both metal surfaces independent of coverage. On both metals, benzene is expected to form multilayers, which is confirmed in this experiment.[42,43,45,54] For Ni(111), the initial short-term and long-term sticking probabilities are approximately 0.99 and increase to 1.00 by a coverage of ~0.25 ML, suggesting a precursor-mediated adsorption

mechanism. This has been previously observed for methyl iodide and formic acid on Ni(111) at low temperatures.[65,66] On Pt(111), the short-term and long-term sticking are initially above 0.99 but decrease to ~0.98 at approximately 0.10 ML. Both sticking probabilities then increase to near unity above ~0.15 ML when the first layer is saturated (see below). The slightly lower average sticking probability in the first layer may be due to the poorer mass-matching in the benzene-Pt(111) collisions than when benzene strikes a benzene multilayer. Poorer mass-matching in gas-surface collisions results in higher probability for quasi-elastic collisions (i.e., less energy loss) and hence lower trapping probability. This also explains the lower sticking probability in the first layer for Pt(111) than Ni(111), since Ni is lighter. It does not explain the initial decrease with coverage seen on Pt(111), which is tiny (~1%) and possibly due to some systematic error.

Heat of Adsorption of Molecular Benzene on Ni(111) at 90 K. In this paper, we define the term *heat of adsorption* as the negative of the differential standard molar enthalpy change for the adsorption reaction, ΔH_{ad}, with the gas and the Ni(111) being at the same temperature as the Ni(111) surface ("standard" here implies only that the gas is at 1 bar as a pure ideal gas). During our experiments, the temperature of the molecular beam was ~300 K, while the Ni(111) sample was held at cryogenic temperatures (e.g., T = 90 K). Thus, the measured heat is corrected by the small difference in the internal energy of the gas in the *directed* molecular beam at 300 K and in a Boltzmann distribution at the sample temperature (T), and then by RT to convert from internal energy change to enthalpy change for the adsorption reaction, as described elsewhere.[15]

The heat of adsorption of benzene on Ni(111) at 90 K is shown in Figure 3.2. At this temperature, benzene is expected to adsorb molecularly, parallel to the surface.[42] Initially, benzene adsorbs with a heat of adsorption of approximately 208 kJ/mol. As coverage increases

up to 0.093 ML, the heat of adsorption decreases linearly with coverage and, as shown in Figure 3.2, is well described by the best-fit line $-\Delta H_{ad} = (208 - 626\ \theta)$ kJ/mol, where θ is coverage in ML. Between 0.093 and 0.13 ML, the heat decreases rapidly in a way that is very similar to a broadened step-function decrease at ~1/9 ML. This coverage corresponds to a (3x3) unit cell, which may be the highest coverage benzene can easily achieve at this low temperature. The broadening may simply be due to the natural inhomogeneity of local coverage, with some regions at higher local coverages reaching 1/9 ML sooner than others, and others with lower local coverage.

By 0.13 ML, the first layer has saturated the surface at 90 K, and the heat has dropped to a nearly constant value of ~60 kJ/mol. X-ray photoelectron spectroscopy experiments measured a coverage of ~0.13 ML before detecting the formation of multilayers at 120 K.[45] This same paper also found that a ($\sqrt{7}$ x $\sqrt{7}$) R19.1° LEED pattern corresponding to 1/7 ML is not observed until 220 K.[45] Therefore, the true saturation coverage of 1/7 ML = 0.143 ML might not be achievable at 90 K since this requires shifting all the benzenes in the adlayer to the less stable hcp hollow sites, which may have an activation energy not accessible at 90 K (even if the sites are only marginally less stable).

Between 0.13 ML and ~0.5 ML, the heat of adsorption of benzene remains 5-15 kJ/mol higher than the final multilayer energy. This is characteristic of benzene forming layers on top of the first monolayer but still being able to weakly interact with the metal below. This result is well explained by previous TPD experiments, which have shown three multilayer peaks (154 K, 136 K, and 146 K). These corresponding to the first physisorbed layer that is likely parallel to the surface, a transition layer, and bulk benzene.[43]

At coverages greater than ~0.5 ML, the heat of adsorption becomes nearly constant, which implies the formation of bulk-like multilayers. Above 0.5 ML, we measure a multilayer adsorption energy of 44.5 ± 1.4 kJ/mol, where the error bars reference the run-to-run standard deviation on the mean of the average heat from 0.5 to 0.8 ML. There are several literature heats of sublimation for benzene measured at various temperatures.[67] Averaging these results give a heat of sublimation of 44.3 kJ/mol at 250 K. This value may be adjusted to 90 K using the heat capacities of solid and gaseous benzene. Using this method results in a heat of sublimation of 49.1 kJ/mol at 90 K. This is consistent with previous TPD experiments of deuterated benzene, which measured an activation energy of desorption for bulk multilayers to be 48.9 ± 2 kJ/mol on Ni(111)[43] and 47.3 ± 3.8 kJ/mol on Pt(111)[54], assuming a prefactor of 10^{13} s^{-1}. Our measured value (44.5 ± 1.4 kJ/mol) is not consistent with these results. One possibility is that we are not forming the ideal bulk state of solid benzene. Our results are at a lower temperature than the above TPD experiments, which may prevent benzene from overcoming the activation energy needed to order into the lowest energy state, at least on the timescale of our measurements (~100 ms). Therefore, we could be probing a less stable multilayer structure here than measured in the higher temperature TPD experiments.

Another possibility is that instead of forming bulk benzene, we are forming the transition layer identified by TPD experiments.[43] As stated in the introduction, the peak that corresponds to bulk benzene desorption does not appear until a higher exposure (1.8 L). This transition layer peak was observed at exposures from 1.0 to 2.4L, and possessed a lower desorption temperature of 136 K, compared to 146 K for bulk benzene. This 10 K difference would approximately result in a 3 kJ/mol difference, which leads to a literature heat of adsorption for transition layer(s) that is well within the error of our “multilayer” heat.

Heat of Adsorption of Molecular Benzene on Pt(111) at 90 K. In order to directly compare the heats of adsorption of molecular benzene on Ni(111) and Pt(111), the adsorption of benzene was studied on a Pt(111) surface under the exact same conditions as the Ni(111) surface. Under these conditions, benzene is expected to adsorb molecularly parallel to the surface, favoring bridge sites but may also adsorb onto hollow and top sites.[42,48] As seen in Figure 3.3, benzene initially adsorbs onto Pt(111) at 90 K with a heat of ~209 kJ/mol, and the heat decreases with coverage. Below 0.096 ML, the heat is well described by the best-fit line $-\Delta H_{ad} = (209 - 817\ \theta)$ kJ/mol. Between 0.096 and 0.13 ML, the heat decreases rapidly like a broadened step-function decrease at ~1/9 ML similar to that seen on Ni(111) above. Again, this broadening may be due to inhomogeneity in local coverage. Up to 0.10 ML, these data agree well with previous calorimetry results on Pt(111) measured instead at 300 K, which gave the red curve shown in Figure 3.3: $-\Delta H_{ad} = (197 - 314\ \theta - 3546\ \theta^2)$ kJ/mol.[37] This literature equation has been adjusted so that its definition of a "monolayer" is identical to the one used in this present paper, and is plotted in Figure 3.3 for comparison. Due to differences in the gas-phase and solid-phase heat capacities of benzene at 300 K and 90 K, we expect the heats of adsorption to be a few kJ/mol higher at 90 K. At the limit of low coverage, this is consistent with our results. As seen, our results at 90 K decrease more rapidly compared to the results at 300 K above 0.10 ML. One possible explanation is that at 90 K, the benzene molecules are not mobile enough on the surface to achieve the more stable configurations reached at 300 K. It is clear from the decrease in heat with coverage that there are repulsive benzene-benzene lateral interactions on the surface. If an incoming molecule lands in a region of high local coverage, the molecules in the local region may not have the mobility needed to move away and generate the most stable global energy minimum. Saturation may be achieved at 90 K when there are still open spaces on the surface,

but none large enough to accommodate benzene molecules. At 300 K, benzene has the mobility to effectively find open adsorption sites, thus maintaining higher heats and allowing a higher saturation coverage. This also explains why the heat of benzene adsorption at 90 K continues to decrease at a slower rate until ~0.15 ML, the literature saturation coverage.[53,54]

Above ~0.14 ML on Pt(111) at 90 K, the heat of adsorption becomes somewhat stable at ~60 kJ/mol. From 0.15 ML to ~0.4 ML, the heat of adsorption slowly decreases, approaching the heat of sublimation. This likely corresponds to additional layers on the surface that continue to interact with the underlying Pt metal.

By 0.5 ML at 90 K, benzene reaches a constant multilayer energy of 44.2 ± 1.1 kJ/mol, where the error bars reference the run-to-run standard deviation on the mean of the average heat from 0.5 to 1.2 ML. This is consistent with the multilayer desorption energies ranging from 47.3 - 48.9 kJ/mol (see above).[43,54]

3.4 DISCUSSION

Energetics of Adsorbed Benzene on Ni(111) and Pt(111): We next analyze the measured enthalpy of molecular adsorption at 90 K on Ni(111) (Figure 3.2) and Pt(111) (Figure 3.3) to calculate the heats of formation of benzene on both surfaces. The heats of adsorption for Ni(111) and Pt(111) are directly compared in Figure 3.4, and seen to be quite similar. At 90 K, the first layer appears to saturate at approximately the same coverage (~1/9 ML) of Ni(111) and Pt(111), as seen in Figure 3.4. Since the lattice parameter of Ni is 11% shorter than Pt, this corresponds to a 24% higher packing density on Ni(111), and thus it seems to be dictated more by the need to achieve registry with the substrate, whereby each benzene seems to require something close to the area of a 3x3 unit cell at this temperature.

We use the integral heat determined from the individual data points up to a coverage of 1/9 ML. The thermodynamic cycles in Figure 3.5 show how to extract the heats of formation of adsorbed benzene on both Ni(111) and Pt(111). On the left-hand side of the figure, all elements are in their standard states and therefore possess a heat of formation of zero. The first step at the bottom is simply the enthalpy of formation of gaseous benzene, 82.9 kJ/mol.[68] The second step at the bottom is our integral enthalpy of adsorption measured by SCAC (-167.7 kJ/mol for Ni(111) and -161.5 kJ/mol for Pt(111)). Adding these values together results in the enthalpy of formation of adsorbed benzene, i.e., the top pathway: -250.6 kJ/mol for Ni(111) and -244.4 kJ/mol for Pt(111).

Since there is no decomposition of benzene and the only difference between gaseous benzene and adsorbed benzene is the adsorbate-surface bond, our measured integral enthalpy of adsorption is also equal to the negative of the benzene-metal bond dissociation enthalpy. Therefore, the benzene-Ni(111) bond enthalpy at 1/9 ML coverage is +167.7 kJ/mol and the benzene-Pt(111) bond enthalpy at 1/9 ML coverage is +161.5 kJ/mol. The corresponding bond energies are found by subtracting RT. This results in a benzene-Ni(111) bond energy of 166.9 kJ/mol at 1/9 ML coverage and a benzene-Pt(111) bond energy at 1/9 ML coverage of 160.7 kJ/mol.

Since the adsorption of benzene was studied at the same conditions on Ni(111) and Pt(111), we may directly compare these results. The first conclusion is that there is only a slight difference in the heats of formation and bond energies of these two species. Benzene is only ~6 kJ/mol more stable on Ni(111) than Pt(111).

Previous TPD experiments show the first layer of benzene molecularly desorbing at ~380 K on Ni(111)[43] and at 505 K[54] on Pt(111). However, the vast majority of the adsorbed benzene

dissociates. On Pt(111), for coverages below ~60% of the first saturation layer, approximately 100% dissociates and none desorbs. It is only at higher coverages than 0.09 ML (i.e., when the heat of adsorption has decreased by >60 kJ/mol) that desorption starts to become competitive with dissociation. At such high coverages, very broad, unresolved desorption peaks were seen at ~350 K and ~505 K. These peak temperatures give desorption activation energies of 88 and 129 kJ/mol, respectively, when analyzed with the Redhead equation assuming a prefactor of 10^{13} s^{-1}.[54] Increasing the prefactor to 7.2×10^{15} s^{-1} for the 350 K peak and 3.7×10^{16} s^{-1} for the 505 K peak (based on the more recent method[69] for more accurate estimates of prefactors) increases the values by a small amount (to 107 and 163 kJ/mol, respectively). These two values are consistent with the differential heats of adsorption at lower coverages, before decomposition occurs.

These values are consistent with the high-coverage heats measured in Figure 3.3. On Ni(111), the initial 0.06 ML, or ~40% of the first chemisorbed layer, decomposes to surface carbon and hydrogen, which immediately desorbs as H_2. At higher coverages, a broad, molecular desorption peak appears at ~380 K.[43] At this temperature, the prefactor may be estimated to be 1.0×10^{16} s^{-1} (by the same method as above). This results in an activation energy for desorption of 118 kJ/mol, which is consistent with the high-coverage heats in Figure 3.2. Unlike on Pt(111), a higher TPD peak at ~500 K is not observed. This is likely due to the activation energy for decomposition (C-H bond dissociation) being lower on Ni(111) compared to Pt(111), since both hydrogen and carbon bind more strongly to Ni(111) than Pt(111).[14] By 500 K in TPD, all the adsorbed benzene has probably already dissociated on Ni(111) but not on Pt(111).

We have shown that methyl adsorbs more strongly to Ni(111) compared to Pt(111) by 24 kJ/mol.[31,65] King's group[70] measured the energetics associated with methylidyne on Ni(100) and

ethylidyne on Pt(111) and their results, after a later correction for an error in calorimeter calibration, gave that the metal-carbon σ bond energies are 37 kJ/mol stronger to Ni(100) than Pt(111).[15] One would thus expect hydrocarbon species to adsorb more strongly onto Ni surfaces compared to Pt surfaces. Our bond energy difference for benzene (6 kJ/mol stronger to Ni than Pt) is less than what might be expected based on these previous results, especially given benzene has six carbon atoms bonded to the metal, and these other adsorbates have fewer. This might be understood by considering TPD studies of molecularly adsorbed methane, which have shown that the peak temperature for methane is 10-15 K higher on Pt(111) than Ni(111), giving bond energies of 14.5 kJ/mol on Pt(111) and 12.1 kJ/mol to Ni(111),[71,72] with both dominated by van der Waals forces. This difference implies that van der Waals (vdW) interactions are stronger for adsorbates on Pt(111) than Ni(111). This is also supported by the effective screened C_6 coefficients for vdW interactions calculated for metal surfaces, which are nearly twice as big for Pt as for Ni.[73] Since benzene adsorption on Pt(111) is well known to have strong contributions from van der Waals interactions[14,16,17,38], this stronger van der Waals interaction might bring the adsorption energy on Pt(111) up closer to Ni(111), as observed here. Thus, the binding of benzene to Ni and Pt(111) is a balance between short- and long-range interactions, similar to its bonding to noble metals.[74]

Comparison to DFT Calculations. The heats of molecular adsorption of benzene onto Ni(111) and Pt(111) measured in this work may be used as benchmarks for comparison to theoretical calculations. Table 3.1 gives several calculated bond energies from various DFT methods and the measured bond energy of adsorbed benzene at the equivalent coverage. All DFT values shown here are calculated for bridge sites, for which all DFT methods agreed is the most stable adsorption site on both Ni(111) and Pt(111) at low coverage. The DFT calculations for both

surfaces have been divided into two sections in Table 3.1: those that contain corrections for van der Waal forces and those that do not. Generally, calculations that contain these corrections are more accurate than those that omitted van der Waal corrections, which tend to underestimate benzene's bond energy by large amounts (often 50 to 100 kJ/mol). These differences are much larger than the expected zero-point energy and heat-capacity corrections, which were not included in this comparison. These calculations might also be biased by small amounts since each reported DFT calculation represents benzene exclusively bound to bridge sites. Previous experimental work has suggested that benzene adsorbs onto a mixture of adsorption sites for both Ni(111) and Pt(111).[45,48] Taking this mixture into account would lower all the theoretical values listed in Table 3.1, which would not change the trend seen here, where most DFT functionals underestimate the adsorption energy of benzene on Pt(111).

3.5 CONCLUSIONS

On Ni(111), benzene adsorbs molecularly at 90 K with a decreasing heat of adsorption in the first 0.093 ML well fit by $-\Delta H_{ad} = (208 - 626\ \theta)$ kJ/mol. On Pt(111), benzene adsorbs molecularly at 90 K with a decreasing heat of adsorption in the first 0.096 ML well fit by $-\Delta H_{ad} = (209 - 817\ \theta)$ kJ/mol. On both surfaces, the heat drops rapidly to ~60 kJ/mol in a broadened step-function at ~1/9 ML. On both Ni(111) and Pt(111), benzene adsorbs with a nearly constant heat of adsorption above 0.5 ML of 44-45 kJ/mol, which is the value for multilayer solid benzene. Using the known enthalpies of the gas-phase benzene, we find a standard enthalpy of formation of adsorbed benzene (ΔH_f^0) of -250.6 kJ/mol on Ni(111) and -244.4 kJ/mol on Pt(111).

These measured energies were compared to DFT from many different studies. We found that DFT calculations that neglect van der Waals routinely underestimate this bond energy, while many DFT functionals that include van der Waals corrections are much more accurate. Benzene binds to Ni(111) only slightly more strongly than to Pt(111), even though C-Ni(111) bonds are usually considerably stronger than C-Pt(111) bonds. This is attributed to van der Waals interactions with benzene being stronger on Pt(111) than Ni(111).

3.6 TABLES AND FIGURES

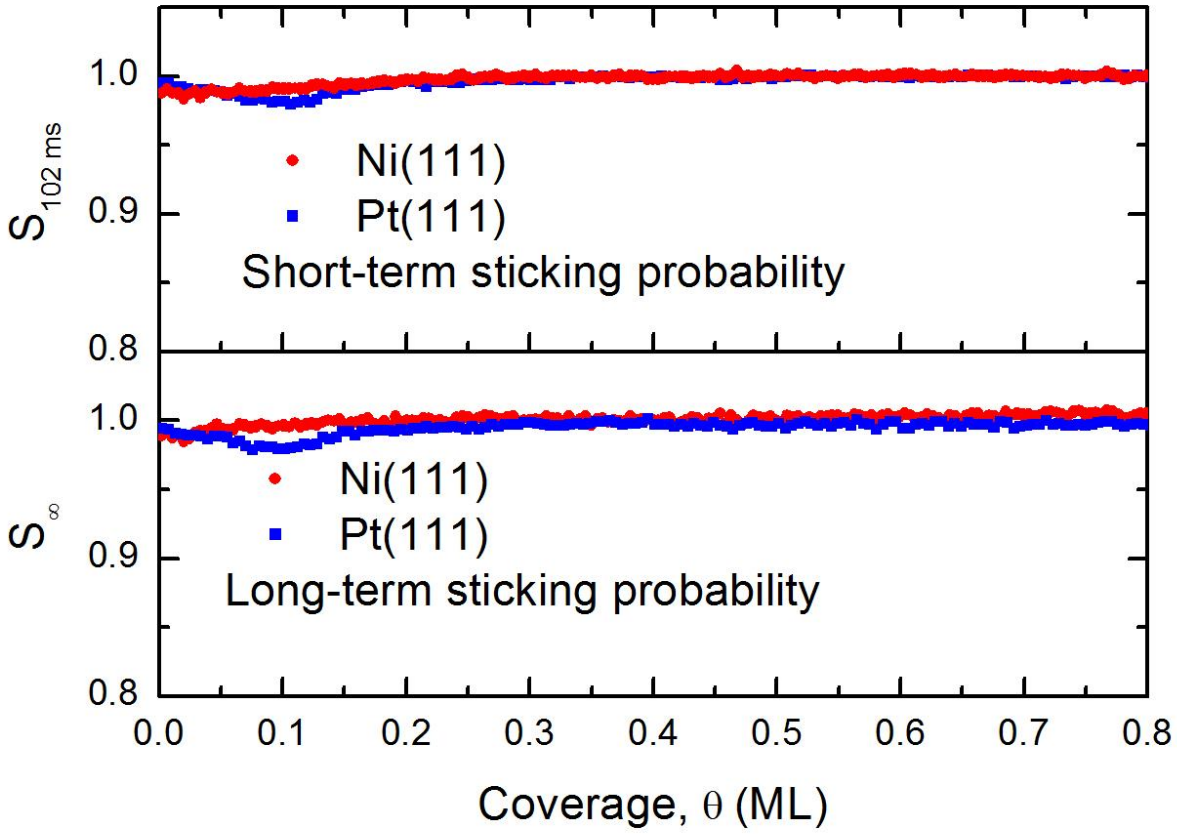

Figure 3.1. Average short-term and long-term sticking probabilities of benzene versus coverage at 90 K on Ni(111) and Pt(111).

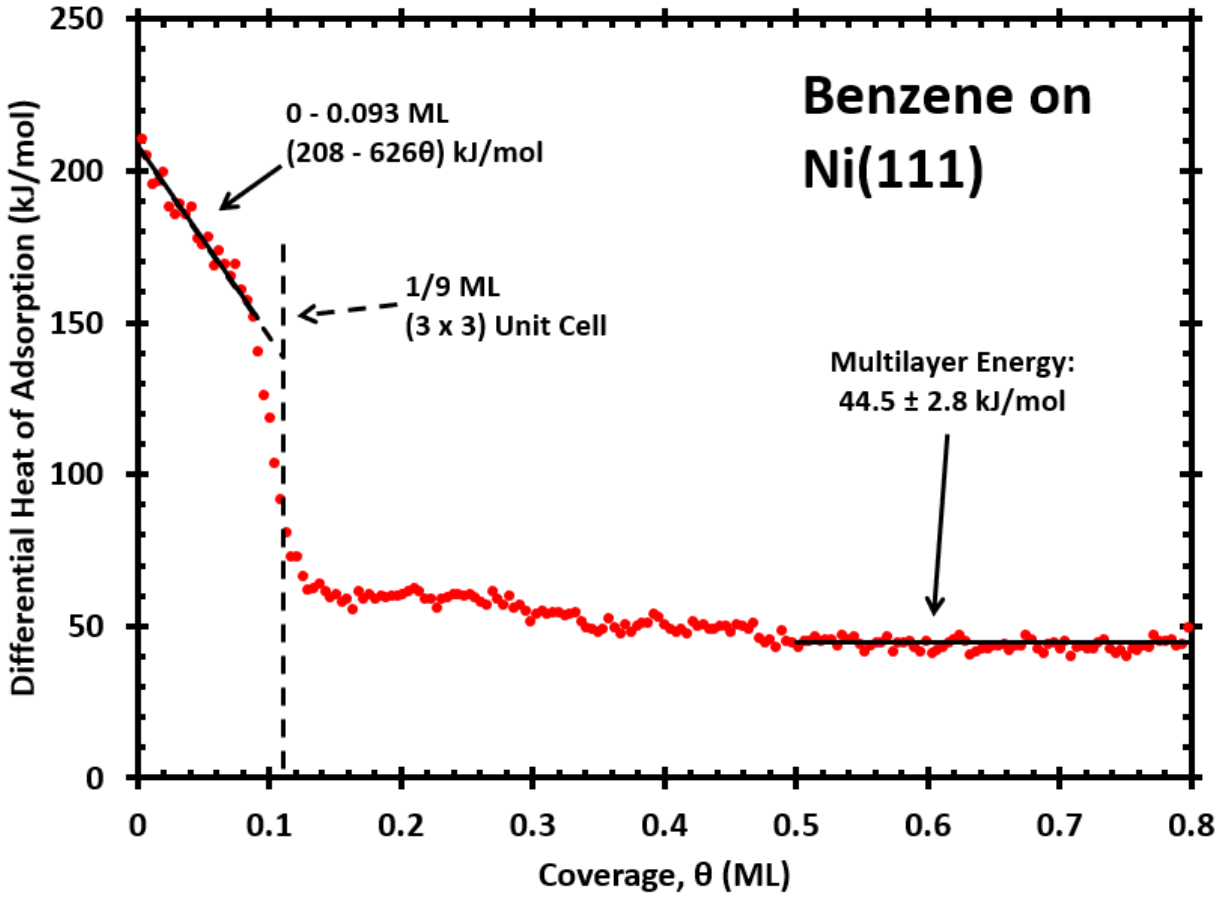

Figure 3.2. Differential heat of adsorption of molecularly adsorbing benzene on Ni(111) at 90 K as a function of adsorbed benzene coverage. Each data point represents a pulse of ~0.002 ML of benzene gas.

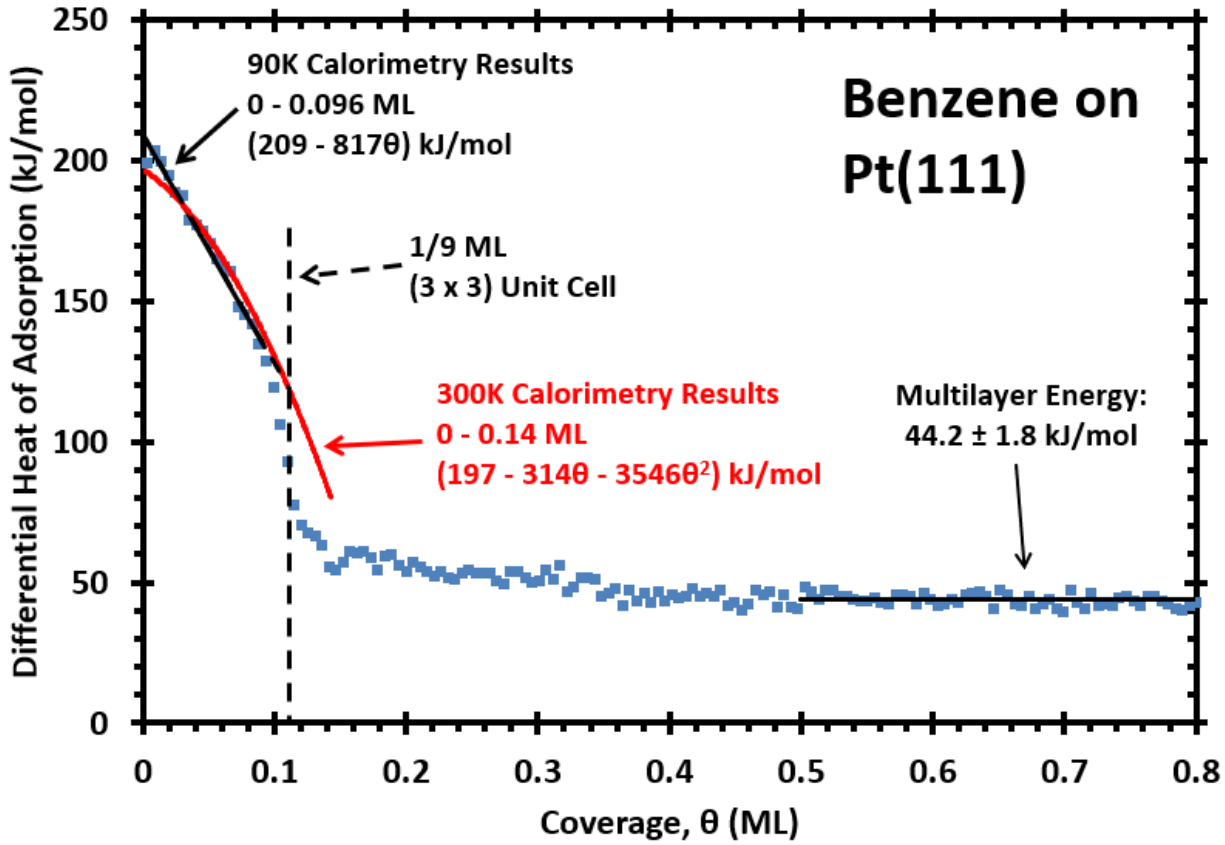

Figure 3.3. Differential heat of adsorption of molecularly adsorbing benzene on Pt(111) at 90 K as a function of adsorbed benzene coverage. Each data point represents a pulse of ~0.005 ML of benzene gas. The red curve shows the previously measured heat of adsorption of molecular benzene at 300 K.[37]

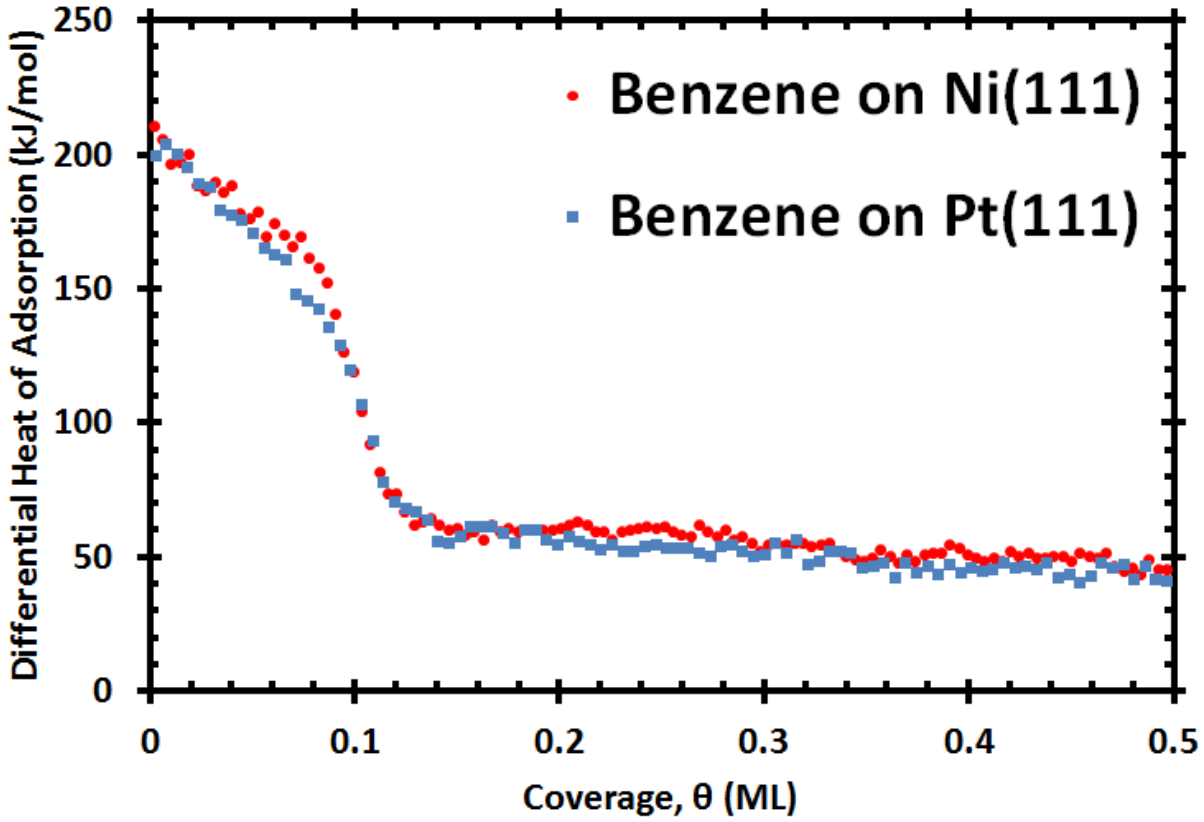

Figure 3.4. Comparison of the differential heat of adsorption of benzene on Ni(111) and Pt(111) at 90 K as a function of adsorbed benzene coverage.

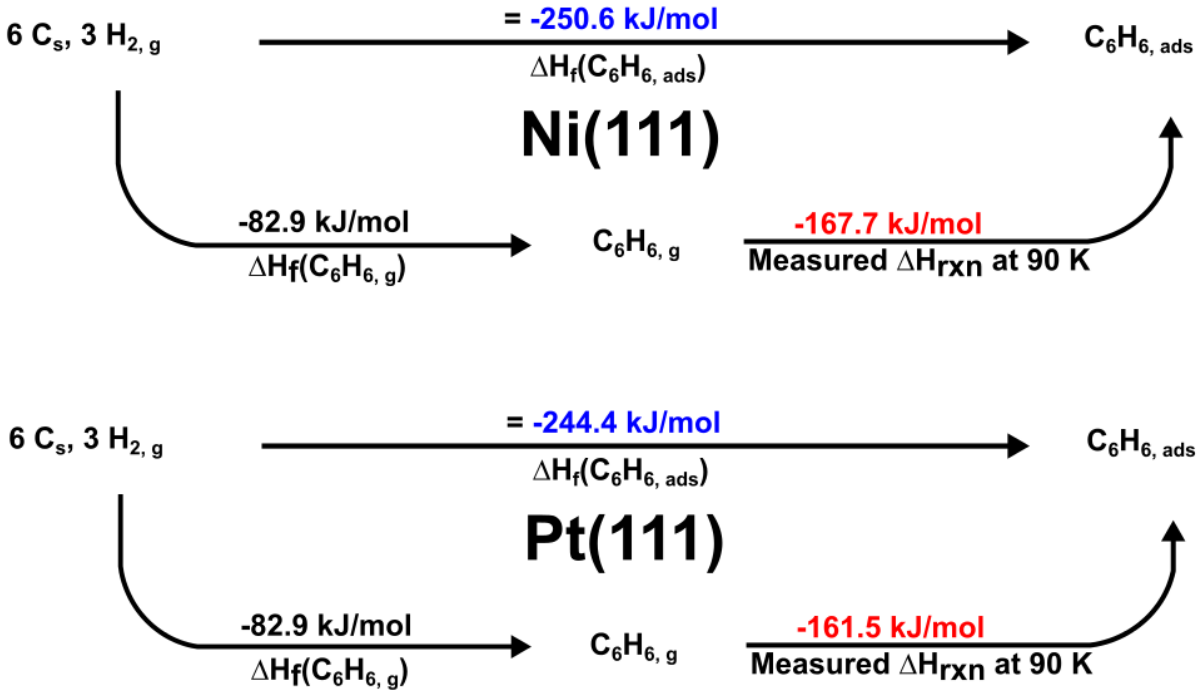

Figure 3.5. Reactions used to determine the heat of formation of molecularly adsorbed benzene on the Ni(111) and Pt(111) surfaces. The values in red correspond to the integral enthalpy of adsorption measured at 90 K for the first 1/9 ML of coverage. The values in blue correspond to the resulting heats of formation of adsorbed benzene.

Table 3.1. Comparison of present calorimetric bond energies of benzene to the Ni(111) and Pt(111) surfaces with calculated values using DFT with periodic boundary conditions. DFT calculations are separated into values that include corrections for van der Waal forces and those that do not.

Benzene on Ni(111)		Bond Energy (kJ/mol)		
Coverage	Functional or Method	DFT	Experimental	Reference
1/16 ML	PBE	95	188	[38]
1/16 ML	revPBE	67	188	[38]
1/16 ML	rPW86	26	188	[38]
1/9 ML	PBE	101	167	[39]
1/16 ML	optB86b-vdW	211	188	[38]
1/16 ML	optB88-vdW	173	188	[38]
1/16 ML	optPBE-vdW	143	188	[38]
Benzene on Pt(111)		Bond Energy (kJ/mol)		
Coverage	Functional or Method	DFT	Experimental	Reference
1/16 ML	PW91	119	183	[56]
1/16 ML	PBE	130	183	[58]
1/16 ML	PBE	115	183	[38]
1/16 ML	revPBE	95	183	[38]
1/16 ML	rPW86	58	183	[38]
1/16 ML	PBE	131	183	[59]
1/9 ML	PBE	86	161	[59]
1/9 ML	PBE	78	161	[16]
1/9 ML	LDA	222	161	[16]
1/9 ML	PBE	78	161	[17]
1/9 ML	PW91	117	161	[60]
1/9 ML	PW91	123	161	[61]
1/9 ML	PW91	87	161	[62]
1/9 ML	PBE	103	161	[63]
1/9 ML	PBE	116	161	[64]
1/25 ML	PBE+vdW^{surf}	212	192	[17]
1/16 ML	PBE+vdW^{surf}	210	183	[38]
1/16 ML	optB86b-vdW	234	183	[38]
1/16 ML	optB88-vdW	195	183	[38]
1/16 ML	optPBE-vdW	171	183	[38]

1/16 ML	PBE-dDsC	207	183	[57]
1/16 ML	PBE-vdW	170	183	[58]
1/16 ML	revPBE-vdW	102	183	[58]
1/16 ML	PW86-vdW2	96	183	[58]
1/16 ML	PBE-vdW	207	183	[59]
1/9 ML	optB88-vdW	178	161	[16]
1/9 ML	vdW-DF	74	161	[16]
1/9 ML	vdW-DF2	33	161	[16]
1/9 ML	PBE-vdW^{surf}	189	161	[16,17]
1/9 ML	PBE+vdW	174	161	[17]
1/9 ML	optPBE-vdW	168	161	[64]

Chapter 4. ENERGETICS OF ADSORBED PHENOL ON NI(111) AND PT(111) BY CALORIMETRY

This chapter reprinted with permission from: S.J. Carey, W. Zhao, Z. Mao, and C.T. Campbell, Energetics of Adsorbed Phenol on Ni(111) and Pt(111) by Calorimetry, Journal of Physical Chemistry C (2018), Article ASAP, DOI: 10.1021/acs.jpcc.8b03155

Chapter Abstract

The heat of adsorption and sticking probability of phenol was measured on Ni(111) at 150K and Pt(111) at 90K using single crystal adsorption calorimetry (SCAC). Phenol adsorbs molecularly with a heat of 200 kJ/mol on terrace sites in the low-coverage limit on Ni(111), giving a standard enthalpy of formation (ΔH_f^0) of $C_6H_5OH_{ad}$ of -272 kJ/mol and with a heat of 220 kJ/mol on terrace sites in the low-coverage limit on Pt(111), giving a standard enthalpy of formation (ΔH_f^0) of $C_6H_5OH_{ad}$ of -271 kJ/mol. The measured energetics for phenol were compared to Density Functional Theory (DFT) calculations from previous literature, showing that DFT functionals that included van der Waals corrections are more accurate, although some calculations on both surfaces, even those with vdW-corrections, still grossly underestimated the bond energy.

4.1 INTRODUCTION

Phenol is the simplest example of an aromatic oxygenate, a class of compounds that are involved in many important catalytic and electrocatalytic reactions on late transition metal surfaces. As such, it is often studied as a model compound to understand surface reactions for

this class of compounds. For example, phenol is often used as a model for studying catalytic and electrocatalytic biomass conversion reactions over Pt, Ni, and other late transition metals.[75–79] In order to better understand how phenol behaves in catalytic reactions, it is critical to know the energetics of phenol on catalyst surfaces. Here, we report the first calorimetric measurements of the adsorption energy of phenol on any transition metal surface, including the bond energies and heats of formation, of phenol adsorbed on two model catalyst surfaces, Ni(111) and Pt(111).

Phenol adsorption onto Ni(111) has been studied with temperature programmed desorption (TPD), vibrational spectroscopy (RAIRS), and Auger electron spectroscopy (AES).[80] These methods found that phenol forms a chemisorbed layer that is parallel to the surface, interacting through its π-bonds with the surface. Multilayers of phenol already start desorbing at the lowest adsorption temperature studied (170K). The first layer mainly decomposes during TPD, as evidenced by desorption peaks for H_2 (starting at ~300 K) and CO (starting at ~420 K).[80]

Phenol adsorption on Pt(111) has been studied with vibrational spectroscopy (HREELS)[81–83], low-energy electron diffraction (LEED)[82], AES[82], TPD[81,83], and X-ray photoelectron spectroscopy (XPS)[83]. Below 200K, phenol adsorbs molecularly, parallel to the surface.[81–83] At low temperatures, multilayers are formed that possess a desorption peak at 195K. There is a transition (second) layer between the chemisorbed first layer and multilayers that interacts weakly with the Pt(111) surface. The adsorption energy of this layer is slightly stronger than the multilayer, as evidenced by a TPD desorption peak at 225K.[83] At 200K, adsorbed phenol dissociates by O-H bond scission, resulting in phenoxy and an adsorbed hydrogen atom.[81,83] Further analysis shows that phenoxy transitions to a η^5-π-adsorption or

oxocyclohexadienyl species.[83] By 490K, this species decomposes to CO and H_2 gas, plus some carbon residue on the surface.[83]

4.2 EXPERIMENTAL

Experiments were performed in a UHV chamber (base pressure $<2 \times 10^{-10}$ mbar) equipped with XPS, AES, low-energy ion scattering spectroscopy (LEIS), LEED, and SCAC. The sample used was a 1 μm thick Ni(111) or Pt(111) single-crystal foil, supplied by Jacques Chevallier at Aarhus University in Denmark. The sample surface was cleaned by Ar^+ ion sputtering and annealing to remove contaminants. This treatment was repeated until impurities were below the detection limit of XPS, and the surface gave a very sharp LEED pattern. Detailed descriptions of the apparatus, molecular beam, sticking probability, heat measurements, and other procedures for SCAC may be found elsewhere.[29,34,35,65]

Briefly, calorimetry was performed by holding the clean metal single crystal at a given temperature and exposing it to a pulsed molecular beam of phenol. The heat of adsorption was measured with a pyroelectric detector pressed against the backside of the sample.[25,35] The sensitivity of the pyroelectric detector was calibrated after each experiment by depositing a known amount of energy into the sample by use of a HeNe (632.8 nm) laser. The sticking probability was measured simultaneously with the heat of adsorption using a quadrupole mass spectrometer, as described previously.[36] We report two types of sticking probabilities, long-term and short-term.[29] The long-term sticking probability, S_∞, is the probability that a gas molecule strikes the Ni(111) or Pt(111) surface, sticks, and remains until the next gas pulse starts ~3 s later. This measurement is used to calculate the adsorbate coverage remaining at the start of the next gas pulse. The short-term sticking probability, $S_{102\ ms}$, is the probability that a gas molecule

strikes the Ni(111) or Pt(111) surface, sticks, and remains at least throughout the time frame of our heat measurement (i.e., the first 102 ms). This is used to calculate the moles of gas-phase reactant that contribute to the measured heat of adsorption, so we can report that value in kilojoules per mole adsorbed.

The molecular beam was created by expanding ~0.3 mbar of phenol (Sigma-Aldrich, >99%) through a microchannel array held at 300 ± 5 K (defining the gas temperature) and then collimated through a series of five liquid nitrogen-cooled orifices. A chopper converts the beam into pulses that are 102 ms long and repeat every 3 s. Coverages are reported in monolayers (ML) and are defined as the number of phenol molecules that adsorb to the surface irreversibly, normalized by the number of metal surface atoms in the Ni(111) surface (1.86×10^{15} Ni atoms/cm^2) or Pt(111) surface (1.50×10^{15} Pt atoms/cm^2). A typical phenol dose was ~0.001-0.002 ML per pulse with a beam spot size previously determined to be 4.36 mm in diameter.[34]

4.3 RESULTS

Sticking Probability. As described previously[29] and above, we measured two types of sticking probabilities: the short-term sticking probability, $S_{102\ ms}$, and the long-term sticking probability, S_∞. Figure 4.1 shows the average short-term and long-term sticking probabilities measured as a function of coverage on both Ni(111) and Pt(111). At these low temperatures, the sticking probability is near unity for both metal surfaces independent of coverage. On both surfaces, multilayer formation is expected and confirmed in this work.[80,83] For Ni(111), both sticking probabilities start and remain very near unity for all experiments. For Pt(111), the initial short-term and long-term sticking probabilities start near unity but decrease slightly over the first 0.1 ML of coverage to ~0.98, then increase to near unity at coverages above 0.15 ML after the first

layer saturates (see below). This behavior was previously observed for benzene adsorption onto Pt(111) at 90K,[84] where the lower average sticking probability in the first layer on Pt(111), compared to Ni(111) or multilayers, was attributed to the poorer mass-matching in the phenol-Pt(111) collisions than when phenol strikes Ni(111) or a phenol multilayer. Poorer mass-matching in the gas-surface collisions results in a higher probability for quasi-elastic collisions and hence lower trapping probability.[85]

Heat of Adsorption of Molecular Phenol on Ni(111) at 150K. In this paper, we define the term *heat of adsorption* as the negative of the differential standard molar enthalpy change for the adsorption reaction, ΔH_{ad}, with the gas and the metal surface being at the same temperature as the metal surface ("standard" here implies only that the gas is at 1 bar as a pure ideal gas). During our experiments, the temperature of the molecular beam was ~300 K, while the Ni(111) sample was held at cryogenic temperatures (e.g., T = 150 K). Thus, the measured heat is corrected by the small difference in the internal energy of the gas in the *directed* molecular beam at its source temperature (300 K) and in a Boltzmann distribution at the sample temperature (T), and then by RT to convert from internal energy change to enthalpy change for the adsorption reaction, as described elsewhere.[15]

Figure 4.2 shows the heat of adsorption of phenol on the Ni(111) surface at 150K. Under these conditions, phenol is expected to adsorb molecularly, parallel to the surface.[80] Phenol initially adsorbs with a heat of 200 kJ/mol. As coverage increases to 0.08 ML, the heat of adsorption decreases linearly with coverage and is well described by the best-fit line $-\Delta H_{ad} = (200 - 295\ \theta)$ kJ/mol, where θ is coverage in ML. At 0.08 ML, the negative slope abruptly increases in magnitude. From 0.08 ML to 0.115 ML, the heat of adsorption is well described by the linear best-fit line $-\Delta H_{ad} = (380 - 2466\ \theta)$ kJ/mol. At 0.115 ML, the negative slope abruptly

decreases in magnitude to near zero. Between 0.115 ML and ~0.28 ML, the heats of adsorption remain almost constant at approximately 85 kJ/mol. This indicates that there exists a transition layer between bulk multilayer phenol and the first chemisorbed layer. By 0.30 ML, we form multilayers of bulk phenol and the heat of adsorption becomes constant at 72.2 ± 1.0 kJ/mol, where the error bars are the run-to-run standard deviation on the mean of the average heat from 0.30 to 0.45 ML. This agrees well the literature values for the heat of sublimation of benzene. Averaging the three literature values given by NIST gives a standard heat of sublimation of 69.0 kJ/mol at 298 K.[86–88] Using the gas phase and solid phase heat capacities of phenol, this average may be adjusted to the experiment temperature of 150K, giving a standard enthalpy of sublimation of 71.2 kJ/mol. This value agrees within 1 kJ/mol of our measured value.

These measurements indicate that the first layer of chemisorbed phenol is completed at 0.115 ML, which is within error of the ideal coverage of 1/9 ML for a (3 x 3) structure. Thus, each phenol occupies approximately nine Ni atoms at saturation. To the best of our knowledge, there is no information as to whether phenol forms an ordered structure on the Ni(111) surface. The saturation coverage of benzene on Ni(111) is 0.13 ML (i.e., 7.7 Ni atoms per benzene) at 90K.[84] This larger area per phenol is not surprising since it has the extra OH group.

Heat of Adsorption of Molecular Phenol on Pt(111) at 90K. Figure 4.3 shows the heat of adsorption of phenol on the Pt(111) surface at 90K. Here, phenol is expected to initially adsorb molecularly, parallel to the surface.[81–83] Phenol adsorbs initially with a heat of adsorption of 220 kJ/mol. From 0 – 0.15 ML, the heat of adsorption decreases linearly with coverage and is well described by the best-fit line $-\Delta H_{ad} = (220 - 808\ \theta)$ kJ/mol. Our saturation coverage of the first layer is within error of that expected for a $(\sqrt{7} \times \sqrt{7})$ R19.1° structure, which corresponds to a coverage of 1/7 = 0.143 ML. Lu et al.[82] adsorbed phenol from aqueous solutions onto a Pt(111)

electrode at room temperature and observed a (3 x 3) structure at saturation using LEED and HREELS, which corresponds to 1/9 ML. Our coverage in UHV may be larger due to the absence of water solvent and the lower adsorption temperature used here.

From 0.15 – 0.30 ML, the heat of adsorption decreases much more slowly and is well described by the best-fit line $-\Delta H_{ad} = (118 - 125\ \theta)$ kJ/mol. The presence of this transition layer agrees well with previous TPD experiments, which found that the second phenol layer binds slightly more strongly, compared to bulk multilayer phenol, by evidence of a higher desorption peak at 225K (compared to 195K for the multilayer).[83] By ~0.3 ML, bulk-like multilayers of phenol are formed and the heat of adsorption becomes constant at 73.2 ± 1.4 kJ/mol, where the error bars are the run-to-run standard deviation on the mean of the average heat from 0.30 to 0.48 ML. Adjusting the standard enthalpy of sublimation reported for bulk phenol (solid) at 298 K[86–88] to 90K using the gas phase and solid phase heat capacities of phenol results in a literature enthalpy of 71.9 kJ/mol. This value agrees within 1.3 kJ/mol with the heat of multilayer adsorption measured in this work.

4.4 DISCUSSION

Energetics of Adsorbed Phenol: The measured enthalpy of molecular adsorption at 150K on Ni(111) (Figure 4.2) and at 90K on Pt(111) (Figure 4.3) may be used to calculate the heats of formation of phenol on both surfaces. These heats for Ni(111) and Pt(111) are compared directly in Figure 4.4, and seen to be similar. We use the integral heat determined from the best fit lines for each adsorption curve up to a coverage of 1/9 ML. The thermodynamic cycles in Figure 4.5 show how to extract the heats of formation of adsorbed phenol on both Ni(111) and Pt(111). On the left-hand side of the figure, all elements are in their standard states and therefore possess a

heat of formation of zero. The first step at the bottom is simply the enthalpy of formation of gaseous phenol, -96kJ/mol.[86–88] The second step at the bottom is our integral enthalpy of adsorption measured by SCAC from 0 to 1/9 ML of coverage (-176 kJ/mol for Ni(111) and -175 kJ/mol for Pt(111)). Adding these values together results in the enthalpy of formation of adsorbed phenol, i.e., the top pathway: -272 kJ/mol for Ni(111) and -271 kJ/mol for Pt(111).

Since there is no decomposition of phenol in these experiments, our measured integral heat is equal to the phenol-metal bond enthalpy. Therefore, at 1/9 ML coverage, the phenol-Ni(111) bond enthalpy is -176 kJ/mol and the phenol-Pt(111) bond enthalpy is -175 kJ/mol. These bond enthalpies may be converted into bond energies by changing sign and subtracting RT. This results in a phenol-Ni(111) bond energy of 175 kJ/mol and phenol-Pt(111) bond energy of 174 kJ/mol, both averaged up to 1/9 ML.

Previous TPD work studying adsorbed phenol on Pt(111) shows a clearly resolved peak at 225K, which corresponds to a second layer, above the 195 K peak for multilayer phenol.[83] This second layer, with a slightly higher heat of adsorption than the multilayer, is also clearly observed in Figure 4.3. Averaging the data points in Figure 4.3 from 0.15 ML to 0.30 ML gives an average adsorption enthalpy of 89.5 kJ/mol for this second layer. Converting this value to an activation energy of desorption (E_{des}) by subtracting ½RT (as explained elsewhere[89]) gives E_{des} = 89.1 kJ/mol. Using this E_{des} in the first-order Redhead equation[89] together its reported TPD peak temperature of 225 K gives a prefactor for desorption of this second layer of 2.5×10^{20} s^{-1}.

Comparison of Phenol Adsorption on Ni(111) and Pt(111): A direct comparison of the heats of adsorption of phenol on Ni(111) at 150K and Pt(111) at 90K is shown in Figure 4.4. Based on the bond energies measured in this work, phenol binds with comparable bond strength to both surfaces. The 1 kJ/mol difference in the integral bond energy at 1/9 ML is well within the error

in our absolute calibration (up to 3%)[35]. By "integral bond energy" here, we mean the bond energy obtained from the average adsorption energy between zero coverage and the stated coverage, or 1/9 ML here. However, this difference changes depending on the chosen coverage. Initially, phenol binds to Pt(111) more strongly than Ni(111), up to a coverage of ~0.04 ML. From ~0.04 ML to ~0.10 ML, the differential heat of adsorption of phenol on Ni(111) is stronger. The higher heat below 0.04 ML on Pt may be due to a larger fraction of step sites on Pt(111), the removal of which requires higher annealing temperatures than Ni(111). Step sites are known to bind aromatic molecules more strongly than terraces on Pt(111).[90] From ~0.10 ML up until the saturation of the second layer, phenol binds stronger to Pt(111) again.

The similarity in first-layer heats of phenol adsorption between Ni(111) and Pt(111) above was also seen for benzene.[84] This was explained for benzene as being due to a cancellation of two opposing effects: stronger intrinsic covalent bonding for Ni-C compared to Pt-C bonds, but stronger van der Waals (vdW) attractions for Pt.[84] The similarity for phenol is not surprising since the nature of the bonding seems to be very similar as with benzene, as indicated by the similar integral bond energies for benzene (-166.9 kJ/mol at 1/9 ML on Ni(111) and -160.7 kJ/mol at 1/9 ML on Pt(111)[84] compared to those above for phenol. There seems to be little contribution to the adsorption energy from oxygen-to-metal bonds since O-Ni bonds should be >50 kJ/mol stronger than O-Pt bonds.[66]

Comparison to DFT Calculations. The heats of molecular adsorption of phenol onto Ni(111) and Pt(111) measured in this work may be used as benchmarks for comparison to theoretical calculations. Table 4.1 gives several calculated bond energies from various DFT methods and the measured integral bond energy of adsorbed phenol at the same coverage. As reviewed in the Introduction, previous experimental measurements on both Ni(111) and Pt(111) had indicated

that the phenol adsorbs molecularly (without bond breaking) with its aromatic ring lying parallel to the metal surface at the conditions of the present calorimetric measurements. The DFT results here are also for such a structure. They do not include zero-point energy corrections. The DFT results for each surface are divided into two sections, those that employ corrections for van der Waals (vdW) forces and those that do not. The calculated DFT results for phenol adsorption on Ni(111) underestimate the bond energy strength by 87-94 kJ/mol, regardless of the inclusion of vdW corrections, which was done with only one functional, PBE-D3. The calculated DFT results for phenol adsorption on Pt(111) ranges from underestimating the energy by 94 kJ/mol to overestimating the energy by 12 kJ/mol. Results that include vdW corrections were less likely to underestimate the energy. However, in some cases, vdW-corrected functionals also underestimated the bond energy to Pt(111) by ~100 kJ/mol. For the closely-related system of benzene on Ni(111), optB86b-vdW and optB88-vdW gave adsorption energies of 211 and 173 kJ/mol, resp., both close to our SCAC value of 188 kJ/mol.[84] Therefore, we believe that the very low value for the DFT energy on Ni(111) for the one study that included vdW corrections in Table 4.1 is probably due to a problem with that particular method (PBE-D3) than due to a general problem with vdW corrections in DFT for Ni(111).

The experiments in Table 4.1 are at 150 and 90 K, whereas the DFT values are for 0 K. The heat capacity difference between solid phenol and gaseous phenol is only 14 J/(mol K) at 150 K and drops to ~10 J/(mol K) at 90 K,[91] and this difference must approach zero at 0 K. Thus, we expect the average heat capacity difference between adsorbed phenol and gaseous phenol to be <30 J/(mol K) in the range from 0 K to the measurement temperature of 90 or 150 K. Thus, the temperature difference between the experiments and the DFT results in Table 4.1 should contribute less than 5 kJ/mol to the energy differences seen there.

To the best of our knowledge, there is no experimental knowledge of the preferred adsorption site of phenol on either surface. Theoretical studies that do not include vdW corrections systematically calculate strongest adsorption to be at bridge sites. Studies that use vdW corrected functionals vary in their adsorption site, preferring either bridge or HCP hollow sites. For phenol, the adsorption site is defined as the site over which the aromatic ring is centered.

4.5 CONCLUSIONS

On Ni(111), phenol adsorbs molecularly at 150 K with a decreasing heat of adsorption in the first 0.08 ML well fit by $-\Delta H_{ad} = (200 - 295\ \theta)$ kJ/mol. From 0.08 ML to 0.115 ML, the heat of adsorption drops more rapidly and is well fit by $-\Delta H_{ad} = (386 - 2529\ \theta)$ kJ/mol. On Pt(111), phenol adsorbs molecularly at 90 K with a decreasing heat of adsorption in the first 0.15 ML well fit by $-\Delta H_{ad} = (220 - 808\ \theta)$ kJ/mol. On both Ni(111) and Pt(111), phenol adsorbs with a nearly constant heat of adsorption above 0.3 ML of 72-74 kJ/mol, which is the value for multilayer solid phenol. Using the known enthalpies of the gas-phase phenol, we find a standard enthalpy of formation of adsorbed phenol (ΔH_f^0) of -272 kJ/mol on Ni(111) and -271 kJ/mol on Pt(111).

These measured energies were compared to DFT from many different studies. We found that DFT calculations that neglect van der Waals corrections are more likely to underestimate this bond energy, while many DFT functionals that include van der Waals corrections are more accurate. However, some calculations on both surfaces, even those with vdW-corrections, still grossly underestimated the bond energy.

4.6 TABLES AND FIGURES

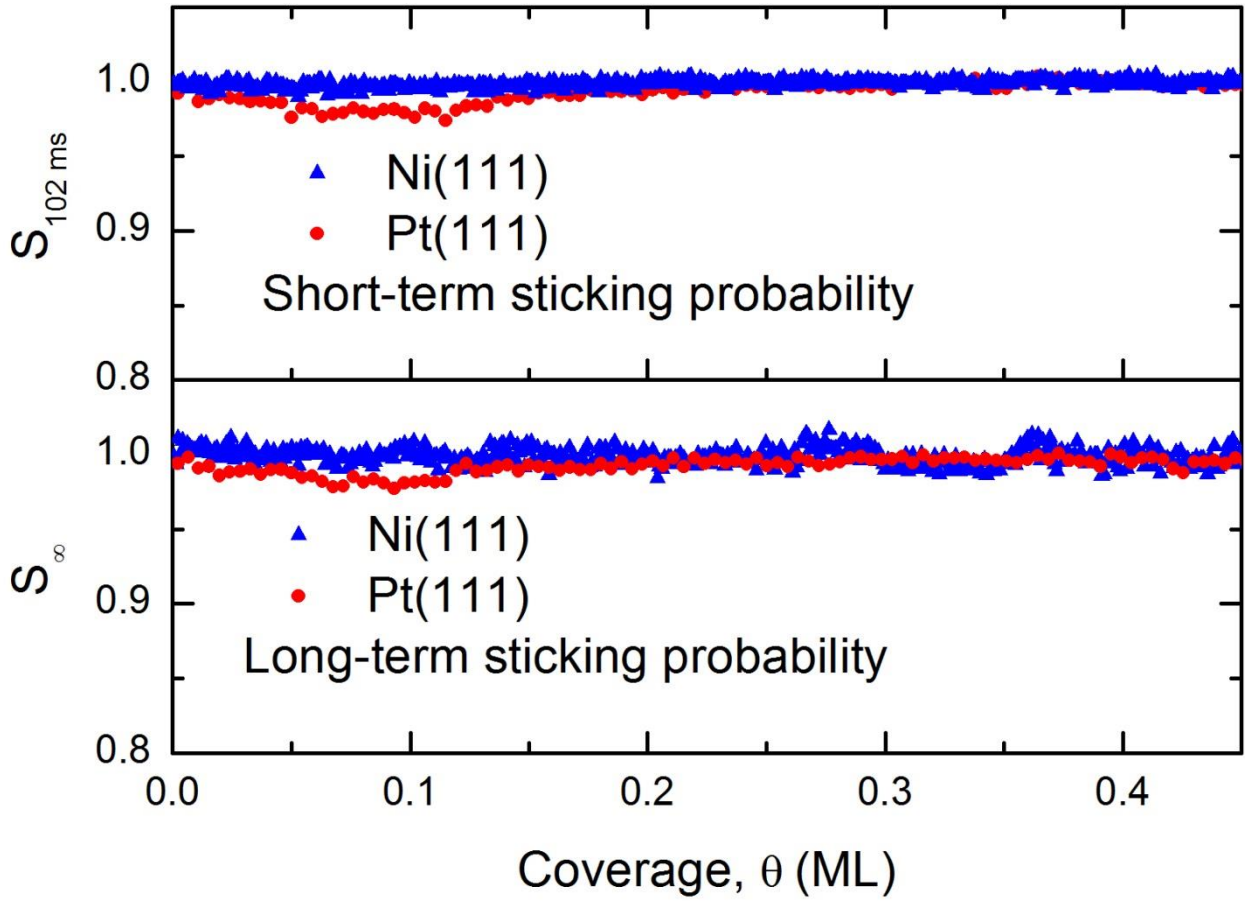

Figure 4.1. Average short-term and long-term sticking probabilities of phenol versus coverage at 90K for Pt(111) and 150K for Ni(111).

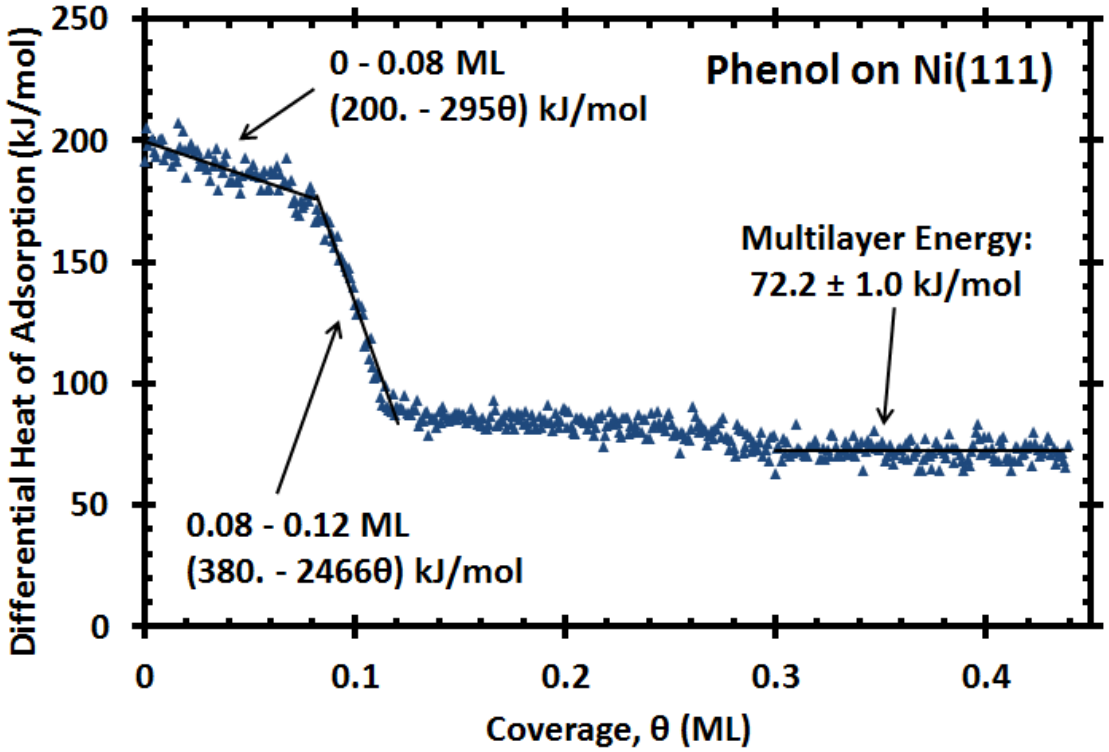

Figure 4.2. Differential heat of adsorption of molecularly adsorbing phenol on Ni(111) at 150K as a function of adsorbed phenol coverage. Each data point represents a pulse of ~0.001 ML of phenol gas.

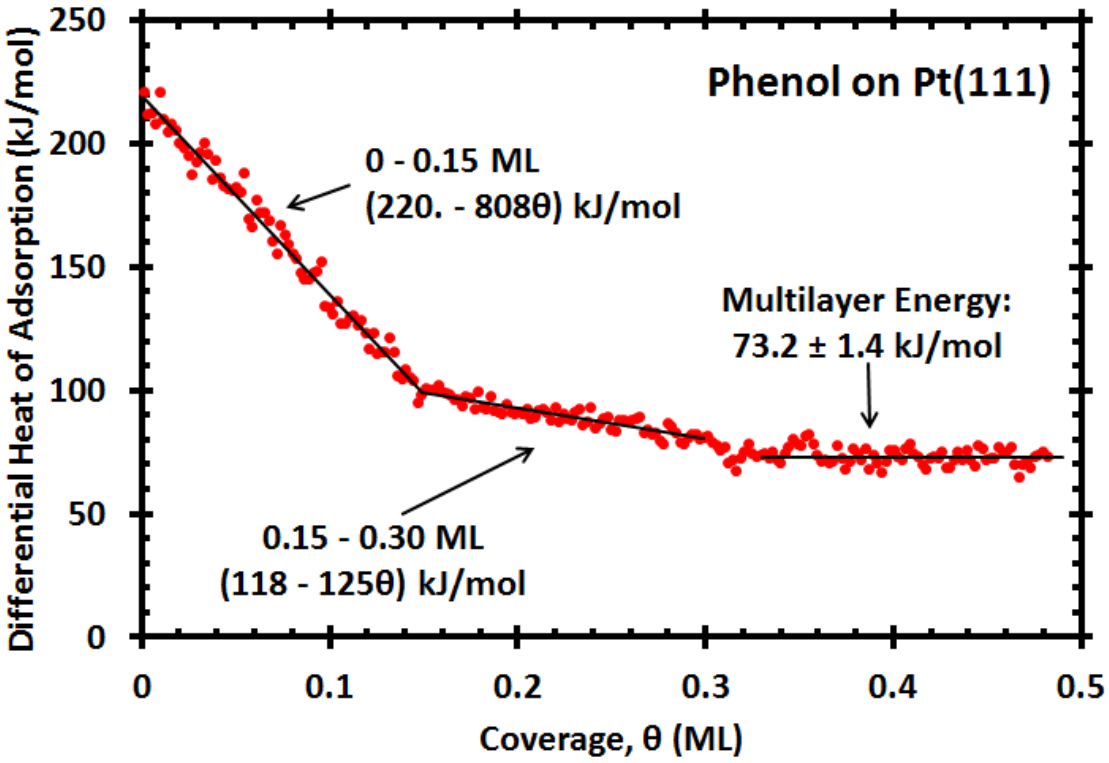

Figure 4.3. Differential heat of adsorption of molecularly adsorbing phenol on Pt(111) at 90K as a function of adsorbed phenol coverage. Each data point represents a pulse of ~0.002 ML of phenol gas.

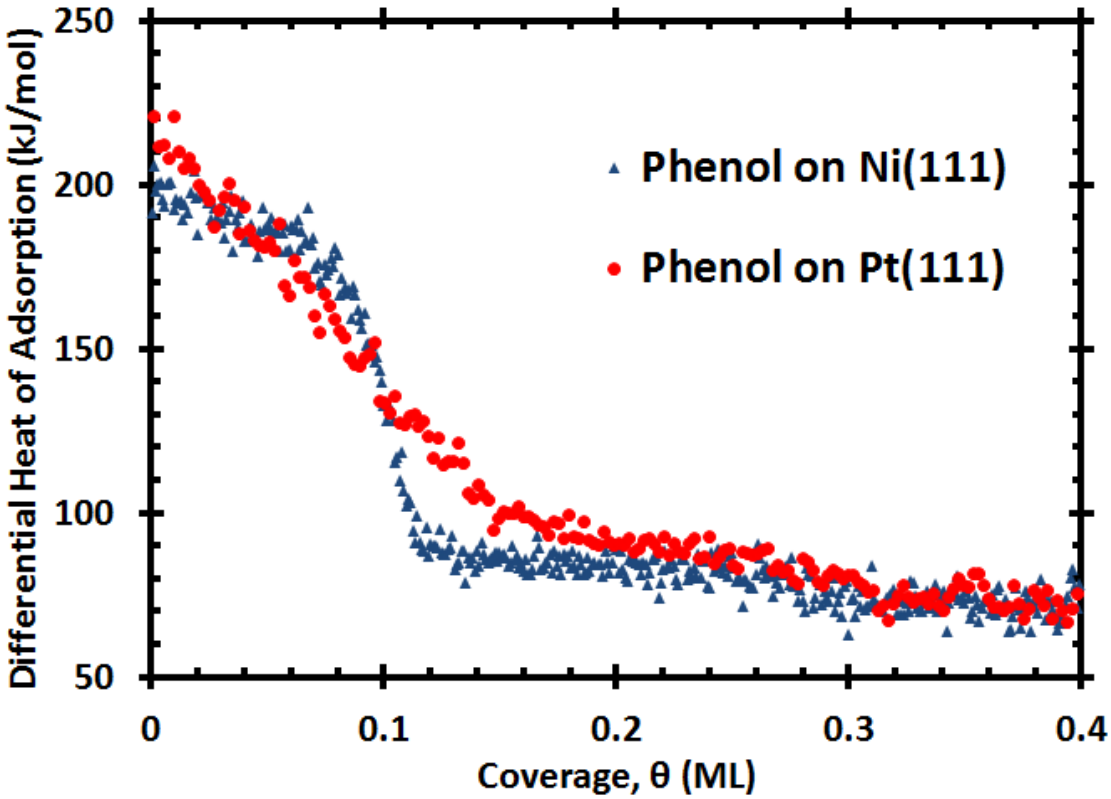

Figure 4.4. Comparison of the differential heat of adsorption of phenol on Ni(111) at 150K and Pt(111) at 90K as a function of adsorbed phenol coverage.

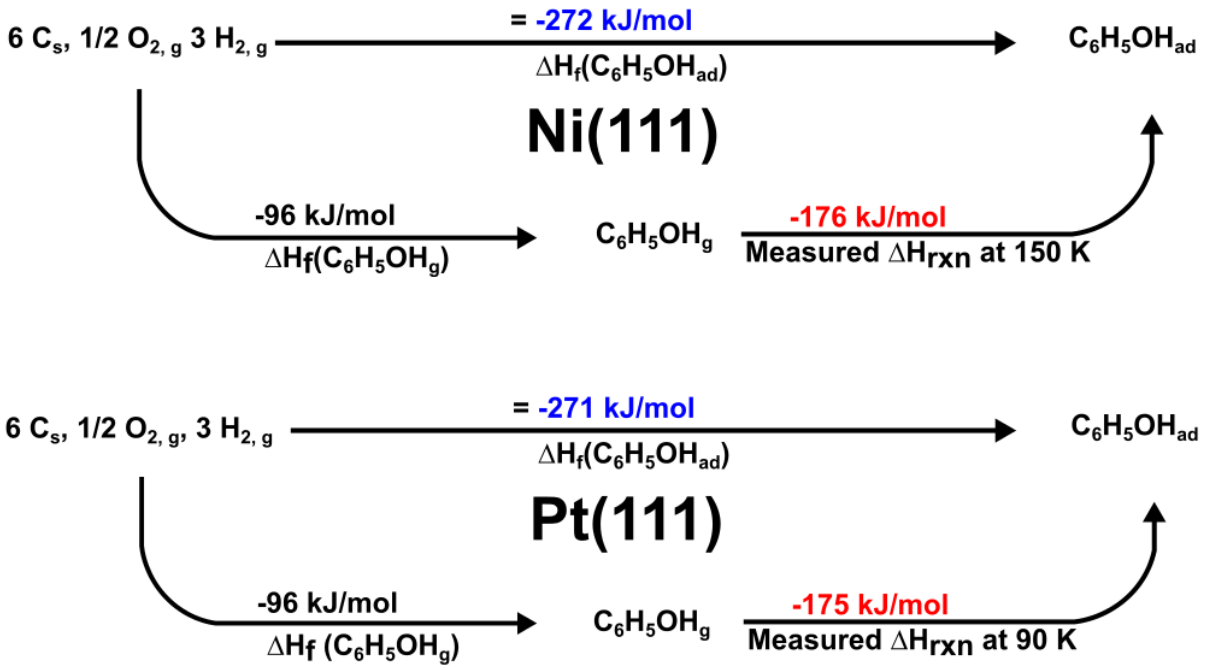

Figure 4.5. Reactions used to determine the heat of formation of molecularly adsorbed phenol on the Ni(111) and Pt(111) surfaces. The values in red correspond to the integral enthalpy of adsorption measured at 90K for Ni(111) and 150K for Pt(111) for the first 1/9 ML of coverage. The values in blue correspond to the resulting heats of formation of adsorbed phenol ($C_6H_5OH_{ad}$).

Table 4.1. Comparison of present calorimetric integral bond energies of phenol to Ni(111) at 150 K and Pt(111) at 90 K with calculated values at 0 K using DFT with periodic boundary conditions.

Phenol on Ni(111)			Bond Energy (kJ/mol)		Reference
Coverage	DFT Functional/Method	DFT Site	DFT	Calorimetry	DFT
1/9 ML	PBE	Bridge	88	175	[39]
1/16 ML	PBE-D3 (includes vdW)	HCP Hollow	96	190	[92]
Phenol on Pt(111)			Bond Energy (kJ/mol)		Reference
Coverage	DFT Functional/Method	DFT Site	DFT	Calorimetry	DFT
1/25 ML	PW91	Bridge	215	203	[93]
1/16 ML	PBE	Bridge	112	194	[94]
1/16 ML	PBE	Bridge	126	194	[58]
1/16 ML	PBE-vdW	HCP Hollow	176	194	[58]
1/16 ML	revPBE-vdW	HCP Hollow	105	194	[58]
1/16 ML	PW86-vdW2	HCP Hollow	100	194	[58]
1/16 ML	PBE-dDsC	Bridge	208	194	[57]
1/16 ML	optB88-vdW	Bridge	199	194	[94]
1/16 ML	PBE-D3 (includes vdW)	HCP Hollow	172	194	[92]

Chapter 5. THE ENERGETICS OF ADSORBED METHYL AND METHYL IODIDE ON NI(111) BY CALORIMETRY: COMPARISON TO PT(111) AND IMPLICATIONS FOR CATALYSIS

This chapter reprinted with permission from: S.J. Carey, W. Zhao, A. Frehner, and C.T. Campbell, Energetics of Adsorbed Methyl and Methyl Iodide on Ni(111) by Calorimetry: Comparison to Pt(111) and Implications for Catalysis, ACS Catalysis (2017), 7(2), 1286-1294, DOI: 10.1021/acscatal.6b02457

Chapter Abstract

The heat of adsorption and sticking probability of methyl iodide were measured on Ni(111) at 100K and 160K using single crystal adsorption calorimetry (SCAC). At 100K, methyl iodide adsorbs molecularly with a heat of 102 kJ/mol on terrace sites in the low-coverage limit, giving a standard enthalpy of formation (ΔH_f^0) of CH_3I_{ad} of -87 kJ/mol. A heat of 122 kJ/mol is also measured on defect sites, probably step edges. Calorimetry of the dissociative adsorption of methyl iodide on Ni(111) at 160K yielded an integral heat of adsorption of -270. kJ/mol at 0.04 ML, providing the energetics of adsorbed methyl, with $\Delta H_f^0[CH_{3,ad}]$ = -71 kJ/mol and a CH_3-Ni(111) bond enthalpy of 218 kJ/mol. This is 22 kJ/mol stronger than the reported value for CH_3-Pt(111) bonds, explaining the greater activity of Ni catalysts for hydrogenolysis compared to Pt. The measured energetics for methyl were compared to Density Functional Theory (DFT) calculations from previous literature, showing that these methods systematically underestimate the bond energy of methyl to Ni(111).

5.1 INTRODUCTION

Adsorbed methyl ($CH_{3,ad}$) is known to be a key intermediate in energy-related catalysis over transition metals, including combustion, partial oxidation, steam reforming and dry reforming of methane, methanation, Fischer-Tropsch, steam reforming and combustion of various other hydrocarbons and oxygenates, methanol decomposition, and several fuel cell reactions. It is also the simplest example of all adsorbed alkyls. Since the critical catalytic parameters of selectivity and activity depend on the thermodynamic stability and energetics of adsorbed intermediates, it is important to measure the energetics of adsorbed methyl. This is especially important for Ni surfaces, since Ni-based catalysts are the most widely used in methane conversion. Here, we report the first direct measurements of the energetics of adsorbed methyl on the Ni(111) surface, produced by the dissociative adsorption of methyl iodide. The only other surface where this energy is known is Pt(111)[95]. We find that methyl binds ~20 kJ/mol more strongly to Ni(111) than to Pt(111).

Under ultrahigh vacuum (UHV) conditions, methyl is stable enough below 150K to be identified on Ni(111) single crystal surfaces[96,97]. Methyl has been produced on Ni(111) through dissociative adsorption of methyl iodide[97] and methane[96] and studied in considerable detail. Those previous studies have shown that methyl iodide adsorbs molecularly at 80K, eventually forming multilayers[97]:

$$CH_3I_g \rightarrow CH_3I_{ad} \quad . \qquad (1)$$

At approximately 120K, multilayer methyl iodide desorption starts and methyl iodide dissociates into an adsorbed methyl group and iodine adatom:[96,97]

$$CH_3I_{ad} \rightarrow CH_{3,ad} + I_{ad} \quad . \qquad (2)$$

Above 150K, adsorbed methyl dissociates to an adsorbed methylidyne and two adsorbed hydrogen atoms:[96]

$$CH_{3,ad} \rightarrow CH_{ad} + 2\,H_{ad} \quad . \quad (3)$$

These adsorbed hydrogen atoms may react with adsorbing methyl groups above 220K to form methane gas:[96]

$$CH_3I_{ad} + H_{ad} \rightarrow CH_{4,g} + I_{ad} \quad . \quad (4)$$

In this work, we report heats of reaction for both the molecular adsorption of methyl iodide and its dissociative adsorption to form coadsorbed methyl and iodine. Dissociative adsorption calorimetry measurements were performed at 160K, a temperature where no methane gas is produced, which indicates that no C-H cleavage has yet occurred in the adsorbed methyl since H_{ad} is known to add to $CH_{3,ad}$ to make methane at even lower temperature.[97] The heat released during this reaction is measured directly using single crystal adsorption calorimetry (SCAC). Since the energy of the adsorbed iodine atoms has been determined previously with TPD studies,[98] we can extract from this heat the enthalpy of formation of adsorbed methyl.

5.2 EXPERIMENTAL

Experiments were performed in a UHV chamber (base pressure $<2 \times 10^{-10}$ mbar) equipped with Auger electron spectroscopy (AES), low-energy electron diffraction (LEED), and SCAC. The apparatus and procedures for SCAC have been described previously.[34,35]

The sample used was a 1 μm thick Ni(111) single-crystal foil, supplied by Jacques Chevallier at Aarhus University in Denmark. The sample surface was cleaned by 1.25 kV Ar^+ ion sputtering to remove sulfur and other contaminants, annealing at 673 K in 1×10^{-7} mbar O_2(g) for 1 min to remove any surface carbon, and then annealing at 1050 K to remove oxygen.

This treatment was repeated until no impurities could be seen in AES, and the surface gave a very sharp Ni(111) LEED pattern. Before calorimetry, the clean Ni(111) sample was brought to thermal equilibrium with the calorimeter and then flash-heated to 1050 K (<2 s) to ensure a clean surface. Thereafter, the sample was brought back into contact with the pyroelectric detector, and within ~5 minutes, thermal equilibrium was re-established, after which the experiment was performed.

Calorimetry was performed by exposing the surface to a pulsed molecular beam of methyl iodide (CH_3I) gas. All gas pulses were 102 ms long and repeated every 5 s. The methyl iodide (Sigma-Aldrich, 99.5%) was outgassed by several freeze−pump−thaw cycles after being put into its reservoir on the vacuum chamber. The methyl iodide reservoir was shielded from light to prevent photolysis. Its purity was verified by mass spectrometry in the beam. The beam was produced by expanding ~1.8 mbar of methyl iodide through a microchannel array held at 299 ± 4 K (which defines the gas temperature) and then collimated through a series of five orifices that were cooled by liquid nitrogen as described previously.[34] Coverages are reported here in monolayers (ML), which we define by the number of nickel surface atoms in the Ni(111) surface (1.86×10^{19} Ni atoms/m^2). Methyl iodide typically contained ~0.0032 ML (8.89×10^{11} molecules) per pulse, with a beam diameter previously determined to be 4.36 mm.[34] In a given run, the dose per pulse was highly precise (<1% pulse-to-pulse variation, determined by the reproducibility of the chopper's beam-open time). The absolute accuracy of the measurement of the number of molecules per pulse was better than the measured 3% accuracy of the combined heat measurement, but how much better is difficult to determine. A more detailed description of the experimental principles and implementation of the molecular beam can be found elsewhere.[29,34] The methyl iodide molecular beam flux was measured by impinging the beam

onto a liquid-nitrogen-cooled quartz crystal microbalance (QCM), precovered with multilayers of methyl iodide to ensure unit sticking probability. Calibration of the QCM has been described previously.[34]

The heat released from the adsorption of each methyl iodide pulse was measured with a pyroelectric polymer ribbon gently pressed against the back side of the Ni(111) sample.[25,35] The sensitivity of this pyroelectric heat detector was calibrated after each experiment by depositing pulses of known energy into the sample using a 632.8 nm HeNe laser. The absolute accuracy of the calorimetric heats is estimated to be better than 3% (i.e., any systematic errors are less than 3%) for systems like those studied here, which have sticking probabilities above 0.8. This is based on comparisons to literature values for standard enthalpies of sublimation of the bulk solid when solids with known enthalpies are formed, specifically multilayers of adsorbed cyclohexene,[29] methanol,[30] methyl iodide,[99] and water[32] on Pt(111). For these molecules, the differences between the measured value and the estimated heat of sublimation based on the literature values for the standard enthalpies of phase transition (after correction for temperature differences using literature values for heat capacities) were −5.6%, −3.3%, <1%, and −5.1%, respectively. Note these differences from bulk sublimation values may be partially due to errors in the literature values or the possibility that we were not producing exactly the most stable phase at these low temperatures (possibly explaining the fact that our heats are lower than the literature values in the two cases where they differ most). However, these differences are all within the error bars (at 95% confidence) of the two values being compared, and therefore they do not have a statistically significant differences. Relative measurements (for example, differences in heat with changes in sample temperature or coverage) are generally much more accurate. By averaging multiple runs, the precision of energy calibration can be improved as much as desired.

Sticking probabilities were measured via the King and Wells method[36] simultaneously with calorimetric measurements. A mass spectrometer, without line-of-sight to the sample, measured the background pressure increase of methyl iodide, CH_3I (g) (m/z = 142) in the chamber. A gold flag was positioned in front of the sample and used to determine the mass spectrometry signal corresponding to 100 % reflection of methyl iodide (zero sticking). The sticking probability of methyl iodide is calculated by integrating the mass spectrometer signal measured from the increase in methyl iodide partial pressure above background when the molecular beam is pulsed onto the sample surface in comparison with the increase in methyl iodide partial pressure resulting when pulsed onto this inert gold flag. We report two types of sticking probabilities, long-term and short-term.[29] The long-term sticking probability, S_∞, is defined as the probability that a gas molecule strikes the Ni(111) surface, sticks, and remains on the surface until the next gas pulse starts, ~5 s later. Its value is used to calculate the adsorbate coverage remaining at the start of the next gas pulse. The short-term sticking probability, $S_{102\ ms}$, is defined as the probability that a gas molecule strikes the Ni(111) surface, sticks, and remains on the surface at least throughout the time of heat measurement on each pulse (i.e., the first 102 ms). Its value is used to calculate the number of moles of gas-phase reactant that contribute to the measured heat of adsorption, allowing us to report that value in kilojoules per mole adsorbed. These the two sticking probabilities equal each other hen there is no desorption between pulses.

The Ni(111) sample and entire calorimeter are cooled by a massive thermal reservoir. One cannot mount a thermocouple directly on the ultrathin single crystal used for calorimetry nor on the sample platen to which it is mounted (because it is transferred from its manipulator to the thermal reservoir during use). The sample temperature was monitored by two thermocouples

spot-welded to the two closest locations, onthe thermal reservoir and the holder of the pyroelectric detector. We averaged these two readings, which differed by ~10 K on average.

5.3 RESULTS

Sticking Probability. As described previously[29] and above, we measured two types of sticking probabilities: the short-term sticking probability, $S_{102\ ms}$, and the long-term sticking probability, S_∞. Figure 5.1 shows the average short-term and long-term sticking probabilities measured as a function of coverage at 100K and 160K. Even though dissociation is occurring at 160 K, the "CH_3I coverages" reported in Figure 5.1, and later figures in this paper, refer to the total amount of CH_3I_g that has adsorbed to the surface, irrespective of the final products produced.

For both temperatures, the sticking probabilities stay near unity independent of coverage, up to nearly saturation coverage at 160 K, indicating a precursor-mediated adsorption mechanism. This type of adsorption has been previously observed for numerous species on Pt(111) at low temperatures[100,37,90,32,30].

At 100K, the short-term and long-term sticking probability remain at unity for all coverages, in agreement with previous experiments.[97] Methyl iodide is thought to be molecularly adsorbed on Ni(111) at 100 K, based on a HREELS study performed by Mims and co-workers[97]. This behavior has also been observed on Pt(111)[101]. At 160K, CH3I is thought to dissociatively adsorb (see below), and multilayers are not expected to form.[97] This is confirmed by our results where the long-term sticking probability at 160 K starts at near unity but starts to rapidly decrease at 1/7 ML and reaches 0 at 0.17 ML. The short-term sticking also starts at unity, sharply decreases at a coverage of 1/7 ML, and reaches a steady-state value of 0.20 at the

saturation coverage of 0.17 ML, where 20% of the molecules in each pulse transiently adsorb on the surface (probably molecularly) but desorb again before the next pulse arrives.

Heat of Adsorption of Molecular Methyl Iodide at 100K: Intact Molecular Adsorption. In this paper, we define the term *heat of adsorption* as the negative of the differential standard molar enthalpy change for the adsorption reaction, ΔH_{ad}, with the gas and the Ni(111) being at the same temperature as the Ni(111) surface ("standard" here implies only that the gas is at 1 bar as a pure ideal gas). During our experiments, the temperature of the molecular beam was ~299 K, while the Ni(111) sample was held at cryogenic temperatures (e.g., T = 100 K). Thus, the measured heat is corrected by the small difference in the internal energy of the gas in the *directed* molecular beam at 299 K and in a Boltzmann distribution at the sample temperature (T), and then by RT to convert from internal energy change to enthalpy change for the adsorption reaction, as described elsewhere.[29]

The heat of adsorption of CH_3I on Ni(111) at 100K is shown in Figure 5.2. At these conditions, CH_3I adsorbs molecularly to the Ni(111) surface.[97] As seen in Figure 5.2, CH_3I initially adsorbs with a heat of 122 kJ/mol in the first gas pulse but drops to 101 kJ/mol by the second data point at 0.005 ML. The heat in the first data point is much higher than subsequent points, which we attribute to defect sites on the surface, probably step edges. As the coverage increases from the limit of low coverage to 0.15 ML, the heat of adsorption decreases linearly with coverage and, as shown in Figure 5.2, is well described by the best-fit straight line: $-\Delta H_{ad} = (102 - 115\ \theta)$ kJ/mol, where θ is coverage in ML, yielding an average (integral) heat of 93 kJ/mol in the first 0.15 ML. The initial defect data point was excluded for this fit and integral heat, so that they both correspond to terrace sites. Using the known enthalpy of formation of CH_3I_g at 100 K (14.6 kJ/mol)[102] and the initial enthalpy of adsorption of methyl iodide on Ni(111) found

by extrapolating the best-fit line for the initial 0.15 ML coverage to 0 coverage (102 kJ/mol), the standard enthalpy of formation of CH_3I_{ad} at 100 K in this low-coverage limit is found to be $\Delta H_f^0(CH_3I_{,ad}) = -87.4$ kJ/mol, again corresponding to terrace sites. The first layer saturation coverage of ~0.15 ML suggests that adsorbed molecular methyl iodide forms a ($\sqrt{7}$ x $\sqrt{7}$) structure, with an ideal coverage of 1/7 ML. This is the highest coverage where every molecule can sit in the same site and avoid occupation of sites that are separated by only two Ni-Ni bond distances (or less). (The van der Waals diameter of a methyl iodide molecule was estimated to be 0.54 nm from its liquid density of 2.28 g/cm^3, assuming close packed spheres in the liquid.)

Using the integral heat of adsorption for the first 0.15 ML (93.5 kJ/mol, based on the above equation and therefore excluding the contribution from defects) gives $\Delta H_f^0(CH_3I_{,ad}) = 78.9$ kJ/mol in this structure. This integral heat of adsorption on terrace sites is slightly larger than the corresponding value of 84 kJ/mol for a coverage of 0.25 ML on Pt(111), also at 100 K.[95] Periodic DFT methods underestimate this heat of adsorption of methyl iodide on Pt(111) by 48 to 68 kJ/mol, which is a common magnitude of error for this class of adsorbates.[14]

An abrupt ~40 kJ/mol decrease in adsorption enthalpy occurs as the first layer completes at ~0.15ML. This rapid decrease is well described by the best-fit line (400 – 2095 θ) kJ/mol over the narrow coverage range shown in Figure 5.2. This abrupt change in slope at approximately 0.15 ML suggests stronger adsorbate-adsorbate repulsions as they must pack more closely than in a ($\sqrt{7}$ x $\sqrt{7}$) overlayer (i.e., closer than 4th-nearest-neighbor sites).

At coverages greater than 0.17 ML, the heat of adsorption becomes nearly constant, implying that additional methyl iodide adsorbs on top of methyl iodide adsorbates, forming multilayers. Above 0.4 ML, the multilayer adsorption energy is 42.1 ± 1.1 kJ/mol, where the error bars reference the run-to-run standard deviation on the mean of the average heat at 0.4 to

0.8 ML. The bulk heat of sublimation at 100K may be estimated by using the heat of sublimation of bulk CH_3I(solid) measured at 207.7K of 40.2 kJ/mol.[103] After correcting this value to 100K by using its gas-phase heat capacity of ~4R[99] and the heat capacity of solid CH_3Br, since the heat capacity of solid CH_3I is not available, of 13 cal/(mol K),[104] the heat of sublimation of bulk methyl iodide at 100 K is estimated to be 37.9 kJ/mol. The multilayer heat measured here from 0.40 to 0.88 ML of 42.1 kJ/mol is 4.2 kJ/mol higher than this literature value. This difference may be due to methyl iodide still feeling some attraction to the underlying metallic Ni(111) surface in the very thin CH_3I film studied here.

Heat of Adsorption of Methyl Iodide at 160K: Dissociative Adsorption. Figure 5.3 shows the heat of adsorption versus coverage for methyl iodide dosed onto Ni(111) at 160K. At 160K, methyl iodide is expected to decompose to an adsorbed methyl and an adsorbed iodine atom without forming multilayers.[97]

The results of this experiment (Figure 5.3) show that initially, methyl iodide adsorbs with a heat of adsorption of 288 kJ/mol in the first data point but drops abruptly to 270 kJ/mol by the second data point (at 0.005 ML) to a much less rapidly changing value. Thus, this first data point is again attributed to defect sites on the surface, probably step sites. Since this first point may have some contribution from terrace sites as well, its heat of 288 kJ/mol is really a lower limit on the heat at step sites. As the coverage increases to 1/7 ML, the slow decrease in heat of adsorption is well described by a second order polynomial of $(271 - 2605\ \theta^2)$ kJ/mol, where θ is coverage in ML. Extrapolating back to zero coverage yields an initial heat of adsorption of 271 kJ/mol (attributed to terrace sites in the ideal absence of defects). The initial data point that was influenced by defects on the surfaces was excluded for this best-fit line. The integral heat of adsorption at 0.040 ML (based on this equation and therefore for terrace sites, specifically

excluding the contribution from defects) is 269.6 kJ/mol. After reaching a coverage of 1/7 ML, the heat of adsorption decreases much more rapidly, as the long-term sticking probability also approaches zero. This coverage of 1/7 ML suggests that coadsorbed methyl and iodine form a ($\sqrt{7}$ x $\sqrt{7}$) coadsorbed structure.

At temperatures lower than 160K (i.e. at 120K, 135K, 150K, and 155K), the decomposition reaction proceeded at a slower rate, such that the heat signal was broadened compared to the signal from laser pulses of the same duration. This indicates that the decomposition time constant for adsorbed methyl iodide becomes comparable to the beam pulse duration (102 ms) at this temperature. At 190K, we observed pulses of methane gas desorbing from the sample after each pulse of the methyl iodide beam (at low coverages), suggesting that the adsorbed methyl product of dissociative adsorption also abstracts hydrogen adatoms from the surface to make methane. This is consistent with TPD studies.[97] A similar effect has been observed at 270K, 300K, and 320K on Pt(111).[95] An experimental study using vibrational spectroscopy concluded that by 150K and above, adsorbed methyl on Ni(111) decomposes to an adsorbed methylidyne and two adsorbed hydrogen atoms.[96] At 160K, we did not observe such methane gas pulses being produced, suggesting that the decomposition of methyl to methylidyne and two adsorbed hydrogen atoms does not occur at a fast enough rate at 160K to evolve methane quickly enough to be observed, nor to affect the heat measurement.

5.4 DISCUSSION

Energetics of Adsorbed Methyl. We next analyze the measured enthalpy of the dissociative adsorption of methyl iodide on Ni(111) at 160 K (Figure 5.3) to determine the heat of formation of adsorbed methyl. We will use the integral heat determined from the polynomial fit (which

neglects the first, defect-related data point) up to a coverage of 0.040 ML. This is high enough to be confident it is not affected by defects but low enough to avoid significant adsorbate-adsorbate interactions. Note that this gives integral enthalpy of adsorption at 0.04 ML of -269.6 kJ/mol, which differs by only 1.4 kJ/mol from its zero-coverage limit (-271 kJ/mol). The thermodynamic cycle in Figure 5.4 shows how this value is used to extract the enthalpy of formation (ΔH_f^0) and Ni-C bond enthalpy for adsorbed methyl. The enthalpy of formation of adsorbed methyl is found by first starting on the left-hand side of the cycle with the elements in their standard states and following the pathway along the bottom half of the cycle. The enthalpy for the lower left-hand step is simply the enthalpy of formation of CH_3I_g, +14.6 kJ/mol.[102] The lower right-hand step is our integral enthalpy of adsorption measured by SCAC at 160 K from 0 to 0.04 ML of coverage, -269.6 kJ/mol. By adding the enthalpies of the lower left- and right-hand steps, a total value of -255 kJ/mol is found. This is the total enthalpy change in taking the elements in their standard states to methyl co-adsorbed with an iodine adatom, and therefore is equal to the sum of the enthalpy of formation of adsorbed methyl with the enthalpy of formation of adsorbed iodine.

The standard enthalpy of formation of atomic iodine on Ni(111), was previously determined with temperature-programmed desorption (TPD) measurements of the desorption rate of iodine adatoms to make iodine gas atoms.[98] However, this paper assumed a pre-exponential factor of desorption of 1.0×10^{10} s^{-1}, which is inconsistent with those determined experimentally for closely related systems.[69,105] To improve this value, we will use two methods to estimate the pre-exponential factor for desorption of this system. First, we estimate it to equal the pre-exponential factor for desorption of atomic iodine from Pt(111), previously determined to be 4.8×10^{13} s^{-1} by analysis of many TPD experiments.[105] Second, we estimate the prefactor by

the method of Campbell et al.,[69] using the reported entropy of gas-phase iodine atoms. We use for this the entropy of I_{gas} at 990K,[106] which is the temperature that iodine adatoms at 0.04 ML coverage reach their maximum desorption rate in that TPD experiment.[98] This gives the pre-exponential factor of desorption to be 3.9×10^{14} s^{-1}. Using the standard first-order Redhead equation[89], the activation energy for desorption for iodine adatoms from Ni(111) was estimated from the reported TPD peak temperature (990 K) and heating rate (3 K/s) using both of these prefactor estimates. These give values of 278 and 294.9 kJ/mol, respectively. Averaging these two values results in a desorption activation energy (E_{des}) of 286±9 kJ/mol, which we will use for the analysis below. (For comparison, the paper with the TPD experiment reported a desorption energy of 214 kJ/mol in the limit of low coverage based on a much lower prefactor.[98]) This value is then converted into an adsorption enthalpy by adding ½ RT to the positive desorption activation energy and changing sign,[70] resulting in an adsorption enthalpy of -291 kJ/mol. Adding this to the standard enthalpy of formation of I_g (107 kJ/mol [106]), the standard enthalpy of formation of iodine on Ni(111), ΔH_f^0 (I_{ad}), was thus estimated to be -184 kJ/mol.

Subtracting this value of ΔH_f^0 (I_{ad}) from the above value of -255 kJ/mol (the total enthalpy change in taking the elements in their standard states to methyl co-adsorbed with an iodine adatom) results in the enthalpy of formation of adsorbed methyl: ΔH_f^0 ($CH_{3,ad}$) = -71 kJ/mol.

By following the upper pathway of this thermodynamic cycle (Figure 5.4) the C-Pt(111) bond enthalpy of adsorbed methyl can be extracted. Again we start on the left-hand side of the cycle with the elements in their standard states, but now follow the upper left-hand step that takes the elements in their standard states to gas phase methyl radical and adsorbed iodine. The enthalpy for this step is determined by adding the known enthalpy of formation of gas phase

methyl (+147 kJ/mol)[107] and adsorbed iodine (-184 kJ/mol, see above) giving an enthalpy for this step of -37 kJ/mol.

The upper right-hand step in the pathway is the adsorption of gas phase methyl onto the Ni(111) surface already containing an adsorbed iodine. The enthalpy for this step is found by subtracting the upper left-hand step from -255 kJ/mol, giving an enthalpy of -218 kJ/mol. Therefore, the H_3C-Ni(111) bond enthalpy is +218 kJ/mol, based on our heat measurement averaged over the coverage range 0 – 0.04 ML at 160 K and other known thermodynamic data. The corresponding C-Ni bond energy of adsorbed methyl on Ni(111) is found by subtracting RT from this bond enthalpy, giving +216 kJ/mol.

It is expected that these energetics for adsorbed methyl determined here at 0.04 ML are not strongly influenced by the presence of the equal coverage of I_{ad}. This is easily seen by the fact that the integral heat at 0.04 ML from Figure 5.3 has decreased by only 2 kJ/mol from its zero-coverage limit. We certainly expect repulsive interactions between coadsorbed methyl and I, since they have been reported based on both experiments and DFT calculations between I_{ad} on Pt(111) and both co-adsorbed t-butyl[108] and CH_2[109]. These repulsions are however reduced to only a few kJ/mol at 0.04 ML and 160 K, probably because the adsorbates diffuse apart to minimize repulsions. This requires only that either methyl or I_{ad} be sufficiently mobile at 160 K, which is expected based on general trends in adsorbate diffusion rates for related systems. Consistent with this, it has been shown that the coadsorption of iodine does not strongly perturb the energies of the methyl groups at this same coverage on Pt(111).[99]

The decrease in heat of adsorption versus coverage in Figure 5.3 resembles a sigmoidal shape that has been truncated halfway to completion. Such a sigmoidal shape is expected when adsorbates have repulsions but are mobile.[110] This truncation could occur due to the decrease in

sticking probability to below 0.2 (see Figure 5.1), at which point we stopped measuring, since heat measurements have large error bars at low sticking probability (resulting from the large relative errors in sticking probability). This decrease in sticking probability could be due the lower exothermic driving force (lower heat of adsorption, Figure 5.3) that accompanies adsorbate-adsorbate repulsions at higher coverage.

The error in the heat of adsorption in Figure 5.3 could be as large as 3% (8 kJ/mol), and that for I_{ad} could be 10 kJ/mol, so the error on the estimated heat of formation of adsorbed methyl above could be as large as 13 kJ/mol. (We neglect here the much smaller error bars on gas-phase thermodynamic values.)

Comparison to DFT Calculations. These heats of molecular and dissociative adsorption of CH_3I, heats of formation of CH_3I_{ad}, $CH_{3,ad}$, and I_{ad}, and bond strength of methyl to Ni(111) measured in this work may be used as benchmarks for comparison to theoretical calculations.

Table 5.1 lists the measured bond energy of adsorbed methyl found in Figure 5.4 at 0.040 ML (+216 kJ/mol) and, for comparison, several calculated bond energies from various theoretical and DFT methods. The experimental bond energy is 18 to 98 kJ/mol higher than the results obtained from DFT with periodic boundary conditions and various common functionals, which are generally thought to be more modern and more accurate than cluster-based approaches. This suggests that these methods systematically underestimate the strength of H_3C-Ni(111) bonding by amounts from 18 to 98 kJ/mol. These differences are much larger than expected zero-point energy and heat-capacity corrections, which we did not include in this comparison. The calorimetric results have coadsorbed iodine atoms, which are expected to very weakly destabilize the methyl groups if they have any lateral interactions at this low coverage

(see above). Any destabilization would make the discrepancy between experimental calorimetry and these periodic DFT results even larger.

Comparison to Pt(111): Why Ni is a Better Catalyst for Hydrogenolysis than Pt.

Previous calorimetry experiments[99] have determined that methyl has a bond energy of 194 kJ/mol to the Pt(111) surface at 0.04 ML (as corrected slightly by Silbaugh and Campbell[15]). This is slightly weaker than the current values to the Ni(111) surface of 216 kJ/mol at the same coverage of 0.04 ML (0.04 ML of both methyl and iodine atoms on both metals). The sigma bond energy of adsorbed methyl is therefore ~22 kJ/mol stronger to Ni(111) than Pt(111). This stronger bonding of alkyls to Ni than Pt helps explain the well-known much higher activity of Ni catalysts than Pt for C-C bond-breaking reactions such as hydrogenolysis.[111,112] That is because a metal should have a lower activation barrier for cleaving a C-C bond in an adsorbed hydrocarbon if the resulting two fragments bond more strongly to that metal, according to the Brønsted–Evans–Polanyi (BEP) relation. Indeed, this new result resolves a confusing aspect of the earlier SCAC results that Ni-C bonds are weaker than Pt-C bonds, since that is inconsistent with the trend in hydrogenolysis activity. Specifically, previous work from King's group[70] had estimated the single metal-carbon sigma bond energies of a C atom bonded to three Ni atoms on Ni(100) and three Pt atoms in a 3-fold hollow site of Pt(111) using SCAC measurements of the heats of adsorption of ethylene to make methylidyne on both Ni(111) and ethylidyne on Pt(111) surfaces. They reported a Ni-C bond energy of 205 kJ/mol in adsorbed methylidyne and a Pt-C bond energy of 237 kJ/mol in adsorbed ethylidyne. This would suggest that Pt should be a better hydrogenolysis catalysis, in contrast to experimental trends.[70] However, this C-Pt bond energy measurement for ethylidyne on Pt(111) was more recently corrected by Silbaugh and Campbell[15] from the original value of 237 kJ/mol to a more accurate 168 kJ/mol due to a calibration error in

the original paper, with methylidyne now binding more strongly to Ni(111) than ethylidyne to Pt(111), the opposite of that originally reported. This corrected value is consistent with our new results above and with the trend in hydrogenolysis activities. In contrast to these experimental results, DFT using the same functional and same coverage give a bond energy of methyl to Ni(111) that is 5 to 57 kJ/mol weaker than to Pt(111) (176 vs 181 kJ/mol by PBE[113], 140 vs 197 kJ/mol by PW91[26,114], and 128 vs 163 by RPBE[36, 45]), inconsistent with their relative hydogenolysis activities.

Energetics of the Activation of Methane on Ni(111), and Comparison to Pt(111).

The thermodynamics of the dry reforming and steam reforming of methane on Ni has been extensively studied using theoretical and experimental methods.[114,115,125–130,117–124] These studies show that the rate-controlling step of both reactions under certain conditions is the dissociation of methane to an adsorbed methyl and a hydrogen adatom:

$$CH_{4,g} \rightarrow CH_{3,ad} + H_{ad}. \quad (5)$$

With the enthalpy of formation of adsorbed methyl on Ni(111) measured in this work (-71 kJ/mol), the known heat of formation of methane gas (-74.6 kJ/mol)[131], and the previously measured heat of formation of hydrogen adatoms on Ni(111) (-47 kJ/mol)[132], the total change in enthalpy of this reaction is determined to be -43 kJ/mol on Ni(111). This is 29 kJ/mol more exothermic than we found on Pt(111).[99]

Given that the dissociative chemisorption of methane is more exothermic on Ni(111) than on Pt(111), one would expect the barrier for this reaction to be smaller on Ni(111) based on the BEP relation. DFT calculations, however, find the barrier to be larger on Ni(111), in spite of finding the reaction to be more exothermic than on Pt(111). For example, recent PBE-based studies at 1/9 ML coverage find zero-point energy corrected barriers of 84.5 and 67.3 kJ/mol on

Ni(111) and Pt(111), respectively.[133] Energy-resolved UHV molecular beam experiments are consistent with this, finding that, at the same collision energy and similar surface temperatures, methane is more reactive on Pt(111) than on Ni(111).[134] Fortunately, a closer consideration of the transition state for dissociation shows that there is no contradiction. The transition states for the dissociation of methane on both Ni(111) and Pt(111) are very similar, with the carbon atom roughly over the top site, the three unreactive C-H bonds angled away from the surface, and the reactive C-H bond angled towards a hollow or bridge site.[113,120,135–139] The barrier height varies little with the orientation of the reactive bond.[113] Using the ¼ ML PBE results reported in Nave et al.[113] for methyl adsorbed at the top site and H adsorbed in an fcc hollow, the *initial* product energy according to DFT is actually 28 kJ/mol lower in energy on Pt(111) than on Ni(111). This is consistent with the lower activation energy and higher molecular beam reactivity on Pt(111) relative to Ni(111). While this top site is the minimum energy binding site for methyl on Pt(111)[113,137], this is not the case on Ni(111) (see Table 5.1), where the fcc hollow is more stable by 32 kJ/mol.[113] Thus, quickly *after* dissociation on Ni(111), the methyl fragment migrates to this hollow site (without any barrier). This lower-energy configuration is the *final* product state relevant to the heat of adsorption measurements reported in this paper. Again using the numbers in Nave et al.[113], DFT results find that the dissociative chemisorption of methane is about 4 kJ/mol more exothermic on Ni(111) than on Pt(111). This is due to PBE getting H_{ad} to be 9 kJ/mol more stable on Ni(111), while methyl itself is still found by PBE to be less stable on Ni(111) than on Pt(111), by 5 kJ/mol. A full DFT-based explanation of the fact that methane dissociation is slightly faster on Pt(111) than on Ni(111) according to molecular beam experiments is presented elsewhere[62]. This explanation is qualitatively consistent with the current results, but inconsistent with standard BEP relations, which state that activation energy

for an elementary step decreases with decreasing reaction enthalpy for that elementary step (unless one considers dissociation to the top-site for methyl on Ni(111) as a true elementary step in this respect). The top site for methyl on Ni(111) is not the true final state for the *full* elementary step where methane dissociates. In spite of the fact that the BEP relation breaks down for methane dissociation rates on Ni versus Pt, it should still be expected to usually be true, and indeed it seems to be valid for C-C bond cleavage reactions, explaining faster hydrogenolysis catalysis on Ni versus Pt (see above).

Steam reforming and partial oxidation of methane often have methane dissociation as a rate-controlling step,[140] so this dissociation activation energy of methane and the related thermodynamic stability of adsorbed methyl certainly must have an impact the relative activity of Ni versus Pt catalysts for these reactions. There is no consensus in the literature about which metal has the highest turnover frequency, presumably due to the fact that catalytic rates are affected in larger magnitude by other details of the catalyst material and reaction conditions.

5.5 CONCLUSIONS

At 100K, methyl iodide adsorbs molecularly on Ni(111), with a decreasing heat of adsorption in the first 1/7 ML well fit by (102 - 115 θ) kJ/mol. From approximately 0.15 ML to 0.17 ML, the heat of adsorption drops much more rapidly. This drop just above 1/7 ML is consistent with the saturation of a ($\sqrt{7}$ x $\sqrt{7}$) structure, and much stronger adsorbate-adsorbate repulsions when the molecules pack more closely than this 4th-nearest-neighbor structure. Above 0.17 ML, methyl iodide adsorbs with a nearly constant heat of adsorption of 42.1 kJ/mol, near the value for multilayer solid methyl iodide.

At 160K, methyl iodide dissociatively adsorbs on the Ni(111) surface to form adsorbed methyl and an iodine adatom. The adsorption heat in the first 1/7 ML is well fit by (271 – 2605 θ^2) kJ/mol, after which the long-term sticking probability approaches zero. Using known enthalpies of formation of gas-phase species and iodine adatoms on Ni(111), we find the standard enthalpy of formation of adsorbed methyl to be $\Delta H_f^0[CH_{3,ad}]$ = -71 kJ/mol and its C-Ni bond enthalpy to be 218 kJ/mol at a coverage of 0.04 ML.

The measured energetics were compared to DFT and cluster calculations from many different studies. These DFT calculations routinely underestimate this bond energy. When compared to previous calorimetric measurements, $CH_{3,ad}$ binds 21 kJ/mol more strongly to Ni(111) than to Pt(111) at a coverage of 0.04 ML. This helps explain why Ni catalysts have a higher activity than Pt for C-C bond-breaking reactions like hydrogenolysis, since the fragments that result from C-C cleavage bind more strongly to Ni than to Pt, so its activation energy should be lower. The results are also consistent with the relative rates of Ni versus Pt catalysts in methane activation and in steam reforming and partial oxidation of methane.

5.6 TABLES AND FIGURES

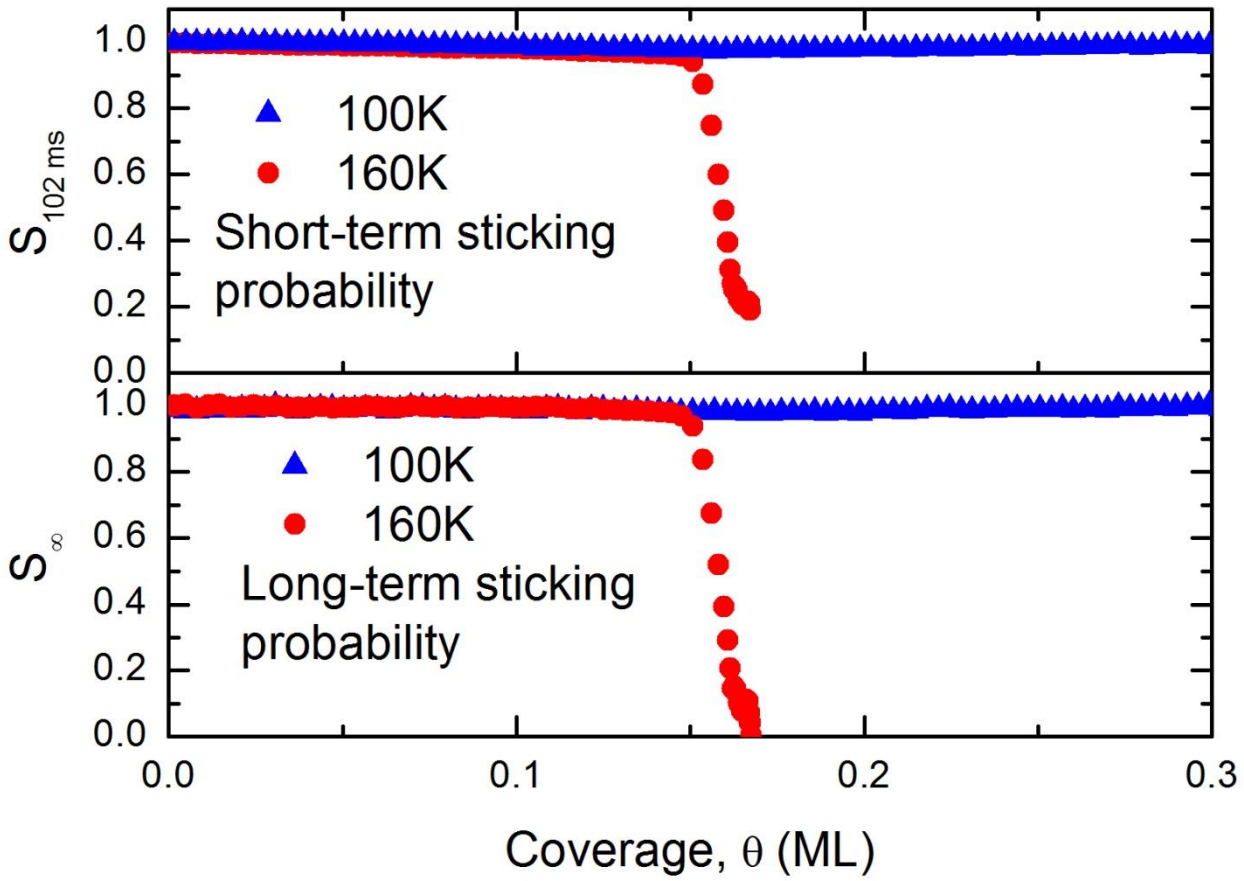

Figure 5.1. The average short-term and long-term sticking probabilities of CH_3I versus the CH_3I coverage on Ni(111) at 100K and 160K. Coverage is defined as the number of CH_3I molecules that adsorb to the surface irreversibly (irrespective of the resulting products), normalized by one monolayer (ML), defined to equal the number of nickel surface atoms in the Ni(111) surface. At 160K, "coverage" by one adsorbed CH_3I molecule really refers to one $CH_{3,ad}$ plus one I_{ad}, whereas at 100 K it is CH_3I_{ad}.

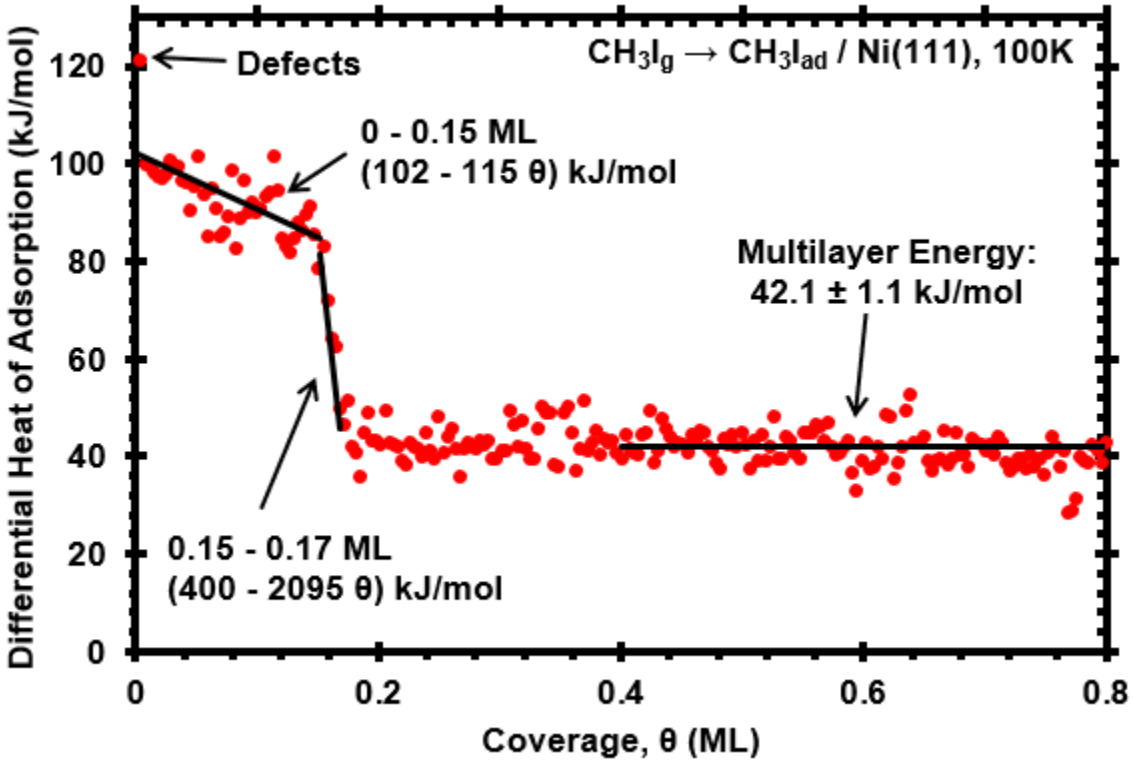

Figure 5.2. Differential heat of adsorption of molecularly adsorbing CH_3I on Ni(111) at 100K as a function of CH_3I_{ad} coverage. Each data point represents a pulse of ~0.0032 ML of CH_3I gas and is the result of averaging eight experiments.

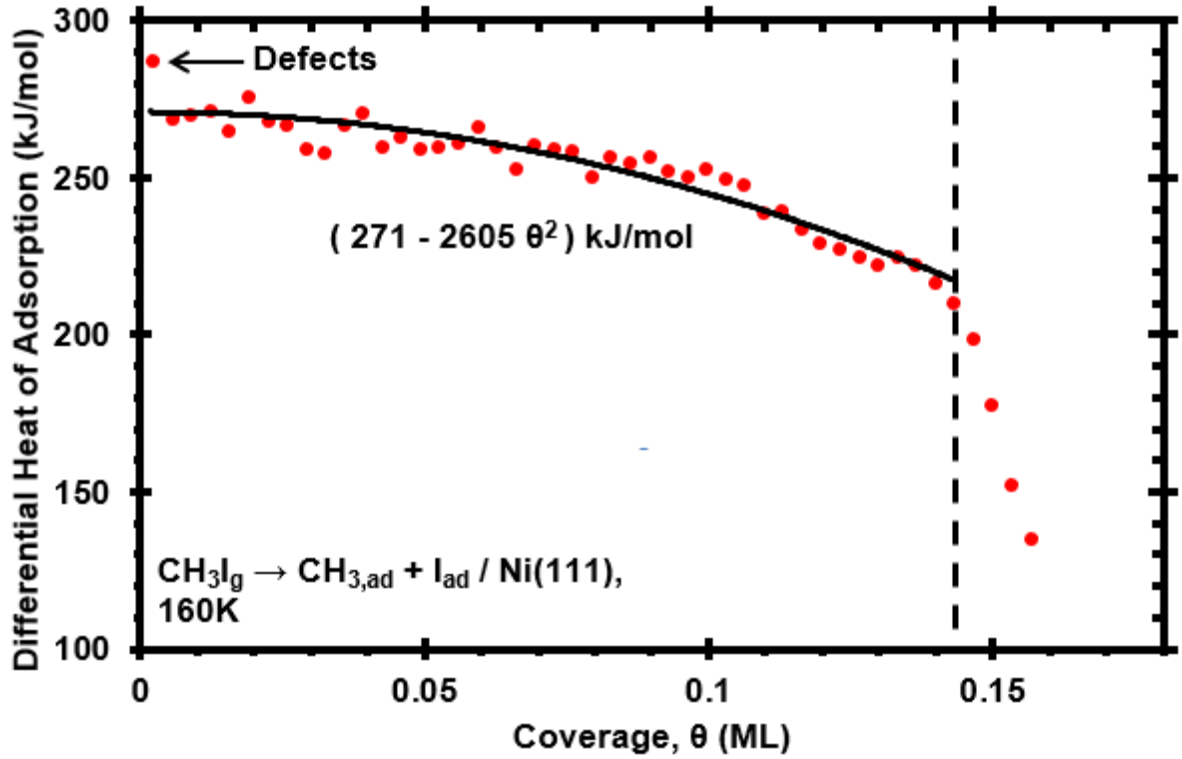

Figure 5.3. Differential heat of dissociative adsorption of CH_3I to adsorbed methyl and an adsorbed iodine atom on Ni(111) at 160K as a function of dissociated CH_3I coverage. Each data point represents a pulse of ~0.0032 ML of CH_3I gas and is the average of nine experimental runs. The vertical dashed line indicates a coverage of 1/7 ML, and the equation is the best fit of that functional form to the data in the range below 1/7 ML.

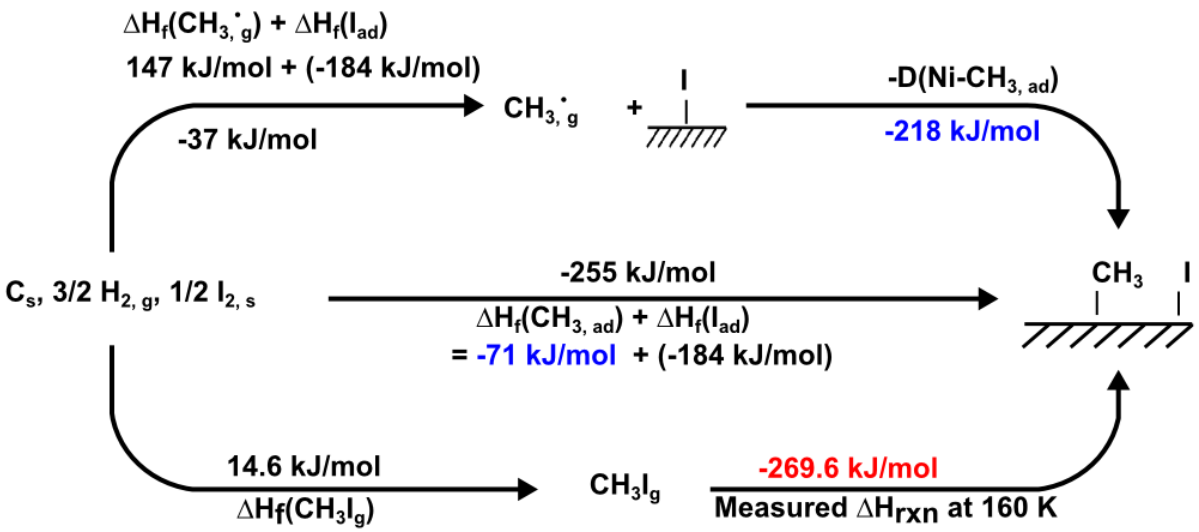

Figure 5.4. The thermodynamic cycle used in calculating the bond enthalpy and heat of formation of adsorbed methyl to the Ni(111) surface. Here, -269.6 kJ/mol is the integral enthalpy of reaction of CH_3I decomposition to an adsorbed methyl and an adsorbed iodine atom measured at 160K for the first 0.040 ML coverage. The other enthalpies are taken from the literature as described in the text.

Table 5.1. Comparison of Present Calorimetric Bond Energies of Methyl to the Ni(111) Surface with Calculated Values Using DFT with Periodic Boundary Conditions (top) and Cluster Methods (bottom).

Coverage or Cluster Size	Functional or Method	Site	Bond energy (kJ/mol)	Ref
0.04 ML with 0.04 ML I_{ad}	Calorimetry		216.	This Paper
Periodic DFT Methods				
1/9 ML	PW-91	Top	167.5	[141]
		Bridge	178.7	
		FCC Hollow	198.3	
		HCP Hollow	194.5	
¼ ML	PW-91	Top	117.7	[114]
		Bridge	132.2	
		FCC Hollow	140.9	
		HCP Hollow	142.8	
1/6 ML	PBE	FCC Hollow	177.5	[142]
¼ ML		Bridge	149.6	
¼ ML		FCC Hollow	174.6	
¼ ML		HCP Hollow	171.7	
¼ ML	PBE	Top	143.9	[113]
¼ ML		Bridge	155.2	
¼ ML		FCC Hollow	175.6	
¼ ML		HCP Hollow	172.5	
¼ ML	PBE	HCP Hollow	164	[143]
¼ ML	PBE	Top	155.6	[144]
¼ ML		Bridge	164.4	
¼ ML		FCC Hollow	178.7	
¼ ML		HCP Hollow	177.0	
¼ ML	RPBE	HCP Hollow	128.3	[116]
¼ ML	RPBE-D3	HCP Hollow	183.3	
Cluster-Based DFT Methods				
3 Atoms	Bond prepared cluster calculations	Hollow	174-205	[145]
1 Atom	Bond prepared cluster calculations	Top	188	[146]
10 Atoms		Top	159	
4 Atoms		Hollow	207.9	
20 Atoms		Hollow	197.5	
22 Atoms		Hollow	192.5	
7 Atoms	Quasi Relativistic Calculations based on DFT-ADF	Top	97	[147]

7 Atoms		Bridge	61	
7 Atoms		Hollow	64	
13 Atoms		Top	179	
13 Atoms		Bridge	152	
13 Atoms		Hollow	143	
28 Atoms	Ab initio valence orbital CI calculations of clusters	Top	141.8	[148]
28 Atoms		Bridge	148.5	
28 Atoms		FCC Hollow	161.9	
28 Atoms		HCP Hollow	161.9	

Chapter 6. THE ENERGETICS OF ADSORBED METHANOL AND METHOXY ON NI(111)

Chapter Abstract

The heat of adsorption of methanol molecularly adsorbed on clean Ni(111) and dissociatively adsorbed on oxygen-precovered Ni(111) were measured by Single-Crystal Adsorption Calorimetry (SCAC). The dissociative adsorption of methanol on oxygen-precovered Ni(111) produces adsorbed methoxy and hydroxyl, resulting in an integral heat of adsorption of -70. kJ/mol at a coverage of 0.25 ML. From this, the heat of formation of this adsorbed methoxy and the dissociation enthalpy of its bond to Ni(111) are estimated to be 233 kJ/mol and 250. kJ/mol. Analyzing previously measured bond enthalpies of monodentate formate and hydroxyl to Ni(111), we find a linear trend with a slope of 1 between of the bond enthalpies of oxygenates to the Ni(111) surface and their corresponding gas-phase hydrogen-ligand bond dissociation enthalpies. We also compare our experimentally measured energetics for adsorbed methanol and adsorbed methoxy with density functional theory (DFT) calculations with periodic boundry conditions from previous literature. These energetic values and trends help clarify selectivity, reaction rate, and activity differences between metal surfaces in reactions involving adsorbed oxygenates.

6.1 INTRODUCTION

Surface methoxy is a key intermediate in many important catalytic reactions on Ni and other transition metal surfaces, such as steam reforming reactions, methanol synthesis, and direct

alcohol fuel cell reactions. Critical catalytic properties, such as the activity, reaction rate, and selectivity, are determined by the energetics of adsorbed intermediates, and they are therefore important to know accurately. The adsorption and decomposition reactions of methanol on Ni(111) have been studied previously.[149–158] However, little is known about the energetics of adsorbed methanol and methoxy on this or any other Ni surfaces. So far, the heat of formation and bond enthalpy of adsorbed methoxy have been measured on only one metal surface, namely Pt(111), using Single-Crystal Adsorption Calorimetry (SCAC) by this group.[30] Here, we report the first calorimetric measurements of the energetics of adsorbed methanol and methoxy on the Ni(111) surface. These energetics are compared to adsorbed methoxy on Pt(111), helping clarify the different catalytic activities for these two transition metals in catalytic reactions involving methoxy intermediates. These experimental results also provide valuable benchmarks for validating the energy accuracy of density functional theory (DFT) methods.

In addition, we compare here the energetics of adsorbed hydroxyl and formate on Ni(111), reported by our group previously,[66,159] with the measurement of adsorbed methoxy here, and find the bond dissociation enthalpies of these three adsorbed oxygenates (hydroxyl, formate, and methoxy) to Ni(111) linearly track their corresponding gas-phase hydrogen-ligand bond dissociation enthalpies with a slope of 1. The same trend with unit slope was also discovered for these same three oxygenates on Pt(111) by this group previously.[160] The difference is that these three oxygenates bind to Ni(111) ~69 kJ/mol more strongly than Pt(111). These findings thus provide a semiempirical method to predict the bond enthalpies and heats of formation of adsorbed oxygenates on these metal surfaces.

Previous studies have found that methanol adsorbs molecularly on Ni(111) below approximately 140K.[153,158] Adsorbed methoxy has been observed on Ni(111) after dosing high

coverages (possibly multilayers) of methanol at temperatures lower than 140K and subsequently heating to 160-240K.[151–153,156–158] Although not known from the literature, we show below that when methanol is dosed to Ni(111) precovered with oxygen adatoms, it dissociates to produce adsorbed methoxy plus –OH in the temperature range 100 to 190 K. This is based on the similarities of heats of reaction and sticking probabilities versus oxygen coverage to prior results for Pt(111), where this reaction is known to occur at similar temperatures.[159]

6.2 EXPERIMENTAL

Experiments were performed in a UHV chamber (base pressure $<2 \times 10^{-10}$ mbar) designed for SCAC. It is equipped with X-ray photoelectron spectroscopy (XPS), Auger electron spectroscopy (AES), low-energy ion scattering spectroscopy (LEIS), and low-energy electron diffraction (LEED). The apparatus and procedures for SCAC have been described in extensive detail previously.[29,34,35] To summarize, the Ni(111) samples used in these experiments are 1 μm thick single-crystal foils and were provided by Jacques Chevallier at Aarhus University. The surface was cleaned by cycles of Ar^+ ion sputtering and annealing to 1120 K. The atomic oxygen-precovered surface was prepared by exposing the clean Ni(111) surface to O_2 at cryogenic temperatures (100-190 K) as described in the literature.[161–163] The heats of adsorption and sticking probability were measured simultaneously as a pulsed molecular beam of methanol was dosed onto the Ni surface. The molecular beam was created by expanding ~2 mbar of methanol through a glass capillary array and collimated through a series of five orifices that are cooled with liquid nitrogen, and then chopped into 102 ms pulses. The heats were measured with a pyroelectric ribbon gently pressed on the backside of the Ni crystal. The short-

term and long-term sticking probabilities were measured with a quadrupole mass spectrometer (QMS) using the King and Wells method.[36]

In this paper, we report coverages in monolayers (ML), which are defined as the number of methanol molecules that adsorb to the surface irreversibly, normalized by the number of nickel surface atoms in the Ni(111) surface (1.86×10^{15} Ni atoms/cm^2). A typical molecular beam flux gives ~0.015 ML (~2.8×10^{12} molecules/pulse).

6.3 RESULTS

Heat of Molecular Adsorption on Clean Ni(111). In this paper, we define the term *heat of adsorption* as the negative of the differential standard molar enthalpy change for the adsorption reaction, $-\Delta H_{ad}$, with the gas and the metal surface being at the same temperature as the metal surface. ("Standard" here implies only that the gas is at 1 bar as a pure ideal gas.) As described previously, this requires a small enthalpy correction on the measured heat since the gas molecule's enthalpy at this temperature is slightly different from the actual experimental molecular beam conditions.[15]

According to the literature,[150,153] methanol molecularly adsorbs on Ni(111) below 160 K and forms multilayers below 140 K. Figure 6.1 shows the heat of adsorption of methanol on Ni(111) at 100K. Initially, methanol adsorbs molecularly with a heat of adsorption of 63.2 ± 0.8 kJ/mol in the limit of low coverage. As coverage increases to 0.4 ML, the heat of adsorption decreases in two linear segments. For the first 0.3 ML, the heat of adsorption is well described by a best fit line (63.2 - 23.9 θ) kJ/mol, where θ is coverage, in monolayers, yielding an average heat of 59.6 kJ/mol. The average (or integral) heat of adsorption up to ¼ ML is 60.2 kJ/mol. Combined with the standard heat of formation of methanol gas of -202 kJ/mol,[164] this gives the

standard heat of formation of adsorbed methanol on Ni(111) to be -262 kJ/mol. After 0.30 ML and up to 0.4 ML, the heats of adsorption decrease much more rapidly and are well described by the best-fit line (99.3 - 142.7 θ) kJ/mol. The sticking probability of methanol is always close to unity at all methanol coverages at 100 K, see Figure 6.6.

These changes in the heat of adsorption could be the result of a model suggested by scanning tunneling microscopy (STM) and DFT studies of methanol on Cu(111), Au(111), and Pt(111).[165,166,167] On these surfaces at cryogenic temperatures, the methanol molecules bond to the surface through their oxygen atom but with the methyl group near the surface, forming hydrogen bonds with their neighbors. This results in clusters of hydrogen-bonded hexamers at low coverages and long hydrogen-bonded chains at higher coverages with the methyl groups pointing outwards. One STM study found that these methanol chains get closer to one another as coverage increases.[165] The decrease in heat with coverage in Figure 6.1 may be due to dipole-dipole and steric repulsions between chains and hexamers as they are forced closer together.

At coverages greater than 0.4 ML, the heat of adsorption becomes nearly constant, implying that additional methanol adsorbs on top of methanol adsorbates, forming multilayers. Above 1.0 ML, the multilayer adsorption energy is 44.0 ± 0.6 kJ/mol. This value is inagreement with the heat of sublimation of bulk methanol (solid) at 100K, 45.3 kJ/mol, calculated from bulk thermodynamic data,[168,169] and with results from a detailed TPD study of multilayer methanol on Au(111) that employed leading edge analysis to determine a sublimation enthalpy of 42.1 – 44.6 kJ/mol[170] (after correction using bulk solid and gas phase heat capacities from 150K down to 100K).

Previous literature reported that exposing clean Ni(111) surface to a high coverage of methanol at a temperature lower than 140K and subsequent heating to 180 – 240 K leads to

adsorbed methoxy and hydrogen.[153,158] Amemiya and co-workers determined that methoxy could also be produced on Ni(111) by directly dosing methanol at 200K.[158] Thus, we performed SCAC experiments of methanol adsorption on clean Ni(111) at temperatures ranging from 180 – 300 K in hopes to produce adsorbed methoxy. However, we observed an initial heat of adsorption that was very similar to that for molecular adsorption of methanol on Ni(111) at 100 K (~63 kJ/mol) and a maximum surface coverage of adsorbed methanol (regardless the products on surface) of ≤ 0.04 ML at 180 to 300 K. It indicates that methanol transiently adsorbs on Ni(111) at these temperatures, but then desorbs again before the next methanol pulse. Thus, we were unable to dissociate the methanol on clean Ni(111). Is at least some of the prior studies mentioned above, it was possible that X-ray, other photon or electron beam damage may have facilitated dissociation.

Heat of Dissociative Adsorption on Oxygen-Precovered Ni(111). After predosing the Ni(111) surface with oxygen adatoms(by the dissociative adsorption of O_2 gas), the heat of adsorption of methanol at temperatures from 100 K to 190 K is considerably higher than the heat of molecular adsorption (~25 kJ/mol higher initially), and the resulting coverage of permanently adsorbed methanol is much higher. According to the studies of methanol dissociatively adsorbing on O-precovered Pt(111)[30] and water dissociatively adsorbed on O-precovered Ni(111)[159], we thus conclude that Reaction (1) occurs to produce adsorbed methoxy and hydroxyl, as:

$$CH_3OH_g + O_{ad} \rightarrow CH_3O_{ad} + OH_{ad} \quad (1)$$

Figure 6.2 shows the heat of adsorption of methanol on oxygen-precovered Ni(111) at 100 K with 0.25 ML of O_{ad} (in red) and a low coverage of O_{ad} (in orange). The heat of adsorption of molecular methanol on clean Ni(111) at 100 K is also reproduced from Figure 6.1

(in blue), for comparison. When the Ni(111) surface is covered with 0.25 ML of O_{ad}, a significantly higher heat of adsorption is observed, ~88 kJ/mol in the limit of low coverage. This heat then decreases linearly with increasing coverage of adsorbed methanol. After ~0.25 ML, the heat of adsorption is the same as that of methanol molecularly adsorbed on clean, O-free Ni(111), suggesting that methanol molecularly adsorbs from 0.25 ML until saturation at ~0.3 ML. In the case of the low coverage of O_{ad}, the heat of adsorption of methanol starts high, close to the curve for 0.25 ML O_{ad}, and more quickly decreases to the same heat as that of molecular adsorption on O-free Ni(111) (the blue curve) at ~0.1 ML. This shows that the coverage dependence of the heats of adsorption of methanol on O-precovered Ni(111) significantly depends on the precoverage of O adatoms, again implying that methanol reacts with O adatoms to form adsorbed methoxy and hydroxyl until all the O_{ad} is consumed. This same reaction was observed on Pt(111) with similar heats.[30]

The heats of adsorption observed at low coverage on the 0.25 ML O_{ad} surface are much higher than what would be expected for simple molecular adsorption. On both Pt(111) and Ni(111), water molecularly coadsorbed with oxygen adatoms releases only ~3 kJ/mol more heat compared to the molecular adsorption of water on clean surfaces.[32,159] We would expect a similar marginal change in heat if methanol molecularly coadsorbed with O_{ad}. In contrast, here the heat is ~25 kJ/mol higher for methanol adsorbed on the O-precovered surface at the limit of low coverage compared to the clean Ni(111), which indicates dissociative adsorption on O-precovered Ni(111). We attribute this much higher heat to methanol reacting with O_{ad} to form adsorbed methoxy and hydroxyl following Reaction (1). This reaction has also been unambiguously observed on O-precovered Pt(111).[30,171] We expect Reaction (1) to proceed until all oxygen is titrated off the surface, after which, methanol continues to adsorb molecularly and

releases the same heat as on clean Ni(111). For the 0.25 ML O_{ad} precovered surface, this reaction completes at ~0.25 ML as expected; for the low coverage experiments, this higher-heat reaction completes at ~0.1 ML (Figure 6.2).

Figure 6.3 shows the more direct comparison for methanol adsorbed on Ni(111) and Pt(111), dissociatively and molecularly. The red curves show SCAC results of methanol on both Ni(111) and Pt(111) predosed with 0.25 ML O_{ad} and the blue curves show SCAC results of methanol on clean Ni(111) and Pt(111). The two curves shown for Pt(111) were published previously[30] and reproduced here for comparison. On Pt(111), an identical reaction scheme to that proposed here for Ni(111) is known to occur.[30] On clean Ni(111) at 155 K and clean Pt(111) at 150 K, methanol adsorbs molecularly and only forms a single layer, and the heats are consistent with the adsorption on clean surfaces at 100 K.[150,171] For the 0.25 ML O-precovered surfaces, methanol reacts with O_{ad} forming adsorbed methoxy and hydroxyl until the 0.25 ML of O_{ad} is titrated. After that, methanol continues to adsorb molecularly until the single layer is finished, releasing the same heat as observed on the clean surfaces at the same coverage. On the O-precovered surface on Ni(111), the heat of adsorption is initially 87 kJ/mol at the limit of low coverage. It decreases linearly until ~0.25 ML and is well described by the linear fit (85.1 – 117.2 θ) kJ/mol. The vertical dashed line at 0.25 ML marks the expected coverage of O_{ad} and represents the point where Reaction (1) completes. After this vertical dashed line, it is clearly observed that the heat of adsorption of methanol on the oxygen-precovered surface has decreased to be the same as on clean Ni(111) at higher coverages. Methanol saturates at ~0.3 ML (see Figure 6.6 for related sticking probability data) for the single layer of adsorbates on Ni(111) at 155 K, smaller than Pt(111) at 150 K (~0.33 ML),[30] which is expected due to Pt(111) having a larger lattice parameter and 19% smaller density of surface atoms than Ni(111).

Further evidence for the formation of methoxy is shown in Figure 6.7 (in supplementary information), which shows the SCAC results for methanol adsorption onto O-precovered Ni(111) at 190 K. At 190 K, we observe the same heats as the O-precovered Ni(111) surface at 100 K and 155 K, but a lower final coverage of ~0.18 ML, due to a lower coverage of O_{ad}. (See also Figure 6.6)

6.4 DISCUSSION

Energetics of Adsorbed Methoxy. From the heats of adsorption measured in this work by calorimetry and available literature values for the heats of formation of adsorbed and gas-phase species, we may extract the heat of formation of methoxy on Ni(111) and its bond enthalpy to this surface. We attribute the integral heat of adsorption from 0 – 0.25 ML on the 0.25 ML oxygen-precovered Ni(111) surface at 155 K (Figure 6.3) of -70. kJ/mol to the heat of Reaction (1). Figure 6.4 shows the thermodynamic cycle, which uses this to extract the heat of formation of adsorbed methoxy and the CH_3O-Ni(111) bond dissociation enthalpy, D(CH_3O-Ni(111)).

This thermodynamic cycle starts on the left-hand side with all atoms in their standard state, which therefore possesses an enthalpy of formation of 0 kJ/mol. Following the bottom path shows the formation of gaseous methanol and an adsorbed oxygen atom, which possess enthalpies of formation of -202 kJ/mol and -240. kJ/mol, respectively.[15,164] The bottom path then tracks the dissocative adsorption of methanol to make adsorbed methoxy plus adsorbed hydroxyl, the enthalpy of which we measured with calorimetry (-70. kJ/mol). This is an exothermic process and the enthalpy of reaction is a negative value, while the values shown in Figure 6.3 are the heats of adsorption, which, by convention, are shown as positive values. Combining the heats of formation and measured reaction enthalpy of the bottom path results in

the total heat of formation of coadsorbed methoxy and hydroxyl, both at 0.25 ML coverage, a value of -512 kJ/mol.

The middle path in the thermodynamic cycle (Figure 6.4) shows this enthalpy change of converting all atoms in their standard states directly to coadsorbed methoxy and hydroxyl. Therefore, the sum of their enthalpies of formation must be equal to the total heat of formation (-512 kJ/mol). The enthalpy of formation of hydroxyl at 0.25 ML on Ni(111) was previously measured to be -279 kJ/mol.[159] Subtracting this enthalpy of formation of adsorbed hydroxyl from the total enthalpy of formation results in the enthalpy of formation of adsorbed methoxy at 0.25 ML coverage: -233 kJ/mol.

Following the top pathway on this thermodynamic cycle (Figure 6.4) shows the method to extract the bond enthalpy of methoxy to Ni(111). This top route starts by converting the standard state elements to a gaseous methoxy radical and an adsorbed hydroxyl, which possess an enthalpy of formation of +17 kJ/mol and -279 kJ/mol, respectively.[107,159] These two species have a total enthalpy of formation of -262 kJ/mol. The difference in enthalpies between these two species and our final state on the far right is negative of the adiabatic CH_3O-Ni(111) bond dissociation enthalpy. Therefore, +250 kJ/mol is the enthalpy for breaking the CH_3O-Ni(111) bond at 0.25 ML coverage (when coadsorbed with 0.25 ML of hydroxyl).

Comparison to DFT Calculations. The bond energy of molecular methanol and methoxy to Ni(111) measured here may be compared to theoretical calculations. Table 6.1 compares computational values obtained by various DFT methods to the experimental values of this work. DFT calculations report integral bond energies of adsorbates at specific coverages. To calculate the bond energy of molecular methanol at a specific coverage, the best-fit line of the measured differential heats of methanol adsorption versus coverage from 0 to 0.30 ML at 100 K (Figure

6.1) is integrated up to the desired coverage. These integral heats (enthalpies) are then converted to bond energies by subtracting RT. The bond energies for methoxy are calculated from thermodynamic cycles similar to that in Figure 6.4 and discussed above but by integrating different coverages to calculate the heat of reaction and used the reported heat of formation of adsorbed hydroxyl at the desired coverage.[159]

For molecular methanol, all reported DFT calculations significantly underestimated the bond energy measured in this work. The weaker bond strength found in these DFT studies than by calorimetry could be due to methanol forming hydrogen-bonded structures, similar to what has been observed in Cu(111) and Au(111).[165,166] These intermolecular hydrogen bonds may not be properly accounted for as these chains would have significantly larger unit cells that what was used in these calculations. These underestimation in bond energy could also be due to underestimating the magnitude of van der Waals and dipole interactions between the adsorbate and the surface. For adsorbed methoxy, PW-91 and PBE perform well, differing from the experimentally determine value by only 0-14 kJ/mol. However, RPBE underestimates the bond energy by 69 kJ/mol. This RPBE paper only reported their calculated results on top sites.[172] Their value of 180 kJ/mol is close to the reported energies of methoxy bound to top sites by another DFT functional, PW-91 (175 kJ/mol).[173]

Comparison to Pt(111). Previous work[30] from this research group studied the adsorption of methanol and methoxy on Pt(111), allowing for a direct comparison between the two metal surfaces. These values are adjusted slightly (by a value of RT_{source}) from the literature to account for a systematic error as discussed elsewhere.[15] Methoxy on Pt(111) at 0.25 ML coverage coadsorbed with 0.25 ML of hydroxyl has a heat of formation of -168 kJ/mol (compared to -233 kJ/mol on Ni(111) under the same conditions) and a bond enthalpy of -185 kJ/mol (compared to

-250. kJ/mol on Ni(111) under the same conditions). These much larger values on Ni(111) are to be expected as it is well known that Ni is more oxophillic than Pt, so that Ni-O bonds should be stronger.

It is interesting to consider how these energetic differences between Ni and Pt manifest themselves in catalysts. Let us consider a simple reaction involving C-O bond cleavage:

$$CH_3O_{ad} \rightarrow CH_{3,ad} + O_{ad} . \quad (2)$$

Using the published heats of formation of $CH_{3,ad} + O_{ad}$ of -71 kJ/mol[65] and -240. kJ/mol[15], respectively, together with the heat of formation of CH_3O_{ad} on Ni(111) of -233 kJ/mol found above give a highly exothermic enthalpy for Reaction (2) of -78 kJ/mol on Ni(111). In contrast, the heats of formation of these three species on Pt (111) of -168 kJ/mol for methoxy[30], -99 kJ/mol for O_{ad}[174], and -50 kJ/mol for methyl[99], give an endothermic enthalpy for Reaction (2) of +19 kJ/mol. Clearly, such simple C-O bond-cleavage reactions that produce O adatoms are much more exothermic (by almost 100 kJ/mol) on Ni than Pt catalysts, and thus should be much faster and have much larger equilibrium constants on Ni catalysts. Similarly, C-O bond forming reactions (like the reverse of Reaction (2)) should be much more facile on Pt than Ni catalysts. In contrast, C-O bond cleavage reactions that involve oxygen transfer to another surface fragment rather than to produce O_{ad} should be similar on Ni and Pt catalysts, as seen for the simple reaction:

$$CH_3O_{ad} + H_{ad} \rightarrow CH_{3,ad} + OH_{ad} . \quad (3)$$

The enthalpy for Reaction (3) is -69 kJ/mol on Ni(111) and quite similar, -54 kJ/mol, on Pt(111). (The heat of formation of H_{ad} is -47 kJ/mol on Ni(111)[15] and -36 kJ/mol on Pt(111).[15] The heat of formation of OH_{ad} is -278 kJ/mol on Ni(111)[159] and -208 kJ/mol on Pt(111).[15,175])

Trends in Bond Enthalpies of Adsorbed Oxygenates. It has previously shown that the ligand-metal σ-bond strengths found in organometallic complexes in liquid solutions strongly correlate with the corresponding gas-phase ligand-hydrogen bond strength.[176–178] Previously this research group found that this trend is also true for ligands (i.e., molecular fragments) bound to Pt(111).[160] Specifically, the adiabatic bond dissociation enthalpies of oxygenate adsorbates to Pt(111) (monodentate formate, hydroxyl, and methoxy) vary linearly with a slope of 1 with the corresponding gas-phase RO-H sigma bond enthalpy but offset by -251 kJ/mol. Analyzing the bond enthalpy of methoxy measured in this work and the bond enthalpies of formate and hydroxyl measured previously[159] on Ni(111), we find this same trend, as shown in Figure 6.5. Figure 6.5 shows the adiabatic bond dissociation enthalpies of three oxygenate adsorbates on both Ni(111) and Pt(111) versus their corresponding gas-phase hydrogen-ligand bond dissociation enthalpies. The data points and trendline for Pt(111) is recreated here from the literature[160] and adjusted slightly to account for systematic error equal to RT_{source}, as discussed elsewhere.[15] A linear trend with a slope of 1 ($y = x - 182$ kJ/mol) is shown on Figure 6.5 to fit the data points for Ni(111) very well and possesses a standard error of 3.9 kJ/mol. The best-fit line of ($y = 1.03\ x - 198$ kJ/mol) is only marginally better with a standard error of 3.8 kJ/mol. The strength of σ-bonds of adsorbed oxygen-bound molecular fragments to Ni(111) varies linearly with the strength of binding of those same fragments to H atoms in gas-phase molecules with a slope of 1.00, but offset by −182 kJ/mol. It is weaker than binding to a H atom, but ~69 kJ/mol stronger than binding to Pt(111), which makes sense because Ni is known to be more oxophillic than Pt. Therefore, we are able to predict the bond enthalpies of other oxygen-bound molecular framents to Ni or Pt through these trend lines. This will probably fail for larger adsorbates, since these will have strong van der Waals attractions to the surface too, that are not

accounted for in the trends in Figure 6.5. Given that these trends of Figure 6.5 hold for both Pt(111) and Ni(111), we expect that the bond enthalpies of small adsorbed oxygenates to other transition metal surfaces will follow a similar trend with a slope near 1.

6.5 CONCLUSIONS

The energetics of the molecular and dissociative adsorption of methanol on Ni(111) were measured by SCAC. At 100 K, the heat of adsorption is well fit by the curve (63.2 - 23.9 θ) kJ/mol from 0 – 0.30 ML and (99.3 - 142.7 θ) kJ/mol from 0.30 – 0.40 ML. The dissociative adsorption of methanol on O-precovered Ni(111) produces adsorbed methoxy and hydroxyl and gives an integral heat of adsorption at 155 K of -70. kJ/mol at a coverage of 0.25 ML (of both products). This gives a heat of formation for adsorbed methoxy of -233 kJ/mol and a bond enthalpy of 250. kJ/mol. We find a linear trend with a slope of 1 between the bond enthalpies of small oxygenates to Ni(111) and Pt(111) and their corresponding gas-phase hydrogen-ligand bond dissociation enthalpies. These values and trends improve our ability to understand the selectivity, reaction rate, and activity differences between metal surfaces in reactions involving adsorbed oxygenates.

6.6 TABLES AND FIGURES

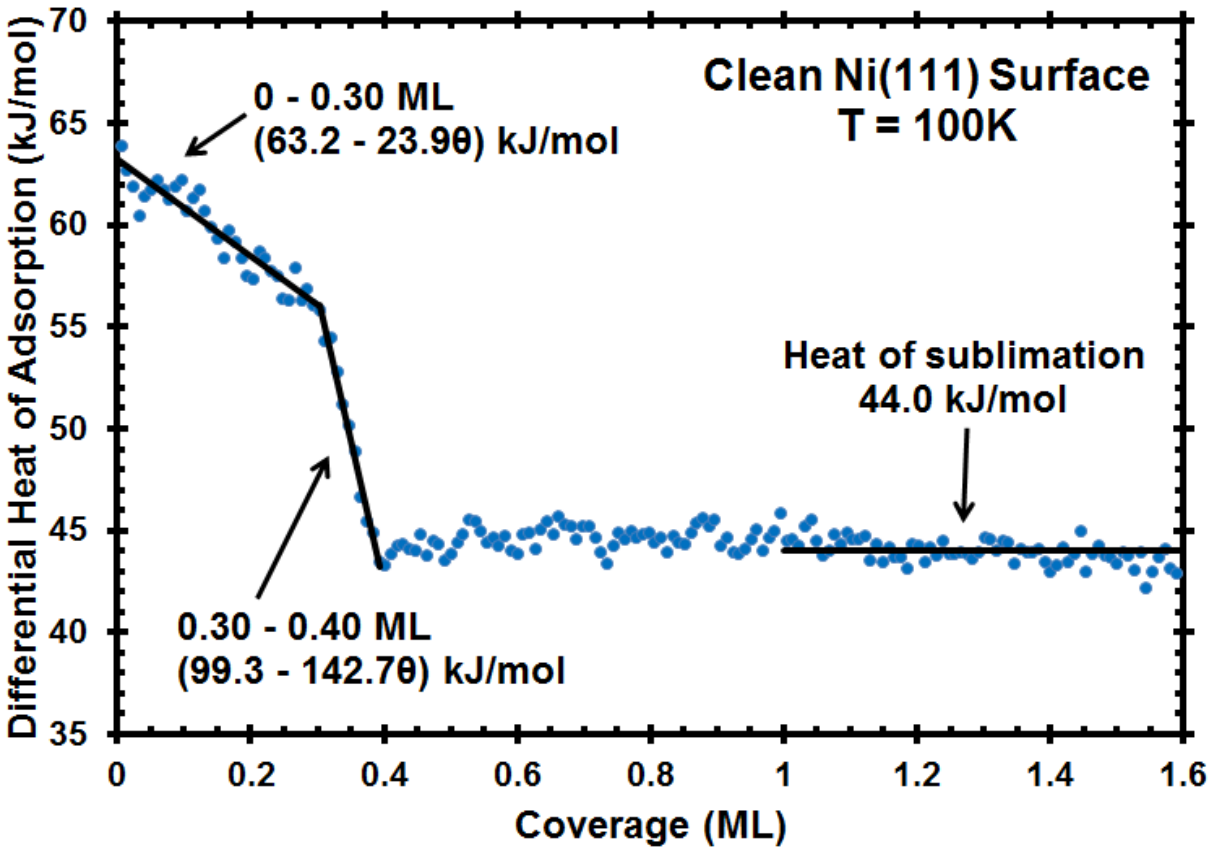

Figure 6.1. Differential heat of adsorption of methanol on the clean Ni(111) surface as a function of methanol coverage at 100 K.

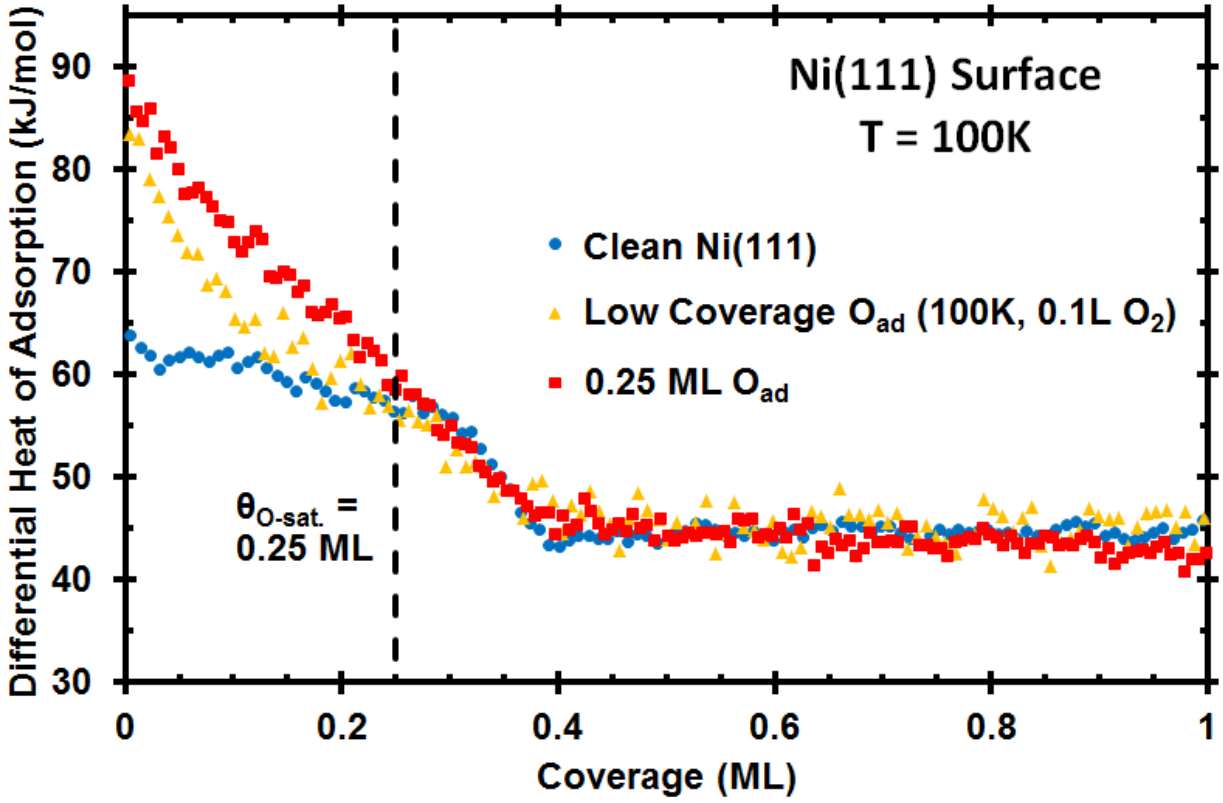

Figure 6.2. Differential heat of adsorption of methanol on Ni(111) at 100K versus total methanol coverage. Each curve represents a different coverage of predosed oxygen adatoms on the surface, including the clean, O-free surface, a low coverage of O_{ad}, and 0.25 ML of O_{ad}. The vertical dashed line at 0.25 ML is where the reaction of methanol with O_{ad} to produce CH_3O_{ad} + OH_{ad} is expected to finish for this highest predose of O_{ad}.

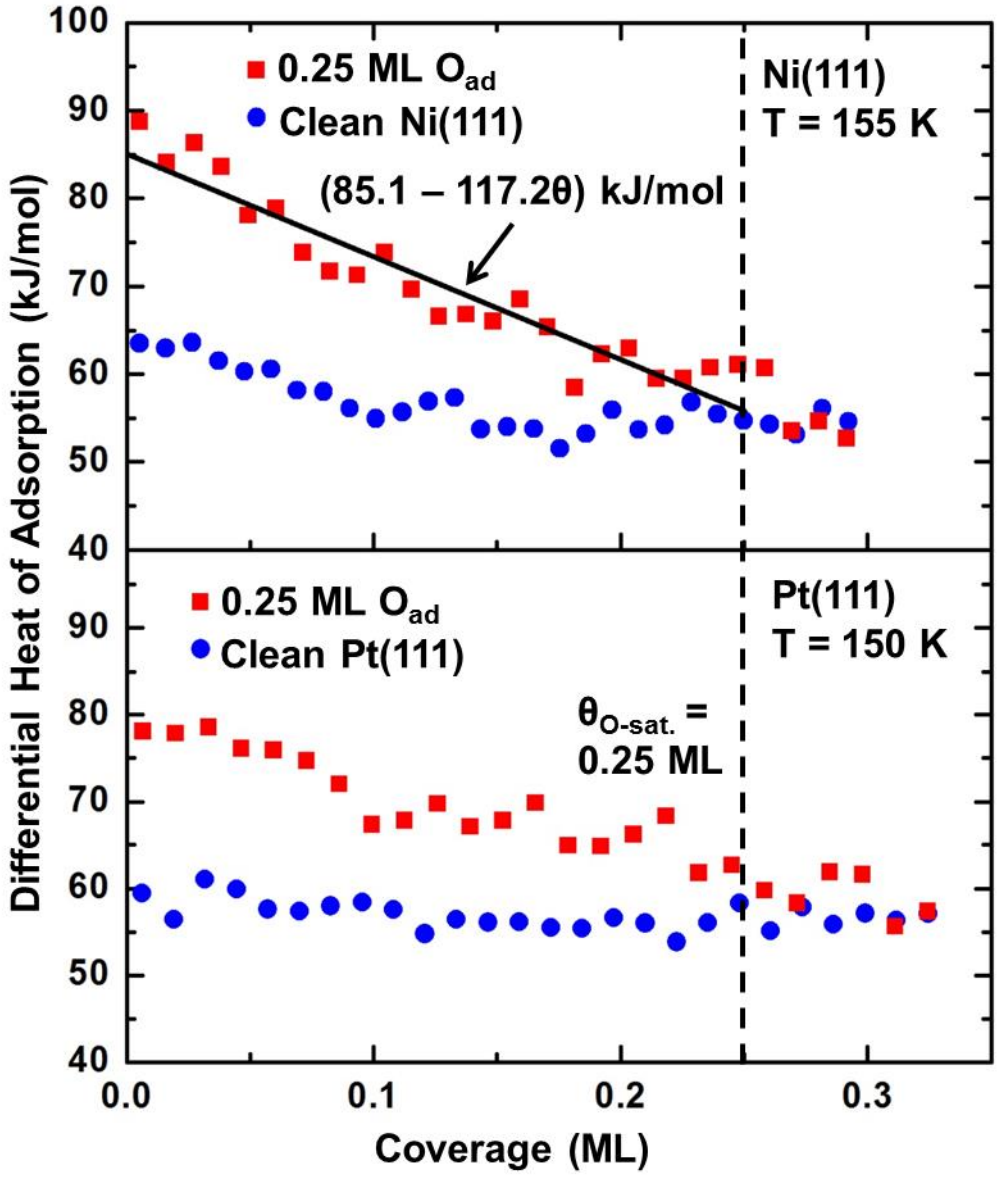

Figure 6.3. Differential heat of adsorption of methanol versus total methanol coverage on Ni(111) at 155 K and on Pt(111) at 150 K at two surface conditions: the clean metal surface and with 0.25 ML precoverage of O_{ad}. The vertical dashed line at 0.25 ML is where the reaction of methanol with O_{ad} to produce CH_3O_{ad} + OH_{ad} is expected to finish.

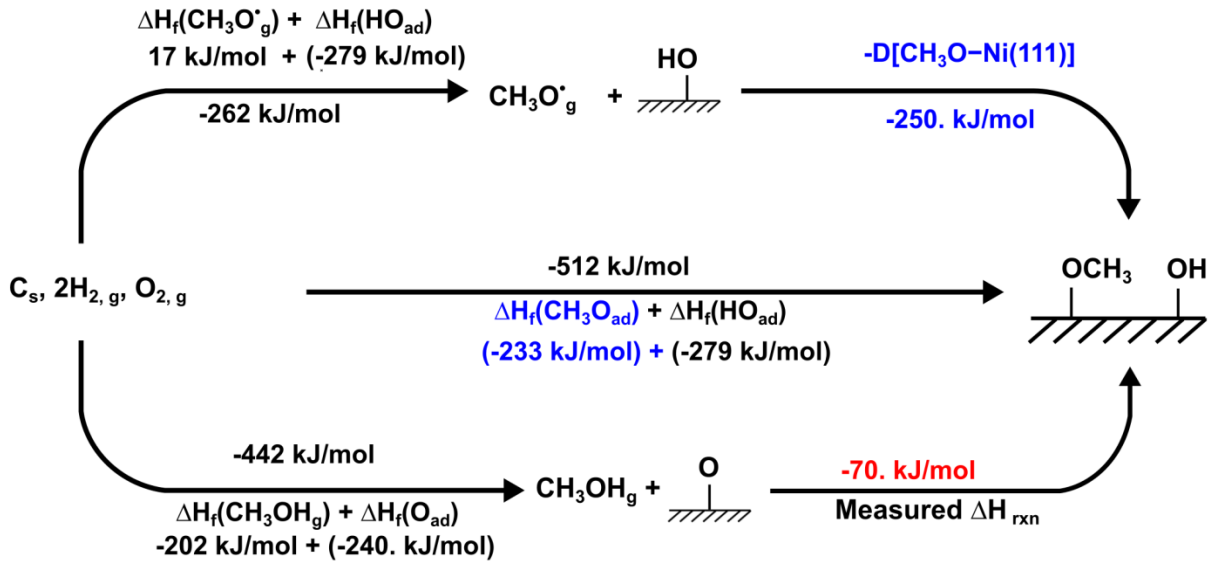

Figure 6.4. Thermodynamic cycle used to calculate the heat of formation and bond dissociation enthalpy of adsorbed methoxy to the Ni(111) surface, which are shown in blue. The red value of -70. kJ/mol is the measured enthalpy of reaction of gaseous methanol onto the surface precovered with 0.25 ML of O_{ad} at 100K producing adsorbed methoxy and hydroxyl. This is the integral or average reaction enthalpy from 0 to 0.25 ML of dissociatively-adsorbed methanol. The other values shown in black are from the literature, as described in the text.

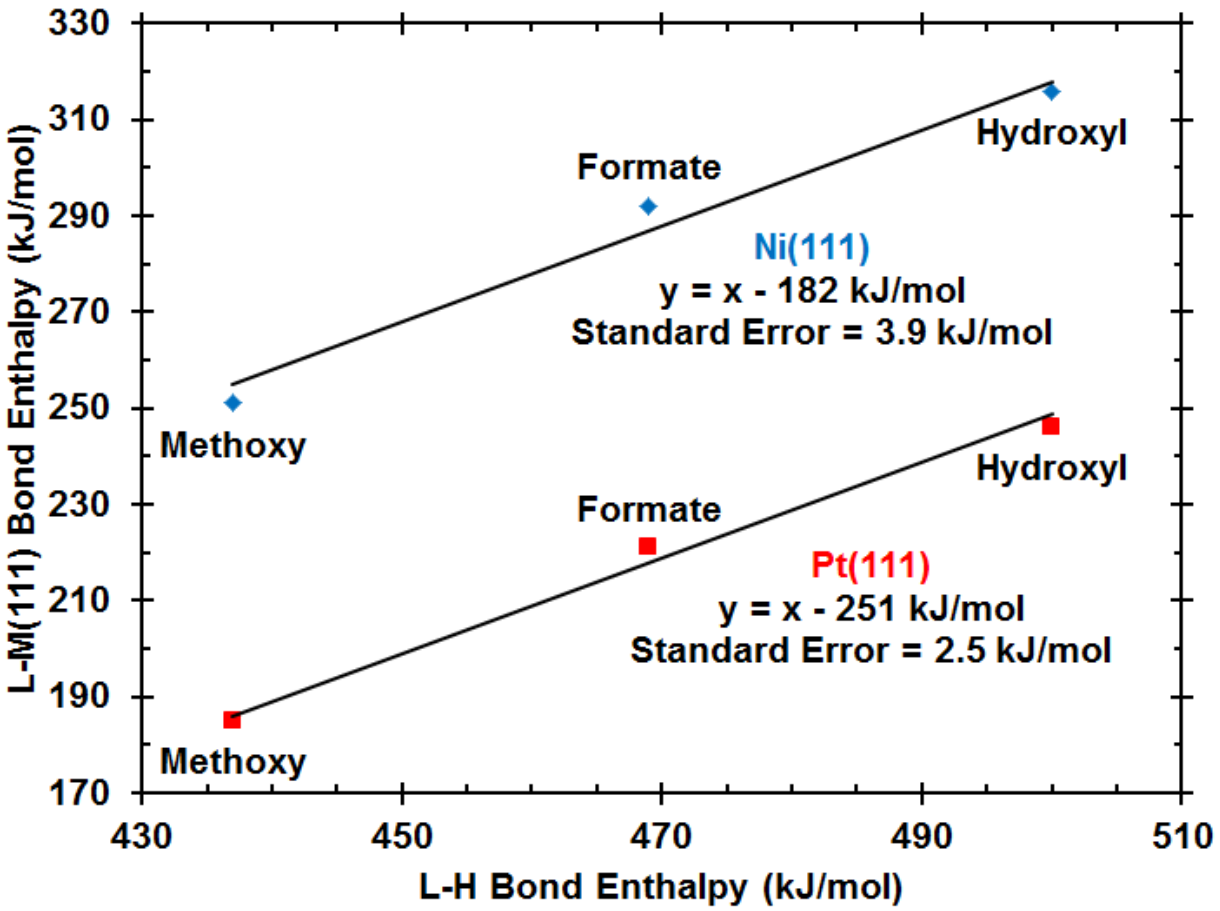

Figure 6.5. Calorimetric bond dissociation enthalpies of three adsorbates on both Ni(111) and Pt(111) versus their corresponding gas-phase hydrogen-ligand bond dissociation enthalpies. These data points are fitted with the linear trendlines shown, each with a slope of 1.

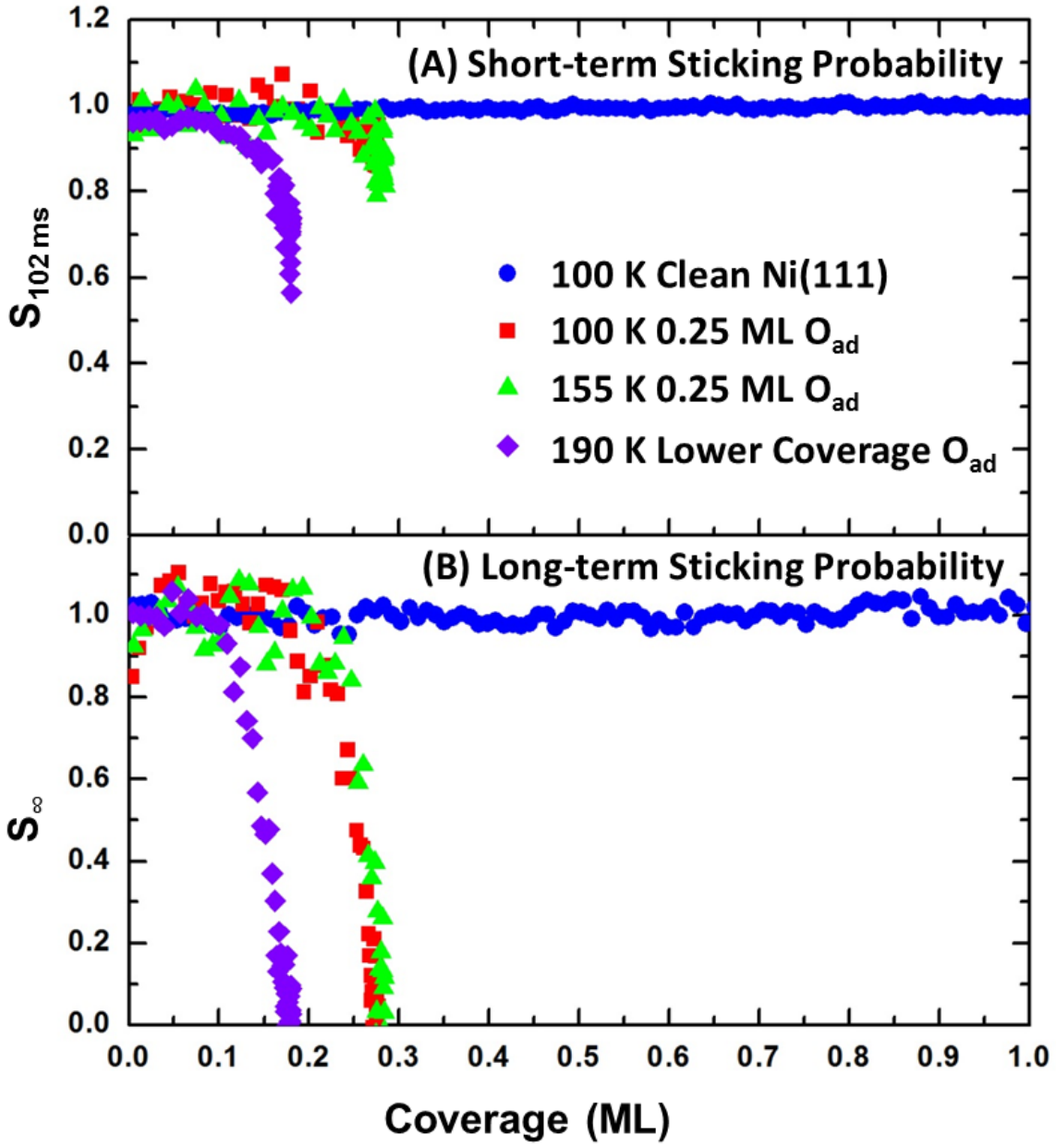

Figure 6.6. Average short-term (A) and long-term (B) sticking probabilities of methanol as a function of total methanol coverage on Ni(111) at several temperatures and surface conditions. Note that the reaction completes at ~0.16 ML for the "lower coverage" of O_{ad}, which we interpret to indicate that this coverage (from 5 L O_2 at 190 K) is ~0.16 ML of O_{ad}.

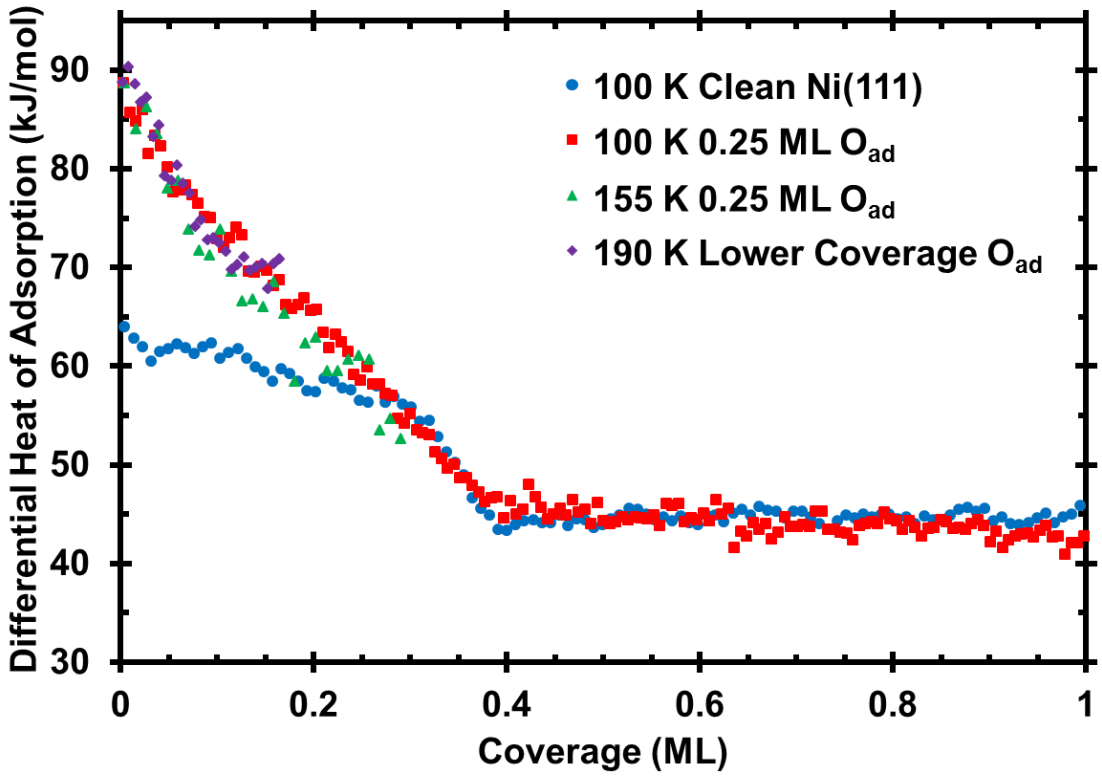

Figure 6.7. Comparison of the differential heats of adsorption of methanol on Ni(111) at several different temperatures and surface conditions as a function of adsorbed methanol coverage. The methanol dissociates to make methoxy and –OH on the oxygen-predosed surfaces, until this titrates all the O_{ad}.

Table 6.1. Comparison of present calorimetric integral bond energies of phenol to the Pt(111) and Ni(111) surface with calculated values using DFT with periodic boundary conditions.

Molecularly Adsorbed Methanol			Bond Energy (kJ/mol)		Reference
Coverage	DFT Functional/Method	DFT Site	DFT	Calorimetry	DFT
1/9 ML	PW-91	Top	24	61	[179]
1/9 ML	PW-91	Top	32	61	[173]
1/6 ML	PBE	Top	16	60	[180]
1/4 ML	RPBE	Top	2	59	[172]
Methoxy			Bond Energy (kJ/mol)		Reference
Coverage	DFT Functional/Method	DFT Site	DFT	Calorimetry	DFT
1/9 ML	PW-91	Hollow	257	257	[179]
1/9 ML	PW-91	FCC Hollow	243	257	[173]
1/6 ML	PBE	FCC Hollow	249	254	[180]
1/6 ML	PW-91	FCC Hollow	264	254	[181]
1/4 ML	RPBE	Top	180	249	[172]

Chapter 7. TRENDS IN BOND ENTHALPIES OF MOLECULAR FRAGMENTS ADSORBED TO SURFACES

Understanding the energetics of chemical reactions on transition metal surfaces is crucial for many technologies, including the development of better catalysts, chemical sensors, surface organo-functionalization, microelectronics and optical device fabrication, bioengineered materials and nanomaterials synthesis. Here, we show how trends in the experimentally-measured bond enthalpies of adsorbed molecular fragments to transition metal surfaces can be understood though simple properties of the metal and the adsorbed molecular fragment (which we will refer to here as the "ligand"). Thus, we correlate bond enthalpies with the electronegativity of the metal, the group electronegativity of the ligand, and the bond enthalpies of the ligand to an H atom. Specifically, we treat four molecular fragments that bind to the metal via their O or C atom, and their adsorption enthalpies to Pt(111) and Ni(111) surfaces, which are the only systems for which the bond enthalpies have been experimentally measured for such molecular fragments.

In this paper, we derive an equation based on Pauling's equation, Pauling electronegativies, and other known bond enthalpies that is able to accurately reproduce these bond enthalpies with standard deviation of only 7.2 kJ/mol relative to experimental values for the limited systems for which data are available (-OH, -OCH_3, -O(O)CH and –CH_3 on Pt(111) and Ni(111)). Our derivation starts with Matcha's bond enthalpy equation, itself an improvement on Pauling's equation.[182] We followed Schock's and Marks' approach of subtracting two of Matcha's Equations in order to establish a relationship between D(L-M(111)), the ligand-metal surface bond enthalpy, and D(L-H), the gas-phase ligand-hydrogen bond enthalpy,[183] but instead

we combined three of Matcha's equations to the same end. Our derivation eliminates the gas-phase M-M dimer bond enthalpy, D(M-M), from Schock's and Marks' equation, which we show is less appropriate for metal surfaces than the revised equation. This term is replaced with D(H-M(111)), the bond enthalpy of a hydrogen adatom to the metal surface, of which values are readily available from previous TPD experiments.

Equilibrium measurements of various organometallic complexes in liquid solutions have resulted in a large database of σ bond enthalpies of many ligands to metal centers.[176–178] Bryndza, Bercaw et al. showed that these metal-ligand bond strengths strongly correlate, with a slope = 1, to the gas-phase ligand-to-hydrogen bond strength.[176] Karp and co-workers found a similar correlation with slope of 1 between the bond enthalpies of oxygen-bound molecular fragments [-OH, -OCH_3, and -O(O)CH] to the Pt(111) surface and their corresponding RO-H bond enthalpies in the gas phase.[160] These bond enthalpies (shown in Figure 7.1) have been corrected slightly from their original value by RT due to a systematic error that has been discussed previously.[15] These relationships provide methods to predict the bond enthalpies of other species to Pt(111) from their corresponding gas-phase hydrogen-to-ligand bond strengths, which are well known.[184]

Figure 7.1 shows that this same Bercaw-type trend also applies to newer bond enthalpies for these same three oxygen-bound species to Ni(111), again with a slope close to 1. All values used in Figure 7.1 are listed in Table 1. Methyl on both Pt(111) and Ni(111) is also shown as a data point on these curves, but these points were not included in the linear fits. Although methyl on Pt(111) lies close to the Pt(111) line, methyl on Ni(111) lies far from its linear trend for oxygenates. This is expected, as Ni is more oxophilic than Pt and is known to bind oxygen

species more strongly than Pt. It is not known that Ni should bind to carbon species so much more strongly than Pt, as it does to oxygen species. As can be seen here in this plot, it does not.

The bond enthalpies of these ligands to metal surfaces depend upon surface coverage. We also list in Table 7.1 the coverages (adsorbates per metal surface atom) used to determine the adsorbate-surface bond enthalpies. These measurements were done in a such way that there was an equal coverage of another ligand on the surface too, specifically –I for methyl and -OH for the oxygenates (or the similar-in-enthalpy H_2O-OH complex it produces). These coverages were chosen as the most reliable coverage to do the analysis in the original papers that reported these bond enthalpies.

Schock and Marks later analyzed Bryndza's trend, applying it to organometallic complexes of different metals.[183] The authors found linear trends between hydrogen-to-ligand bond enthalpies and metal-ligand bond enthalpies of different classes of ligands, such as halogens, oxygenates, or carbonates, to each metal element. Each trend possessed a slope that was close to one but each metal had a different y-axis offset. To explain these offsets, Schock and Marks derived a new equation that used Pauling's bond ionicity and bond enthalpy relationships. Their derivation used an equation of Matcha, which was found to give far better agreement than Pauling's original equations in correlating bond enthalpies with the electronegativity differences between species[182]:

$$D(A-B) = \frac{1}{2}[D(A-A) + D(\mathrm{B}-B)] + (439\ \mathrm{kJ/mol})[1 - e^{-0.219(X_A - X_B)^2}] \qquad (7.1)$$

Species "A" and "B" refer to the metal (M), the ligand (L), or hydrogen (H). Here, X_I is the electronegativity of species I (which is a group electronegativity when I is the ligand) and D(I-J) is the I-J bond enthalpy. This equation can be written in three possible ways relating the enthalpies of bonds between ligands, metal atoms, and hydrogen:

$$D(M-L) = \frac{1}{2}[D(M-M) + D(L-L)] + (439\ \text{kJ/mol})[1 - e^{-0.219(X_M - X_L)^2}] \quad (7.2)$$

$$D(L-H) = \frac{1}{2}[D(H-H) + D(L-L)] + (439\ \text{kJ/mol})[1 - e^{-0.219(X_H - X_L)^2}] \quad (7.3)$$

$$D(M-H) = \frac{1}{2}[D(H-H) + D(M-M)] + (439\ \text{kJ/mol})[1 - e^{-0.219(X_H - X_M)^2}] \quad (7.4)$$

Schock and Marks subtracted Eq. (7.3) from Eq. (7.2) to produce a new equation directly relating the metal-ligand bond enthalpy with the ligand-hydrogen bond enthalpy[183]:

$$D(M-L) = D(L-H) + \frac{1}{2}[D(M-M) - D(H-H)] + (439\ \text{kJ/mol})[e^{-0.219(X_H - X_L)^2} - e^{-0.219(X_M - X_L)^2}] \quad (7.5)$$

The term D(M-M) refers to the metal-metal bond enthalpy in the gas-phase metal dimer in their treatment. We applied this equation to the data in Figure 7.1, as shown in Figure 7.2, and found that it places all four ligands for each metal surface very near to a straight line with slope of 1. Unlike the simple trend employed by Bryndza, Bercaw et al. in Figure 7.1, Eq. (7.5) allows *both* oxygen-bound and carbon-bound species to fall very close to the same line for each metal. However, there is still a large offset between different metals, with the Ni(111) line ~60 kJ/mol above the Pt(111) line. All values used to calculate the data points used in Figure 7.2 are listed in Table 7.1 (or its footnotes) along with their sources from the literature.[185]

Equation (7.5) was originally derived to be applied to organometallic complexes. We postulated that in applying it to ligands bound to solid metal surfaces, it would be more reasonable to replace the metal-metal bond enthalpy in the gas-phase metal dimer for D(M-M) with the metal-metal bond enthalpy in the bulk solid metal phase. Here, we estimate that as equal to the bulk heat of sublimation of the metal divided by six (the number of nearest-neighbor bonds formed per metal atom in making solid FCC metals like Ni and Pt from gaseous atoms), or 94.3 kJ/mol for Pt and 71.7 kJ/mol for Ni.[186] When plotted in this way, both Pt(111) and Ni(111)

show a linear correlation with a slope close to 1 and small standard deviations (≤ 7.3 kJ/mol), as shown in Figure 7.3. This value for D(M-M) provides a major improvement compared to Figure 1.1, as the offset between Ni(111) and Pt(111) drops from 60 to only 20 kJ/mol, clearly capturing better the essential physics involved in ligand-surface bonding.

We found that this equation may be improved further by subtracting Eq. (7.3) and Eq. (7.4) from Eq. (7.2), which results in:

$$D(M-L) = D(H-L) + D(M-H) - D(H_2) + (439\ \text{kJ/mol})\left[e^{-0.219(X_H - X_L)^2} + e^{-0.219(X_H - X_M)^2} - e^{-0.219(X_M - X_L)^2} - 1\right] \quad (7.6)$$

Figure 7.4 shows our calorimetrically measured surface bond enthalpies plotted as a function of the right-hand side of Equation (7.6). All values used to plot Figure 7.4 are listed in Table 7.1 or its footnotes. This plot accurately fits all four adsorbates on both Pt(111) and Ni(111) into a *single* line with a slope close to 1 and a standard deviation of 7.1 kJ/mol. This line is defined by:

$$D(M-L) = D(H-L) + D(M-H) - D(H-H) + \left(439\,\frac{\text{kJ}}{\text{mol}}\right)\left[e^{-0.219(X_H - X_L)^2} + e^{-0.219(X_H - X_M)^2} - e^{-0.219(X_M - X_L)^2} - 1\right] - \left(54\,\frac{\text{kJ}}{\text{mol}}\right) \quad (7.7)$$

The excellent agreement found here between experimental adsorbate-surface bond enthalpies and equation (7.7) offers new insight into the energetics of many adsorbates on late transition metal catalyst surfaces.

From this equation, we may draw several insights into chemical bonds to surfaces. First, the adsorbate bond enthalpy is directly correlated with the difference in electronegativity between the metal and ligand. A larger difference in electronegativity implies a bond more ionic in character, resulting in a stronger bond. Second, a stronger gas-phase ligand-hydrogen bond directly correlates with surface adsorbate's bond strength while the difference in electronegativity inversely correlates with surface adsorbate's bond strength. These terms are

related in such a way that the stronger the ligand can bind to a hydrogen atom, the stronger that ligand can bind to a metal surface, while correcting for the ionic character of this ligand-hydrogen bond. In other words, the stronger the ligand can bind to hydrogen while possessing a lower difference in electronegativity, the stronger the surface adsorbate bond will be. Third, and in a similar manner, the hydrogen atom's adsorption enthalpy directly correlates with the ligand adsorption enthalpy, while correcting for the ionic character of the hydrogen-surface bond. A stronger adsorbate bond will result from a stronger hydrogen-surface bond while maintaining similar electronegativities (i.e., $X \approx 2.2$).

We discovered the accuracy of Eq. (7.7) before we had measured the bond enthalpy of methoxy to Ni(111). To further test this equation, we measured that bond enthalpy, which was previously unknown. The details of that measurement are presented elsewhere (See Chapter 6). As can be seen, this value falls within 4 kJ/mol of the trend line established by the line of unit slope, which best fit the earlier seven adsorbate/surface systems, which suggests some predictive ability of Eq. (7.7).

This fitted line in Figure 7.4 allows the bond enthalpy of these adsorbates to several metals to be predicted using their group electronegativity, hydrogen-ligand bond strength, and hydrogen-surface bond strength. In Table 7.2, the predicted bond enthalpies of these molecular fragments bound to Cu(111), Pd(111), Fe(111), and Rh(111) surfaces are listed.

There are several limitations to the predictive ability of Eq. (7.7). First, each of the shown species is bound to the surface via a single σ bond. This trend will likely not hold for adsorbates that form multiple bonds to the surface (such as bidentate formate[33,66] or methylidyne[95]) since one bond influences the other. Other types of bonds, such as those that include π bonds (such as adsorbed CO) will also not be expected to fit this trend. Second, all

adsorbates shown here are adsorbed on top sites. This trend may not hold for adsorbates bound to bridge or hollow sites. Third, this equation cannot predict the effects of bonding that arise from van der Waals attractions to the surface. As an example, the energetics of tert-butyl bonding to the Pt(111) surface have been measured previously, showing a bond enthalpy of 215 kJ/mol.[108] Using the $(CH_3)C_3$-H bond enthalpy of 400 kJ/mol[187] and assuming a group electronegativity for t-butyl of 2.3 (equal to the electronegativity of methyl), Eq. (7.6) predicts a bond enthalpy that is 50 kJ/mol weaker than this measured value. We attribute the higher experimental bond enthalpy to the van der Waal attractions between t-butyl and the Pt(111) surface. The difference may be larger since approximation for t-butyl's group electronegativity may be inaccurate.

In conclusion, we show trends in the bond enthalpies of adsorbates to transition metal surfaces. We also derived a new equation that allows for semi-empirical estimations of the strength of σ bonds of small molecular fragments ($-CH_3$, $-OCH_3$, -O(O)CH, -OH) to Pt(111) and Ni(111). We find that these bond enthalpies vary linearly with a slope of 1 in relation to the right-hand side of Eq. (7.6) with an offset of -54 kJ/mol (i.e., as in Eq. (7.7)).

7.1 TABLES AND FIGURES

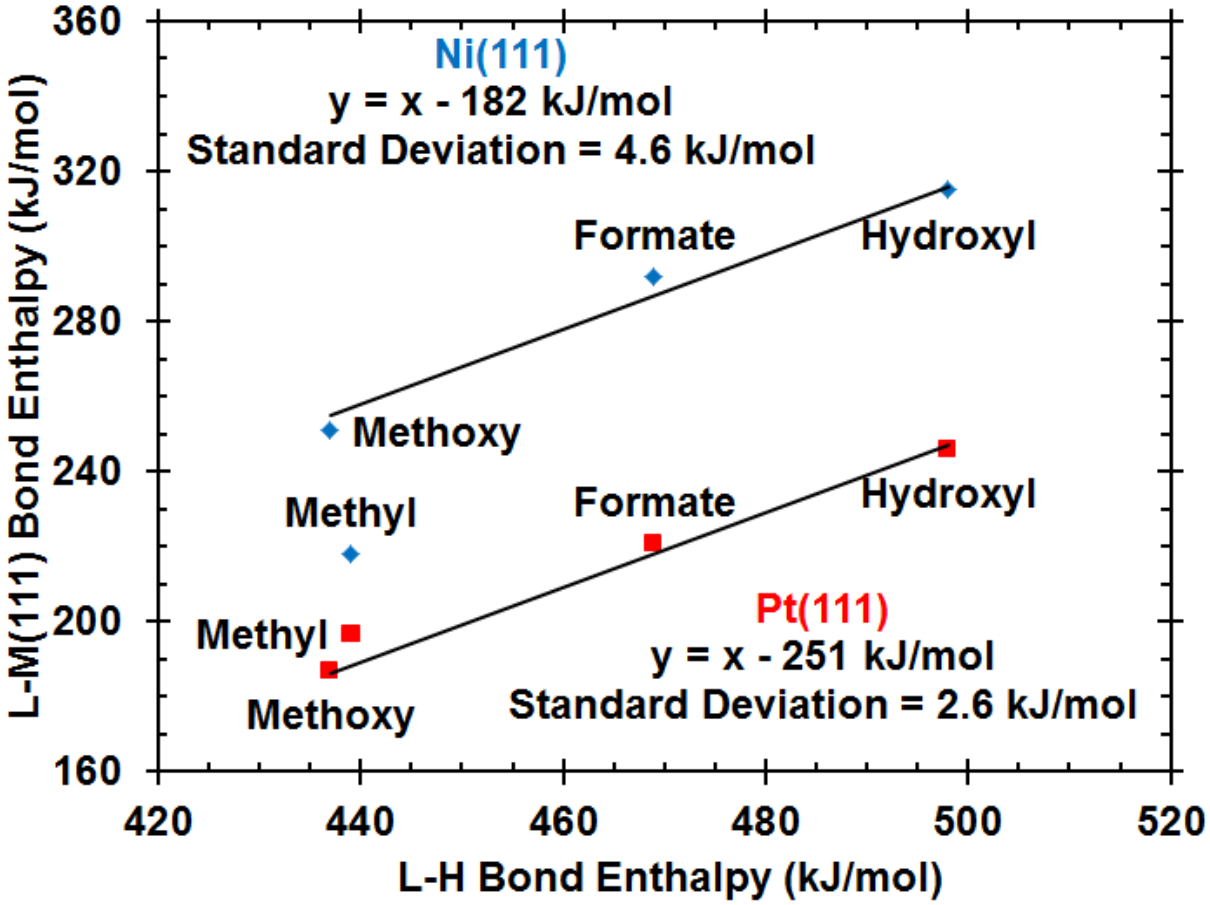

Figure 7.1. Calorimetrically measured bond enthalpies of four adsorbates to both Pt(111) and Ni(111) versus their corresponding gas-phase hydrogen-ligand bond dissociation enthalpies. The two lines shown, one for each metal and each with a slope of 1, fit the three oxygen-bound adsorbed species well.

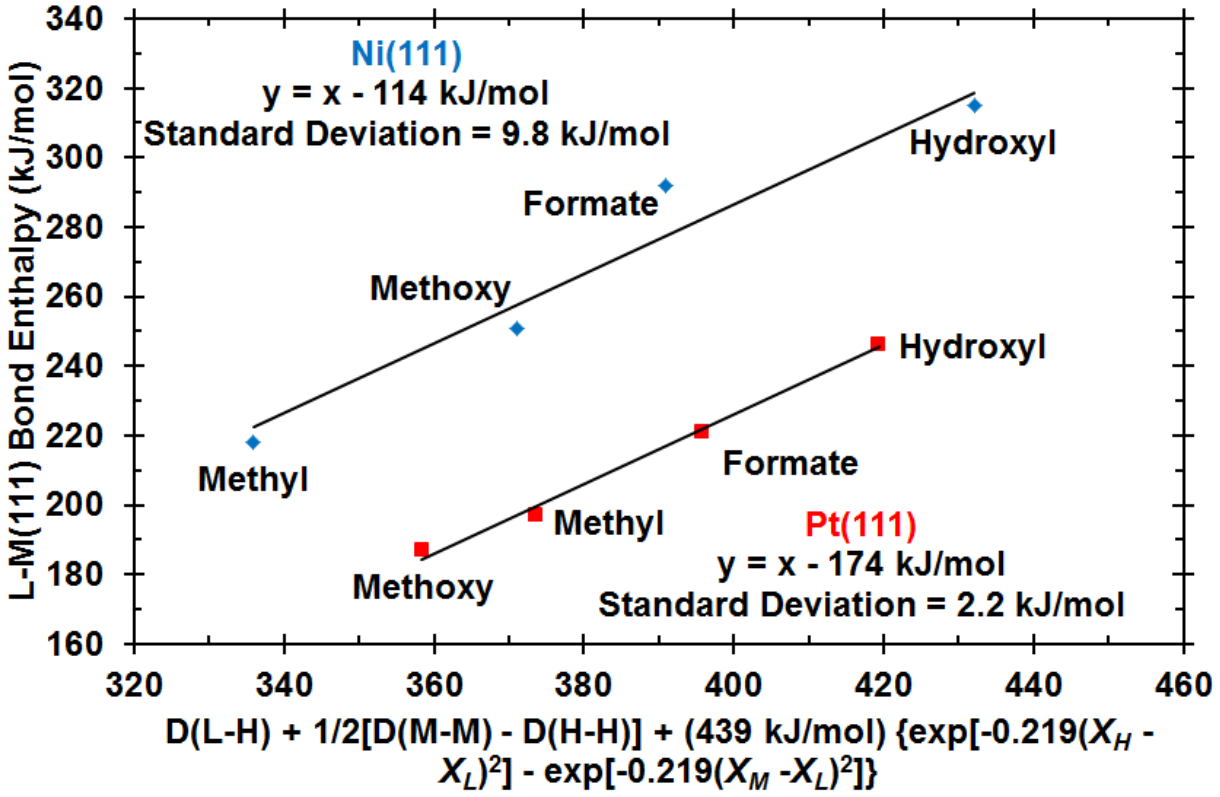

Figure 7.2. Calorimetrically measured bond enthalpies of four adsorbates to both Pt(111) and Ni(111) as a function of the right-hand side of Eq. (7.5) (i.e., correlation proposed by Schock and Marks.[183] Two lines, one for each metal surface and each with a slope of 1, fit well all four adsorbates shown here. The gas-phase metal dimer bond enthalpy is used here for D(M-M).

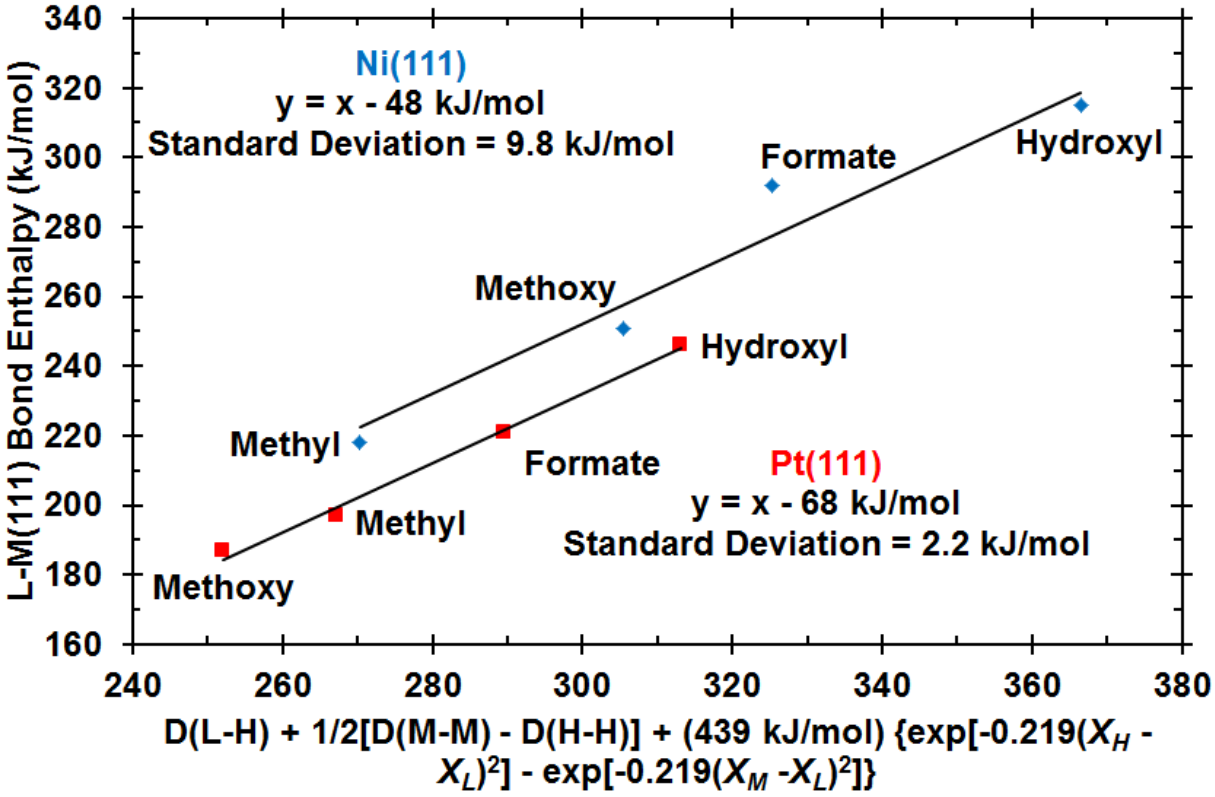

Figure 7.3. Same as Figure 7.2, except that the solid-phase metal-metal bond enthalpy is used for D(M-M) here.

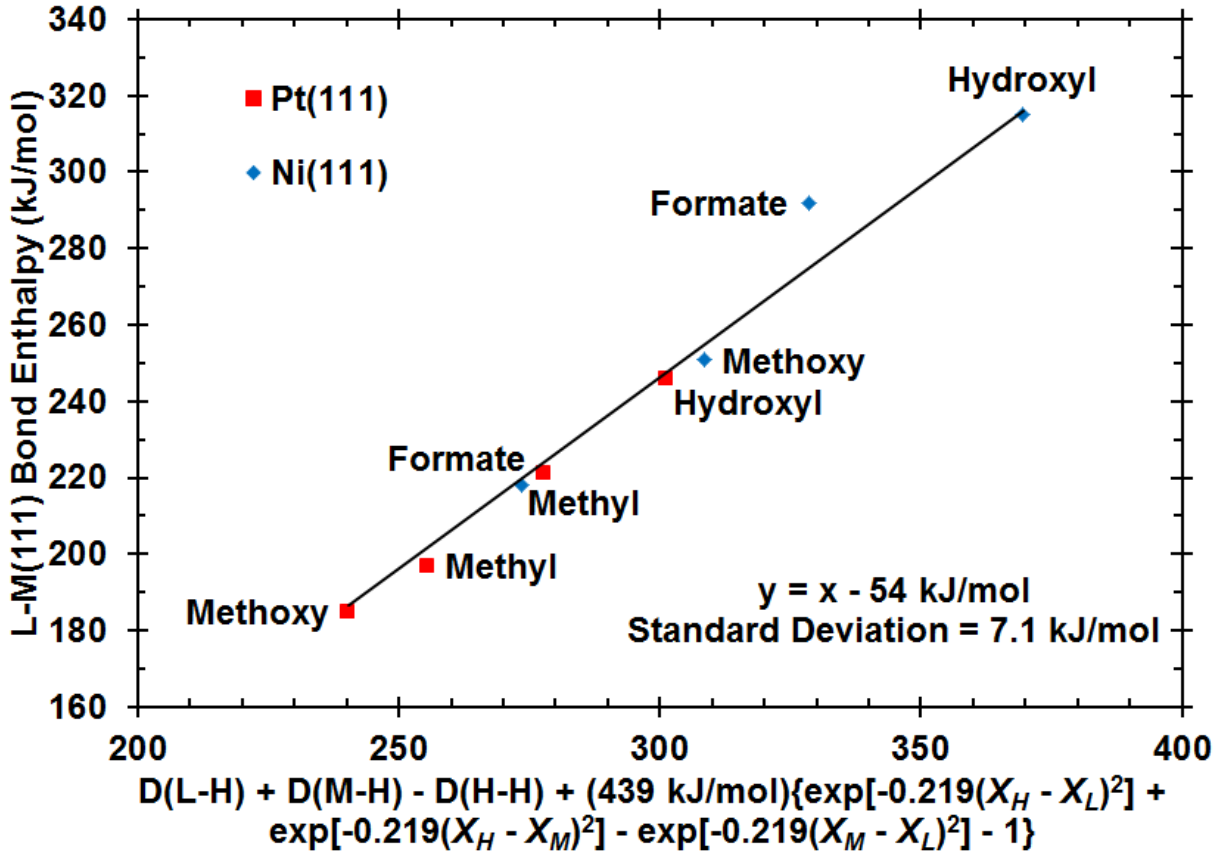

Figure 7.4. Calorimetrically measured bond enthalpies of four adsorbates to both Pt(111) and Ni(111) as a function of the right-hand side of Eq. (7.6), i.e., the equation derived in this work. A single line with a slope of 1 (i.e., Eq. (7.7)) fits all four adsorbates on both metal surfaces well.

Table 7.1. Gas-phase ligand-hydrogen bond enthalpy, and calorimetrically measured adsorbate bond enthalpy to Pt(111) and Ni(111) for five different ligands, all in kJ/mol. Also listed are the group electronegativities of the ligands (X_L) and the metal electronegativities (X_M), from the literature.

Ligand	***X_I***	**D(L-H) Bond Enthalpy (kJ/mol)**	**D(L-Pt(111)) Bond Enthalpy (kJ/mol)**	**(L-Ni(111)) Bond Enthalpy (kJ/mol)**	***Coverage (ML)***
-H	2.2, Ref. [188]	436, Ref. [189]	254, Ref. [15]	265, Ref. [15]	0.25
-OD	3.51, Ref. [188]	498, Ref. [184]	244, Ref. [175]	314, Ref. [159]	0.5
$-OCH_3$	2.68, Ref. [188]	437, Ref. [184]	185, Ref. [30]	249, Ref. (See Chapter 6)	0.25
$-O(O)CH_3$	3.52, Ref. [188]	469, Ref. [189]	220, Ref. [33]	290, Ref. [66]	Pt: 0.25 Ni: 0.20
$-CH_3$	2.27, Ref. [188]	439, Ref. [189]	195, Ref. [95]	216, Ref. [65]	0.04
Pt	2.28, Ref. [186]		94 (solid); 307 (gas-phase dimer), Ref. [186]		
Ni	1.91, Ref. [186]			72 (solid); 203 (gas-phase dimer), Ref. [186]	

Table 7.2. Predicted bond enthalpies of adsorbates on four surfaces using the fitted line in Figure 7.4, based on Eq. (7.7).

Ligand	D(L-Cu(111)) (kJ/mol)	D(L-Pd(111)) (kJ/mol)	D(L-Fe(111)) (kJ/mol)	D(L-Rh(111)) (kJ/mol)
-H	218	262	262	253
-OD	271	271	322	247
$-OCH_3$	210	210	261	186
$-O(O)CH_3$	229	242	280	224
$-CH_3$	173	212	219	201

REFERENCES

(1) Chorkendorff, I.; Niemantzverdriet, J. W. *Concepts of Modern Catalysis and Kinetics*; WILEY-VCH Verlag GmbH & Co. KGaA: Weinheim, 2003.

(2) Farrauto, R. J.; Bartholomew, C. H. *Fundamentals of Industrial Catalytic Processes*, First.; Blackie Academic & Professional: New York, 1997.

(3) Besenbacher, F. Design of a Surface Alloy Catalyst for Steam Reforming. *Science (80-.).* **1998**, *279* (5358), 1913–1915.

(4) Greeley, J.; Nørskov, J. K. Large-Scale, Density Functional Theory-Based Screening of Alloys for Hydrogen Evolution. *Surf. Sci.* **2007**, *601* (6), 1590–1598.

(5) Studt, F.; Abild-Pedersen, F.; Bligaard, T. Identification of Non-Precious Metal Alloy Catalysts for Selective Hydrogenation of Acetylene. *Science (80-.).* **2008**, *320* (5881), 1320–1322.

(6) Greeley, J.; Nørskov, J. K.; Kibler, L. A.; El-Aziz, A. M.; Kolb, D. M. Hydrogen Evolution over Bimetallic Systems: Understanding the Trends. *ChemPhysChem* **2006**, *7* (5), 1032–1035.

(7) Greeley, J.; Stephens, I. E. L.; Bondarenko, a S.; Johansson, T. P.; Hansen, H. a; Jaramillo, T. F.; Rossmeisl, J.; Chorkendorff, I.; Nørskov, J. K. Alloys of Platinum and Early Transition Metals as Oxygen Reduction Electrocatalysts. *Nat. Chem.* **2009**, *1* (7), 552–556.

(8) Nørskov, J. K.; Bligaard, T.; Rossmeisl, J.; Christensen, C. H. Towards the Computational Design of Solid Catalysts. *Nat. Chem.* **2009**, *1* (1), 37–46.

(9) Greeley, J.; Mavrikakis, M. Alloy Catalysts Designed from First Principles. *Nat. Mater.* **2004**, *3* (11), 810–815.

(10) Greeley, J.; Jaramillo, T. F.; Bonde, J.; Chorkendorff, I. B.; Nørskov, J. K. Computational High-Throughput Screening of Electrocatalytic Materials for Hydrogen Evolution. *Nat. Mater.* **2006**, *5* (11), 909–913.

(11) Mavrikakis, M. Computational Methods: A Search Engine for Catalysts. *Nat. Mater.* **2006**, *5* (11), 847–848.

(12) Norskov, J. K.; Abild-Pedersen, F.; Studt, F.; Bligaard, T. Density Functional Theory in Surface Chemistry and Catalysis. *Proc. Natl. Acad. Sci.* **2011**, *108* (3), 937–943.

(13) Alayoglu, S.; Nilekar, A. U.; Mavrikakis, M.; Eichhorn, B. Ru-Pt Core-Shell Nanoparticles for Preferential Oxidation of Carbon Monoxide in Hydrogen. *Nat. Mater.* **2008**, *7* (4), 333–338.

(14) Wellendorff, J.; Silbaugh, T. L.; Garcia-Pintos, D.; Nørskov, J. K.; Bligaard, T.; Studt, F.; Campbell, C. T. A Benchmark Database for Adsorption Bond Energies to Transition Metal Surfaces and Comparison to Selected DFT Functionals. *Surf. Sci.* **2015**, *640*, 36–44.

(15) Silbaugh, T. L.; Campbell, C. T. Energies of Formation Reactions Measured for Adsorbates on Late Transition Metal Surfaces. *J. Phys. Chem. C* **2016**, *120* (44), 25161–25172.

(16) Liu, W.; Carrasco, J.; Santra, B.; Michaelides, A.; Scheffler, M.; Tkatchenko, A. Benzene Adsorbed on Metals: Concerted Effect of Covalency and van Der Waals Bonding. *Phys.*

Rev. B **2012**, *86* (24), 245405.
(17) Liu, W.; Ruiz, V. G.; Zhang, G. X.; Santra, B.; Ren, X.; Scheffler, M.; Tkatchenko, A. Structure and Energetics of Benzene Adsorbed on Transition-Metal Surfaces: Density-Functional Theory with van Der Waals Interactions Including Collective Substrate Response. *New J. Phys.* **2013**, *15* (5), 053046.
(18) Klimeš, J.; Bowler, D. R.; Michaelides, A. Chemical Accuracy for the van Der Waals Density Functional. *J. Phys. Condens. Matter* **2010**, *22* (2), 022201.
(19) Klimeš, J.; Bowler, D. R.; Michaelides, A. Van Der Waals Density Functionals Applied to Solids. *Phys. Rev. B* **2011**, *83* (19), 195131.
(20) Klimeš, J.; Michaelides, A. Perspective: Advances and Challenges in Treating van Der Waals Dispersion Forces in Density Functional Theory. *J. Chem. Phys.* **2012**, *137* (12), 120901.
(21) Bučko, T.; Hafner, J.; Lebègue, S.; Ángyán, J. G. Improved Description of the Structure of Molecular and Layered Crystals: Ab Initio DFT Calculations with van Der Waals Corrections. *J. Phys. Chem. A* **2010**, *114* (43), 11814–11824.
(22) Vanin, M.; Mortensen, J. J.; Kelkkanen, A. K.; Garcia-Lastra, J. M.; Thygesen, K. S.; Jacobsen, K. W. Graphene on Metals: A van Der Waals Density Functional Study. *Phys. Rev. B* **2010**, *81* (8), 081408.
(23) Starr, D. E.; Campbell, C. T. Low-Temperature Adsorption Microcalorimetry: Pb on MgO(100) †. *J. Phys. Chem. B* **2001**, *105* (18), 3776–3782.
(24) Borroni-Bird, C. E.; King, D. A. An Ultrahigh Vacuum Single Crystal Adsorption Microcalorimeter. *Rev. Sci. Instrum.* **1991**, *62* (9), 2177–2185.
(25) Stuckless, J. T.; Frei, N. A.; Campbell, C. T. Pyroelectric Detector for Single-Crystal Adsorption Microcalorimetry: Analysis of Pulse Shape and Intensity. *Sensors Actuators, B Chem.* **2000**, *62* (1), 13–22.
(26) Ford, D. C.; Xu, Y.; Mavrikakis, M. Atomic and Molecular Adsorption on Pt(111). *Surf. Sci.* **2005**, *587* (3), 159–174.
(27) Peng, G.; Sibener, S. J.; Schatz, G. C.; Ceyer, S. T.; Mavrikakis, M. CO 2 Hydrogenation to Formic Acid on Ni(111). *J. Phys. Chem. C* **2012**, *116* (4), 3001–3006.
(28) Grabow, L. C.; Mavrikakis, M. Mechanism of Methanol Synthesis on Cu through CO 2 and CO Hydrogenation. *ACS Catal.* **2011**, *1* (4), 365–384.
(29) Lytken, O.; Lew, W.; Harris, J. J. W.; Vestergaard, E. K.; Gottfried, J. M.; Campbell, C. T. Energetics of Cyclohexene Adsorption and Reaction on Pt(111) by Low-Temperature Microcalorimetry. *J. Am. Chem. Soc.* **2008**, *130* (31), 10247–10257.
(30) Karp, E. M.; Silbaugh, T. L.; Crowe, M. C.; Campbell, C. T. Energetics of Adsorbed Methanol and Methoxy on Pt(111) by Microcalorimetry. *J. Am. Chem. Soc.* **2012**, *134* (50), 20388–20395.
(31) Silbaugh, T. L.; Karp, E. M.; Campbell, C. T. Surface Kinetics and Energetics from Single Crystal Adsorption Calorimetry Lineshape Analysis: Methyl from Methyl Iodide on Pt(1 1 1). *J. Catal.* **2013**, *308*, 114–121.
(32) Lew, W.; Crowe, M. C.; Karp, E.; Campbell, C. T. Energy of Molecularly Adsorbed Water on Clean Pt(111) and Pt(111) with Coadsorbed Oxygen by Calorimetry. *J. Phys. Chem. C* **2011**, *115* (18), 9164–9170.
(33) Silbaugh, T. L.; Karp, E. M.; Campbell, C. T. Energetics of Formic Acid Conversion to Adsorbed Formates on Pt(111) by Transient Calorimetry. *J. Am. Chem. Soc.* **2014**, *136* (10), 3964–3971.

(34) Ajo, H. M.; Ihm, H.; Moilanen, D. E.; Campbell, C. T. Calorimeter for Adsorption Energies of Larger Molecules on Single Crystal Surfaces. *Rev. Sci. Instrum.* **2004**, *75* (11), 4471–4480.
(35) Lew, W.; Lytken, O.; Farmer, J. A.; Crowe, M. C.; Campbell, C. T. Improved Pyroelectric Detectors for Single Crystal Adsorption Calorimetry from 100 to 350 K. *Rev. Sci. Instrum.* **2010**, *81* (2), 1–9.
(36) King, D. A.; Wells, M. G. Molecular Beam Investigation of Adsorption Kinetics on Bulk Metal Targets: Nitrogen on Tungsten. *J. Vac. Sci. Technol.* **1972**, *9* (2), 905–905.
(37) Ihm, H.; Ajo, H. M.; Gottfried, J. M.; Bera, P.; Campbell, C. T. Calorimetric Measurement of the Heat of Adsorption of Benzene on Pt(111). *J. Phys. Chem. B* **2004**, *108* (38), 14627–14633.
(38) Yildirim, H.; Greber, T.; Kara, A. Trends in Adsorption Characteristics of Benzene on Transition Metal Surfaces: Role of Surface Chemistry and van Der Waals Interactions. *J. Phys. Chem. C* **2013**, *117* (40), 20572–20583.
(39) Delle Site, L.; Alavi, a.; Abrams, C. Adsorption Energies and Geometries of Phenol on the (111) Surface of Nickel: An Ab Initio Study. *Phys. Rev. B* **2003**, *67* (19), 1–3.
(40) Tkatchenko, A.; Romaner, L.; Hofmann, O. T.; Zojer, E.; Ambrosch-Draxl, C.; Scheffler, M. Van Der Waals Interactions Between Organic Adsorbates and at Organic/Inorganic Interfaces. *MRS Bull.* **2010**, *35* (06), 435–442.
(41) Liu, W.; Tkatchenko, A.; Scheffler, M. Modeling Adsorption and Reactions of Organic Molecules at Metal Surfaces. *Acc. Chem. Res.* **2014**, *47* (11), 3369–3377.
(42) Lehwald, S.; Ibach, H.; Demuth, J. E. Vibration Spectroscopy of Benzene Adsorbed on Pt(111) and Ni(111). *Surf. Sci.* **1978**, *78* (3), 577–590.
(43) Steinrück, H.-P.; Huber, W.; Pache, T.; Menzel, D. The Adsorption of Benzene Mono- and Multilayers on Ni(111) Studied by TPD and LEED. *Surf. Sci.* **1989**, *218* (2–3), 293–316.
(44) Schaff, O.; Fernandez, V.; Hofmann, P.; Schindler, K. M.; Theobald, A.; Fritzsche, V.; Bradshaw, A. M.; Davis, R.; Woodruff, D. P. Coverage-Dependent Changes in the Adsorption Geometry of Benzene on Ni{111}. *Surf. Sci.* **1996**, *348* (1–2), 89–99.
(45) Papp, C.; Fuhrmann, T.; Tränkenschuh, B.; Denecke, R.; Steinrück, H. P. Site Selectivity of Benzene Adsorption on Ni(111) Studied by High-Resolution x-Ray Photoelectron Spectroscopy. *Phys. Rev. B - Condens. Matter Mater. Phys.* **2006**, *73* (23), 1–9.
(46) Huber, W.; Steinrück, H.-P.; Pache, T.; Menzel, D. The Electronic Structure and Molecular Symmetry of Pure Benzene and Benzene Coadsorbed with CO on Ni(111). *Surf. Sci.* **1989**, *217* (1–2), 103–126.
(47) Horsley, J. A.; Stöhr, J.; Hitchcock, A. P.; Newbury, D. C.; Johnson, A. L.; Sette, F. Resonances in the K Shell Excitation Spectra of Benzene and Pyridine: Gas Phase, Solid, and Chemisorbed States. *J. Chem. Phys.* **1985**, *83* (12), 6099.
(48) Weiss, P. S.; Eigler, D. M. Site Dependence of the Apparent Shape of a Molecule in Scanning Tunneling Micoscope Images: Benzene on Pt{111}. *Phys. Rev. Lett.* **1993**, *71* (19), 3139–3142.
(49) Cemic, F.; Dippel, O.; Hasselbrink, E. Resonant Electron Scattering from Benzene Chemisorbed on Pt(111). *Surf. Sci.* **1995**, *342* (1–3), 101–110.
(50) Somers, J.; Bridge, M. .; Lloyd, D. .; McCabe, T. An Arups Investigation of Benzene on Pt(111): Evidence for Distortion. *Surf. Sci. Lett.* **1987**, *181* (3), L167–L170.
(51) Wander, A.; Held, G.; Hwang, R. Q.; Blackman, G. S.; Xu, M. L.; de Andres, P.; Van

Hove, M. A.; Somorjai, G. A. A Diffuse LEED Study of the Adsorption Structure of Disordered Benzene on Pt(111). *Surf. Sci.* **1991**, *249* (1–3), 21–34.
(52) Mate, C. M.; Somorjai, G. A. Carbon Monoxide Induced Ordering of Benzene on Pt(111) and Rh(111) Crystal Surfaces. *Surf. Sci.* **1985**, *160* (2), 542–560.
(53) Tsai, M. C.; Muetterties, E. L. Platinum Metal Surface Chemistry of Benzene and Toluene. *J. Am. Chem. Soc.* **1982**, *104* (9), 2534–2539.
(54) Campbell, J. M.; Seimanides, S.; Campbell, C. T. Problng Ensemble Effects In Surface Reactions. 2. Benzene Adsorption on Clean and Bismuth-Covered Pt(111). *J. Phys. Chem. B* **1989**, *92* (17), 815.
(55) Cemic, F.; Dippel, O.; Hasselbrink, E. Resonant Electron-Scattering from Benzene Chemisorbed on Pt(111). *Surf. Sci.* **1995**, *342* (1–3), 101–110.
(56) Sabbe, M. K.; Laín, L.; Reyniers, M.-F.; Marin, G. B. Benzene Adsorption on Binary Pt3M Alloys and Surface Alloys: A DFT Study. *Phys. Chem. Chem. Phys.* **2013**, *15* (29), 12197.
(57) Réocreux, R.; Huynh, M.; Michel, C.; Sautet, P. Controlling the Adsorption of Aromatic Compounds on Pt(111) with Oxygenate Substituents: From DFT to Simple Molecular Descriptors. *J. Phys. Chem. Lett.* **2016**, *7* (11), 2074–2079.
(58) Peköz, R.; Donadio, D. Effect of van Der Waals Interactions on the Chemisorption and Physisorption of Phenol and Phenoxy on Metal Surfaces. *J. Chem. Phys.* **2016**, *145* (10), 104701.
(59) Zhang, R.; Hensley, A. J.; McEwen, J.-S.; Wickert, S.; Darlatt, E.; Fischer, K.; Schöppke, M.; Denecke, R.; Streber, R.; Lorenz, M.; et al. Integrated X-Ray Photoelectron Spectroscopy and DFT Characterization of Benzene Adsorption on Pt(111), Pt(355) and Pt(322) Surfaces. *Phys. Chem. Chem. Phys.* **2013**, *15* (47), 20662.
(60) Saeys, M.; Reyniers, M. F.; Marin, G. B.; Neurock, M. Density Functional Study of Benzene Adsorption on Pt(111). *J. Phys. Chem. B* **2002**, *106* (30), 7489–7498.
(61) Morin, C.; Simon, D.; Sautet, P. Density-Functional Study of the Adsorption and Vibration Spectra of Benzene Molecules on Pt(111). *J. Phys. Chem. B* **2003**, *107* (13), 2995–3002.
(62) Morin, C.; Simon, D.; Sautet, P. Intermediates in the Hydrogenation of Benzene to Cyclohexene on Pt(1 1 1) and Pd(1 1 1): A Comparison from DFT Calculations. *Surf. Sci.* **2006**, *600* (6), 1339–1350.
(63) Gao, W.; Zheng, W. T.; Jiang, Q. Dehydrogenation of Benzene on Pt(111) Surface. *J. Chem. Phys.* **2008**, *129* (16).
(64) K, A. P.; Chatanathodi, R. Adsorption of Benzene on Low Index Surfaces of Platinum in the Presence of van Der Waals Interactions. *Surf. Sci.* **2017**, *664*, 8–15.
(65) Carey, S. J.; Zhao, W.; Frehner, A.; Campbell, C. T.; Jackson, B. Energetics of Adsorbed Methyl and Methyl Iodide on Ni(111) by Calorimetry: Comparison to Pt(111) and Implications for Catalysis. *ACS Catal.* **2017**, *7* (2), 1286–1294.
(66) Zhao, W.; Carey, S. J.; Morgan, S. E.; Campbell, C. T. Energetics of Adsorbed Formate and Formic Acid on Ni(111) by Calorimetry. *J. Catal.* **2017**, *352*, 300–304.
(67) Stephenson, R. M.; Malanowski, S. *Handbook of the Thermodynamics of Organic Compounds*; Springer Netherlands: Dordrecht, 1987.
(68) Roux, M. V.; Temprado, M.; Chickos, J. S.; Nagano, Y. Critically Evaluated Thermochemical Properties of Polycyclic Aromatic Hydrocarbons. *J. Phys. Chem. Ref. Data* **2008**, *37* (4), 1855–1996.

(69) Campbell, C. T.; Árnadóttir, L.; Sellers, J. R. V. Kinetic Prefactors of Reactions on Solid Surfaces. *Zeitschrift für Phys. Chemie* **2013**, *227* (9–11), 1–20.
(70) Brown, W.; Kose, R.; King, D. Femtomole Adsorption Calorimetry on Single-Crystal Surfaces. *Chem. Rev.* **1998**, *98* (97), 797–831.
(71) Tait, S. L.; Dohnálek, Z.; Campbell, C. T.; Kay, B. D. N-Alkanes on Pt(111) and on C(0001)/Pt(111): Chain Length Dependence of Kinetic Desorption Parameters. *J. Chem. Phys.* **2006**, *125* (23), 234308.
(72) Beckerle, J. D.; Johnson, A. D.; Ceyer, S. T. Collision-induced Desorption of Physisorbed CH 4 from Ni(111): Experiments and Simulations. *J. Chem. Phys.* **1990**, *93* (6), 4047–4065.
(73) Ruiz, V. G.; Liu, W.; Tkatchenko, A. Density-Functional Theory with Screened van Der Waals Interactions Applied to Atomic and Molecular Adsorbates on Close-Packed and Non-Close-Packed Surfaces. *Phys. Rev. B* **2016**, *93* (3), 035118.
(74) Liu, W.; Maaß, F.; Willenbockel, M.; Bronner, C.; Schulze, M.; Soubatch, S.; Tautz, F. S.; Tegeder, P.; Tkatchenko, A. Quantitative Prediction of Molecular Adsorption: Structure and Binding of Benzene on Coinage Metals. *Phys. Rev. Lett.* **2015**, *115* (3), 036104.
(75) Singh, N.; Song, Y.; Gutiérrez, O. Y.; Camaioni, D. M.; Campbell, C. T.; Lercher, J. A. Electrocatalytic Hydrogenation of Phenol over Platinum and Rhodium: Unexpected Temperature Effects Resolved. *ACS Catal.* **2016**, *6* (11), 7466–7470.
(76) Zhao, C.; He, J.; Lemonidou, A. A.; Li, X.; Lercher, J. A. Aqueous-Phase Hydrodeoxygenation of Bio-Derived Phenols to Cycloalkanes. *J. Catal.* **2011**, *280* (1), 8–16.
(77) Zhao, C.; Kou, Y.; Lemonidou, A. A.; Li, X.; Lercher, J. A. Hydrodeoxygenation of Bio-Derived Phenols to Hydrocarbons Using RANEY® Ni and Nafion/SiO 2 Catalysts. *Chem. Commun.* **2010**, *46* (3), 412–414.
(78) Song, Y.; Gutiérrez, O. Y.; Herranz, J.; Lercher, J. A. Aqueous Phase Electrocatalysis and Thermal Catalysis for the Hydrogenation of Phenol at Mild Conditions. *Appl. Catal. B Environ.* **2016**, *182* (11), 236–246.
(79) Ilikti, H.; Rekik, N.; Thomalla, M. Electrocatalytic Hydrogenation of Phenol in Aqueous Solutions at a Raney Nickel Electrode in the Presence of Cationic Surfactants. *J. Appl. Electrochem.* **2002**, *32* (6), 603–609.
(80) Myers, A. K.; Benziger, J. B. Effect of Substituent Groups on the Interaction of Benzene with Nickel(111). *Langmuir* **1989**, *5* (6), 1270–1288.
(81) Zhuang, S. X.; Wei, X. M.; Wang, Y. S.; Zhai, R. S. A HREELS Study of the Interaction of Cyclohexanone and Phenol with Pt(111) Surface. *Chinese Chem. Lett.* **1996**, *7* (7), 661–662.
(82) Lu, F.; Salaita, G. N.; Laguren-Davidson, L.; Stern, D. A.; Wellner, E.; Frank, D. G.; Batina, N.; Zapien, D. C.; Walton, N.; Hubbard, A. T. Characterization of Hydroquinone and Related Compounds Adsorbed at Pt(111) from Aqueous Solutions: Electron Energy-Loss Spectroscopy, Auger Spectroscopy, LEED, and Cyclic Voltammetry. *Langmuir* **1988**, *4* (3), 637–646.
(83) Ihm, H.; White, J. M. Stepwise Dissociation of Thermally Activated Phenol on Pt(111). *J. Phys. Chem. B* **2000**, *104* (26), 6202–6211.
(84) Carey, S. J.; Zhao, W.; Campbell, C. T. Energetics of Adsorbed Benzene on Ni(111) and Pt(111) by Calorimetry. *Surf. Sci.* **2018**.
(85) Weinberg, W. H.; Merrill, R. P. A Simple Classical Model for Trapping in Gas–Surface

Interactions. *J. Vac. Sci. Technol.* **1971**, *8* (6), 718–724.
(86) Parsons, G. H.; Rochester, C. H.; Wood, C. E. C. Effect of 4-Substitution on the Thermodynamics of Hydration of Phenol and the Phenoxide Anion. *J. Chem. Soc. B Phys. Org.* **1971**, 533.
(87) Cox, J. D. The Heats of Combustion of Phenol and the Three Cresols. *Pure Appl. Chem.* **1961**, *2* (1–2), 125.
(88) Andon, R. J. L.; Biddiscombe, D. P.; Cox, J. D.; Handley, R.; Harrop, D.; Herington, E. F. G.; Martin, J. F. 1009. Thermodynamic Properties of Organic Oxygen Compounds. Part I. Preparation and Physical Properties of Pure Phenol, Cresols, and Xylenols. *J. Chem. Soc.* **1960**, 5246.
(89) Redhead, P. A. Thermal Desorption of Gases. *Vacuum* **1962**, *12* (4), 203–211.
(90) Gottfried, J. M.; Vestergaard, E. K.; Bera, P.; Campbell, C. T. Heat of Adsorption of Naphthalene on Pt(111) Measured by Adsorption Calorimetry. *J. Phys. Chem. B* **2006**, *110* (35), 17539–17545.
(91) Yaws, C. L. *Yaw's Handbook of Thermodynamic and Physical Properties of Chemical Compounds*; Knovel, 2003.
(92) Yoon, Y.; Rousseau, R.; Weber, R. S.; Mei, D.; Lercher, J. A. First-Principles Study of Phenol Hydrogenation on Pt and Ni Catalysts in Aqueous Phase. *J. Am. Chem. Soc.* **2014**, *136* (29), 10287–10298.
(93) Honkela, M. L.; Björk, J.; Persson, M. Computational Study of the Adsorption and Dissociation of Phenol on Pt and Rh Surfaces. *Phys. Chem. Chem. Phys.* **2012**, *14* (16), 5849.
(94) Li, G.; Han, J.; Wang, H.; Zhu, X.; Ge, Q. Role of Dissociation of Phenol in Its Selective Hydrogenation on Pt(111) and Pd(111). *ACS Catal.* **2015**, *5* (3), 2009–2016.
(95) Karp, E. M.; Silbaugh, T. L.; Campbell, C. T. Energetics of Adsorbed CH 3 and CH on Pt(111) by Calorimetry: Dissociative Adsorption of CH 3 I. *J. Phys. Chem. C* **2013**, *117* (12), 6325–6336.
(96) Yang, Q. Y.; Maynard, K. J.; Johnson, a D.; Ceyer, S. T. The Structure and Chemistry of {CH_3} and {CH} Radicals Adsorbed on {Ni(111)}. *J. Chem. Phys.* **1995**, *102* (111), 7734–7749.
(97) Castro, M. E.; Chen, J. G.; Hall, R. B.; Mims, C. A. Reactions of "Hot" Methyl Groups with Surface Hydrogen during CH 3 −I Bond Scission on Ni(111). *J. Phys. Chem. B* **1997**, *101* (20), 4060–4070.
(98) Myli, K. B.; Grassian, V. H. Atomic Iodine Desorption from Single Crystal Nickel Surfaces. *Langmuir* **1995**, *11* (15), 849–852.
(99) Karp, E. M.; Silbaugh, T. L.; Campbell, C. T. Energetics of Adsorbed CH 3 on Pt(111) by Calorimetry. *J. Am. Chem. Soc.* **2013**, *135* (13), 5208–5211.
(100) Jiang, L. Q.; Koel, B. E. Hydrocarbon Trapping and Condensation on Platinum (111). *J. Phys. Chem.* **1992**, *96* (22), 8694–8697.
(101) Henderson, M. A.; Mitchell, G. E.; White, J. M. The Chemisorption of Methyl Halides (Cl, Br and I) on Pt(111). *Surf. Sci.* **1987**, *184* (1–2), L325–L331.
(102) Cox, J. D.; Pilcher, G. *Thermochemistry of Organic and Organometallic Compounds*; Academic Press: New York, 1970.
(103) Wren, D. J.; Vikis, A. C. Vapour Pressure of CH3I in the Temperature Range 176 to 227 K. *J. Chem. Thermodyn.* **1982**, *14* (5), 435–437.
(104) Egan, C. J.; Kemp, J. D. Methyl Bromide. The Heat Capacity, Vapor Pressure, Heats of

Transition, Fusion and Vaporization. Entropy and Density of the Gas. *J. Am. Chem. Soc.* **1938**, *60* (9), 2097–2101.
(105) Labayen, M.; Furman, S. A.; Harrington, D. A. A Thermal Desorption Study of Iodine on Pt(111). *Surf. Sci.* **2003**, *525* (1–3), 149–158.
(106) M.W. Chase Jr. *NIST-JANAF Themochemical Tables, Fourth Edition*; American Institute of Physics for the National Institute of Standards and Technology: Woodbury, N.Y., 1998; Vol. Monograph.
(107) Tsang, W. *Energetics of Organic Free Radicals*; Blackie Academic & Professional: Glasgow, U.K, 1996.
(108) Silbaugh, T. L.; Giorgi, J. B.; Xu, Y.; Tillekaratne, A.; Zaera, F.; Campbell, C. T. Adsorption Energy of Tert -Butyl on Pt(111) by Dissociation of Tert -Butyl Iodide: Calorimetry and DFT. *J. Phys. Chem. C* **2014**, *118* (1), 427–438.
(109) Wolcott, C. A.; Green, I. X.; Silbaugh, T. L.; Xu, Y.; Campbell, C. T. Christopher A. Wolcott, † Isabel X. Green, ‡ Trent L. Silbaugh, † Ye Xu, § and Charles T. Campbell * , † , ‡ † ‡. **2014**, No. 111.
(110) Miller, A. R.; Roberts, J. K. *The Adsorption of Gases on Solids*; Cambridge (England) University Press, 1949.
(111) Sinfelt, J. H. Catalysis by Metals. P. H. Emmett Award Address. *Catal. Rev.* **1974**, *9* (1), 145–166.
(112) Sinfelt, J. H. Specificity in Catalytic Hydrogenolysis by Metals. *Adv. Catal.* **1973**, *23*, 91–119.
(113) Nave, S.; Jackson, B. Methane Dissociation on Ni(111) and Pt(111): Energetic and Dynamical Studies. *J. Chem. Phys.* **2009**, *130* (111), 054701.
(114) Michaelides, A.; Hu, P. A First Principles Study of CH3 Dehydrogenation on Ni(111). *J. Chem. Phys.* **2000**, *112* (May 2013), 8120–8125.
(115) Blaylock, D. W.; Ogura, T.; William, H. G.; Gregory, J. O. B. Computational Investigation of Thermochemistry and Kinetics of Steam Methane Reforming on Ni(111) under Realistic Conditions. *J. Phys. Chem. C* **2009**, *113* (111), 4898–4908.
(116) Li, J.; Croiset, E.; Ricardez-Sandoval, L. Effect of Carbon on the Ni Catalyzed Methane Cracking Reaction: A DFT Study. *Appl. Surf. Sci.* **2014**, *311*, 435–442.
(117) Bradford, M. C. J.; Vannice, M. A. Catalytic Reforming of Methane with Carbon Dioxide over Nickel Catalysts II. Reaction Kinetics. *Appl. Catal. A Gen.* **1996**, *142* (1), 97–122.
(118) Bengaard, H. S.; Nørskov, J. K.; Sehested, J.; Clausen, B. S.; Nielsen, L. P.; Molenbroek, A. M.; Rostrup-Nielsen, J. R. Steam Reforming and Graphite Formation on Ni Catalysts. *J. Catal.* **2002**, *209* (2), 365–384.
(119) Wang, S. G.; Liao, X. Y.; Hu, J.; Cao, D. B.; Li, Y. W.; Wang, J.; Jiao, H. Kinetic Aspect of CO2 Reforming of CH4 on Ni(1 1 1): A Density Functional Theory Calculation. *Surf. Sci.* **2007**, *601* (5), 1271–1284.
(120) Watwe, R. M.; Bengaard, H. S.; Rostrup-Nielsen, J. R.; Dumesic, J. A.; Nørskov, J. K. Theoretical Studies of Stability and Reactivity of CHx Species on Ni(111). *J. Catal.* **2000**, *189* (1), 16–30.
(121) Wei, J.; Iglesia, E. Isotopic and Kinetic Assessment of the Mechanism of Reactions of CH 4 with CO2 or H2O to Form Synthesis Gas and Carbon on Nickel Catalysts. *J. Catal.* **2004**, *224* (2), 370–383.
(122) Rostrup-Nielsen, J.; Bak Hansen, J.-H. CO2-Reforming of Methane over Transition Metals. *Journal of Catalysis*. 1993, pp 38–49.

(123) Michaelides, A.; Hu, P. Methyl Chemisorption on Ni(111) and C-H-M Multicentre Bonding: A Density Functional Theory Study. *Surf. Sci.* **1999**, *437* (3), 362–376.
(124) Zhu, Y. A.; Chen, D.; Zhou, X. G.; Yuan, W. K. DFT Studies of Dry Reforming of Methane on Ni Catalyst. *Catal. Today* **2009**, *148* (3–4), 260–267.
(125) Cui, Y.; Zhang, H.; Xu, H.; Li, W. Kinetic Study of the Catalytic Reforming of CH4 with CO2 to Syngas over Ni/α-Al2O3 Catalyst: The Effect of Temperature on the Reforming Mechanism. *Appl. Catal. A Gen.* **2007**, *318*, 79–88.
(126) Michaelides, A.; Hu, P. A Density Functional Theory Study of CH[Sub 2] and H Adsorption on Ni(111). *J. Chem. Phys.* **2000**, *112* (13), 6006.
(127) Olsbye, U.; Wurzel, T.; Mleczko, L. Kinetic and Reaction Engineering Studies of Dry Reforming of Methane over a Ni/La/Al2O3 Catalyst. *Ind. Eng. Chem. Res.* **1997**, *36* (12), 5180–5188.
(128) Pakhare, D.; Spivey, J. A Review of Dry (CO 2) Reforming of Methane over Noble Metal Catalysts. *Chem. Soc. Rev.* **2014**, *43* (22), 7813–7837.
(129) Wang, S. G.; Cao, D. B.; Li, Y. W.; Wang, J.; Jiao, H. Chemisorption of CO2 on Nickel Surfaces. *J. Phys. Chem. B* **2005**, *109* (40), 18956–18963.
(130) Helveg, S.; López-Cartes, C.; Sehested, J.; Hansen, P. L.; Clausen, B. S.; Rostrup-Nielsen, J. R.; Abild-Pedersen, F.; Nørskov, J. K. Atomic-Scale Imaging of Carbon Nanofibre Growth. *Nature* **2004**, *427* (6973), 426–429.
(131) Manion, J. A. Evaluated Enthalpies of Formation of the Stable Closed Shell C1 and C2 Chlorinated Hydrocarbons. *J. Phys. Chem. Ref. Data* **2002**, *31* (1), 123.
(132) Behm, R. J.; Christmann, K.; Ertl, G.; Van Hove, M. A.; Weinberg, W. H. Chemisorption Geometry of Hydrogen on a Ni(111) Surface. *Surf. Sci.* **1979**, *89* (111), 403.
(133) Guo, H.; Jackson, B. Mode-Selective Chemistry on Metal Surfaces: The Dissociative Chemisorption of CH4 on Pt(111). *J. Chem. Phys.* **2016**, *144* (18), 184709.
(134) Bisson, R.; Sacchi, M.; Dang, T. T.; Yoder, B.; Maroni, P.; Beck, R. D. State-Resolved Reactivity of CH 4 (2ν 3) on Pt(111) and Ni(111): Effects of Barrier Height and Transition State Location. *J. Phys. Chem. A* **2007**, *111* (49), 12679–12683.
(135) Yang, H.; Whitten, J. L. Dissociative Chemisorption of CH4 on Ni(111). *J. Chem. Phys.* **1992**, *96* (7), 5529.
(136) Kratzer, P.; Hammer, B.; Nørskov, J. K. A Theoretical Study of CH4 Dissociation on Pure and Gold-Alloyed Ni(111) Surfaces. *J. Chem. Phys.* **1996**, *105* (13), 5595.
(137) Henkelman, G.; Arnaldsson, A.; Jónsson, H. Theoretical Calculations of CH[Sub 4] and H[Sub 2] Associative Desorption from Ni(111): Could Subsurface Hydrogen Play an Important Role? *J. Chem. Phys.* **2006**, *124* (4), 044706.
(138) Psofogiannakis, G.; St-Amant, A.; Ternan, M. Methane Oxidation Mechanism on Pt(111): A Cluster Model DFT Study. *J. Phys. Chem. B* **2006**, *110* (111), 24593–24605.
(139) Lozano, A.; Shen, X. J.; Moiraghi, R.; Dong, W.; Busnengo, H. F. Cutting a Chemical Bond with Demon's Scissors: Mode- and Bond-Selective Reactivity of Methane on Metal Surfaces. *Surf. Sci.* **2015**, *640*, 25–35.
(140) German, E. D.; Sheintuch, M. Methane Steam Reforming Rates over Pt, Rh and Ni(111) Accounting for H Tunneling and for Metal Lattice Vibrations. *Surf. Sci.* **2016**, 10.1016/j.susc.2016.03.024.
(141) Che, F.; Zhang, R.; Hensley, A. J.; Ha, S.; McEwen, J.-S. Density Functional Theory Studies of Methyl Dissociation on a Ni(111) Surface in the Presence of an External Electric Field. *Phys. Chem. Chem. Phys.* **2014**, *16* (6), 2399–2410.

(142) Wang, S.-G.; Cao, D.-B.; Li, Y.-W.; Wang, J.; Jiao, H. CH4 Dissociation on Ni Surfaces: Density Functional Theory Study. *Surf. Sci.* **2006**, *600* (16), 3226–3234.
(143) An, W.; Zeng, X. C.; Turner, C. H. First-Principles Study of Methane Dehydrogenation on a Bimetallic Cu/Ni(111) Surface. *J. Chem. Phys.* **2009**, *131* (17), 174702.
(144) Mueller, J. E.; van Duin, A. C. T.; Goddard, W. A. Structures, Energetics, and Reaction Barriers for CHx Bound to the Nickel (111) Surface. *J. Phys. Chem. C* **2009**, *113* (111), 20290–20306.
(145) Siegbahn, P.; Panas, I. A Theoretical Study of CH , Chemisorption and Ni(111) Surfaces on the Ni(100). *Surf. Sci.* **1990**, *240*, 37–49.
(146) Schüle, J.; Siegbahn, P.; Wahlgren, U. A Theoretical Study of Methyl Chemisorption on Ni(111). *J. Chem. Phys.* **1988**, *89* (11), 6982.
(147) Burghgraef, H.; Jansen, A. P. J.; van Santen, R. A. Methane Activation and Dehydrogenation on Nickel and Cobalt: A Computational Study. *Surf. Sci.* **1995**, *324* (2–3), 345–356.
(148) Yang, H.; Whitten, J. L. Ab Initio Chemisorption Studies of CH3 on Ni(111). *J. Am. Chem. Soc.* **1991**, *113* (18), 6442–6449.
(149) Erskine, J. L.; Bradshaw, A. M. The Electronic Structure and Orientation of the Surface Methoxy Species on Ni(111). *Chem. Phys. Lett.* **1980**, *72* (2), 260–263.
(150) Rubloff, G. W.; Demuth, J. E. Ultraviolet Photoemission and Flash-Desorption Studies of the Chemisorption and Decomposition of Methanol on Ni(111). *J. Vac. Sci. Technol.* **1977**, *14* (1), 419.
(151) Russell, J. N.; Chorkendorff, I.; Yates, J. T. Methanol Decomposition on Ni(111): Investigation of the C-O Bond Scission Mechanism. *Surf. Sci.* **1987**, *183* (3), 316–330.
(152) Gates, S. M.; Russell, J. N.; Yates, J. T. Observation of a Deuterium Kinetic Isotope Effect in the Chemisorption and Reaction of Methanol on Ni(111). *Surf. Sci.* **1984**, *146* (1), 199–210.
(153) Demuth, J. E.; Ibach, H. Observation of a Methoxy Species on Ni(111) by High-Resolution Electron Energy-Loss Spectroscopy. *Chemical Physics Letters*. 1979, pp 395–399.
(154) Zenobi, R.; Xu, J.; Yates, J. T.; Persson, B. N. J.; Volokitin, A. I. FTIR Overtone Spectroscopy on Surfaces. The C—O Mode in Chemisorbed Methoxy on Ni(111). *Chemical Physics Letters*. 1993, pp 414–419.
(155) Schaff, O.; Hess, G.; Fritzsche, V.; Fernandez, V.; Schindler, K.; Theobald, A.; Hofmann, P.; Bradshaw, A. M.; Davis, R.; Woodruff, D. P. The Structure of the Surface Methoxy Species on Ni(111). **1995**, *333*, 201–206.
(156) Schaff, O.; Hess, G.; Fernandez, V.; Schindler, K.-M.; Theobald, a.; Hofmann, P.; Bradshaw, a. M.; Fritzsche, V.; Davis, R.; Woodruff, D. P. Quantitative Determination of Molecular Adsorption Structures Using Photoelectron Diffraction: The Methoxy Species. *J. Electron Spectros. Relat. Phenomena* **1995**, *75* (95), 117–128.
(157) Gates, S. M.; Russell, J. N.; Yates, J. T. Scanning Kinetic Spectroscopy (SKS): A New Method for Investigation of Surface Reaction Processes. *Surf. Sci.* **1985**, *159* (1), 233–255.
(158) Amemiya, K.; Kitajima, Y.; Yonamoto, Y.; Terada, S.; Tsukabayashi, H.; Yokoyama, T.; Ohta, T. Oxygen K-Edge x-Ray-Absorption Fine-Structure Study of Surface Methoxy Species on Cu(111) and Ni(111). *Phys. Rev. B* **1999**, *59* (3), 2307–2312.
(159) Zhao, W.; Carey, S. J.; Mao, Z.; Campbell, C. T. Adsorbed Hydroxyl and Water on

Ni(111): Heats of Formation by Calorimetry. *ACS Catal.* **2018**, *8* (2), 1485–1489.
(160) Karp, E. M.; Silbaugh, T. L.; Campbell, C. T. Bond Energies of Molecular Fragments to Metal Surfaces Track Their Bond Energies to H Atoms. *J. Am. Chem. Soc.* **2014**, *136* (11), 4137–4140.
(161) Zion, B. D.; Hanbicki, A. T.; Sibener, S. J. Kinetic Energy Effects on the Oxidation of Ni(111) Using O2 Molecular Beams. *Surf. Sci.* **1998**, *417* (2–3), L154–L159.
(162) Norton, P. R.; Tapping, R. L. Photoelectron Spectroscopic Study of the Interaction of Nickel and Oxygen. *Faraday Discuss. Chem. Soc.* **1975**, *60*, 71.
(163) Holloway, P. H.; Hudson, J. B. Kinetics of the Reaction of Oxygen with Clean Nickel Single Crystal Surfaces. *Surf. Sci.* **1974**, *43* (1), 141–149.
(164) Chao, J.; Rossini, F. D. Heats of Combustion, Formation, and Isomerization of Nineteen Alkanols. *J. Chem. Eng. Data* **1965**, *10* (4), 374–379.
(165) Baber, A. E.; Lawton, T. J.; Sykes, E. C. H. Hydrogen-Bonded Networks in Surface-Bound Methanol. *J. Phys. Chem. C* **2011**, *115* (18), 9157–9163.
(166) Lawton, T. J.; Carrasco, J.; Baber, A. E.; Michaelides, A.; Sykes, E. C. H. Hydrogen-Bonded Assembly of Methanol on Cu(111). *Phys. Chem. Chem. Phys.* **2012**, *14* (33), 11846.
(167) Murphy, C. J.; Carrasco, J.; Lawton, T. J.; Liriano, M. L.; Baber, A. E.; Lewis, E. A.; Michaelides, A.; Sykes, E. C. H. Structure and Energetics of Hydrogen-Bonded Networks of Methanol on Close Packed Transition Metal Surfaces. *J. Chem. Phys.* **2014**, *141* (1), 014701.
(168) Tauer, K. J.; Lipscomb, W. N. On the Crystal Structures, Residual Entropy and Dielectric Anomaly of Methanol. *Acta Crystallogr.* **1952**, *5* (5), 606–612.
(169) Carlson, H. G.; E. F. Westrum, J. Methanol: Heat Capacity, Enthalpies of Transition and Melting, and Thermodynamic Properties from 5 - 300 K. *J. Chem. Phys.* **1971**, *54* (1971), 1464–1471.
(170) Green, S. D.; Bolina, A. S.; Chen, R.; Collings, M. P.; Brown, W. a.; McCoustra, M. R. S. Applying Laboratory Thermal Desorption Data in an Interstellar Context: Sublimation of Methanol Thin Films. *Mon. Not. R. Astron. Soc.* **2009**, *398* (1), 357–367.
(171) Sexton, B. A. Methanol Decomposition on Platinum (111). *Surf. Sci.* **1981**, *102* (1), 271–281.
(172) Remediakis, I. N.; Abild-Pedersen, F.; Nørskov, J. K. DFT Study of Formaldehyde and Methanol Synthesis from CO and H2 on Ni(111) †. *J. Phys. Chem. B* **2004**, *108* (38), 14535–14540.
(173) Kelly, T. G.; Stottlemyer, A. L.; Ren, H.; Chen, J. G. Comparison of O-H, C-H, and C-O Bond Scission Sequence of Methanol on Tungsten Carbide Surfaces Modified by Ni, Rh, and Au. *J. Phys. Chem. C* **2011**, *115* (14), 6644–6650.
(174) Karp, E. M.; Campbell, C. T.; Studt, F.; Abild-Pedersen, F.; Norskov, J. K. Energetics of Oxygen Adatoms, Hydroxyl Species and Water Dissociation on Pt(111). *J. Phys. Chem. C* **2012**, *116* (49), 25772–25776.
(175) Lew, W.; Crowe, M. C.; Karp, E.; Lytken, O.; Farmer, J. a; Líney, a; Schoenbaum, C.; Campbell, C. T. The Energy of Adsorbed Hydroxyl on Pt (111) by Microcalorimetry Rnad. **2011**, No. 111, 11586–11594.
(176) Bryndza, H. E.; Fong, L. K.; Paciello, R. A.; Tam, W.; Bercaw, J. E. Relative Metal-Hydrogen, -Oxygen, -Nitrogen, and -Carbon Bond Strengths for Organoruthenium and Organoplatinum Compounds; Equilibrium Studies of Cp*(PMe3)2RuX and

(DPPE)MePtX Systems. *J. Am. Chem. Soc.* **1987**, *109* (5), 1444–1456.
(177) Bryndza, H. E.; Domaille, P. J.; Tam, W.; Fong, L. K.; Paciello, R. A.; E. Bercaw, J. Comparison of Metal-Hydrogen, -Oxygen, -Nitrogen and -Carbon Bond Strengths and Evaluation of Functional Group Additivity Principles for Organoruthenium and Organoplatinum Compounds. *Polyhedron* **1988**, *7* (16–17), 1441–1452.
(178) Bulls, A. R.; Bercaw, J. E.; Manriquez, J. M.; Thompson, M. E. Relative Bond Dissociation Energies for Early Transition Metal Alkyl, Aryl, Alkynyl and Hydride Compounds. Equilibration of Metallated Cyclopentadienyl Derivatives of Peralkylated Hafnocene and Scandocene with Hydrocarbons and Dihydrogen. *Polyhedron* **1988**, *7* (16–17), 1409–1428.
(179) Kramer, Z. C.; Gu, X. K.; Zhou, D. D. Y.; Li, W. X.; Skodje, R. T. Following Molecules through Reactive Networks: Surface Catalyzed Decomposition of Methanol on Pd(111), Pt(111), and Ni(111). *J. Phys. Chem. C* **2014**, *118* (23), 12364–12383.
(180) Wang, G.; Zhou, Y.; Morikawa, Y.; Nakamura, J. Kinetic Mechanism of Methanol Decomposition on Ni (111) Surface : A Theoretical Study. *J. Phys. Chem. B* **2005**, *109* (111), 12431–12442.
(181) Ren, R.; Niu, C.; Bu, S.; Zhou, Y.; Lv, Y.; Wang, G. Why Is Metallic Pt the Best Catalyst for Methoxy Decomposition? *J. Nat. Gas Chem.* **2011**, *20* (1), 90–98.
(182) Matcha, R. L. Theory of the Chemical Bond. 6. Accurate Relationship between Bond Energies and Electronegativity Differences. *J. Am. Chem. Soc.* **1983**, *105* (15), 4859–4862.
(183) Schock, L. E.; Marks, T. J. Organometallic Thermochemistry. Metal Hydrocarbyl, Hydride, Halide, Carbonyl, Amide, and Alkoxide Bond Enthalpy Relationships and Their Implications in Pentamethylcyclopentadienyl and Cyclopentadienyl Complexes of Zirconium and Hafnium. *J. Am. Chem. Soc.* **1988**, *110* (23), 7701–7715.
(184) McMillen, D. F.; Golden, D. M. Hydrocarbon Bond Dissociation Energies. *Annu. Rev. Phys. Chem.* **1982**, *33* (1), 493–532.
(185) *Progress in Physical Organic Chemistry*; Streitwieser, A., Taft, R. W., Eds.; Progress in Physical Organic Chemistry; John Wiley & Sons, Inc.: Hoboken, NJ, USA, 1968.
(186) *Handbook of Chemistry and Physics*, 49th ed.; Weast, R. C., Ed.; The Chemical Rubber Co.: Cleveland, OH, 1968.
(187) Brewer, L.; Rosenblatt, G. M. Dissociation Energies and Free Energy Functions of Gaseous Monoxides; 1969; pp 1–83.
(188) *Progress in Physical Organic Chemistry*; Streitwieser, A., Taft, R. W., Eds.; Progress in Physical Organic Chemistry; John Wiley & Sons, Inc.: Hoboken, NJ, USA, 1968.
(189) Blanksby, S. J.; Ellison, G. B. Bond Dissociation Energies of Organic Molecules. *Acc. Chem. Res.* **2003**, *36* (4), 255–263.

CURRICULUM VITAE

EDUCATION

University of Washington, Seattle, Washington

Ph.D. in Chemistry, Intended Graduation: June 2018
Dual Degree in Nanotechnology and Molecular Engineering
Ph.D. Advisor: Dr. Charles T. Campbell

University of Arizona, Tucson, Arizona

B.S. in Chemistry, Mathematics Minor, May 2013
GPA: Chemistry: 3.49, Mathematics: 3.56, Cumulative: 3.54
Honors College

RESEARCH EXPERIENCES

University of Washington Seattle, WA
Graduate Student with Dr. Charles T. Campbell August 2013-present

- Measured the adsorption energies of irreversibly adsorbed, catalytically important molecules and molecular fragments (methanol, water, hydroxyl, methyl, formate, formic acid, benzene, phenol) on transition metal and metal oxide single crystal surfaces (Pt, Ni, NiO) using single crystal adsorption calorimetry. These adsorption energies are used to provide fundamental insight to the catalytic properties of more complex real catalysts including surface bond strengths, accuracy of DFT measurements, and catalytic activity.
- Prepared samples in an ultra-high vacuum ($<2x10^{-10}$ torr) chamber utilizing X-ray Photoelectron Spectroscopy, Auger Electron Spectroscopy, argon sputtering, annealing techniques, and Low Energy Electron Diffraction.
- Repaired ultra-high vacuum instruments, electronic systems, and gas manifold systems

Fritz-Haber Institute Berlin, Germany
Graduate Student with Dr. Hans-Joachim Freund August-December 2016

- Studied the adsorption of CO_2 and D_2O on CaO_2 and Fe_3O_4 surfaces using single crystal adsorption calorimetry and infrared adsorption spectroscopy. These studies complimented a larger collaboration of several research groups to better understand these surfaces.
- Prepare oxide thin film samples for analysis

University of Arizona Tucson, AZ
Research Assistant with Dr. Stephen Kukolich August 2010-May 2013

- Synthesized organometallic and organic compounds using air-free chemistry techniques, inert gas glove-box systems, and isotopic substitutions.
- Measured the microwave spectrum of organometallic molecules and hydrogen bound species using a Flygare-Belle Microwave Spectrometer.
- Calculated the rotational properties and chemical structures of systems in terms of bond lengths and angles.

Argonne National Laboratory Argonne, IL
Science Undergraduate Laboratory Intern with Dr. Nancy Kariuki May-August 2012

- Synthesized platinum nanoparticles for the oxygen reduction reaction and deposited these structures onto novel transition metal silicide supports
- Analyzed electrocatalysts with cyclic voltammetry

Argonne National Laboratory Argonne, IL
Science Undergraduate Laboratory Intern with Dr. John Schlueter May-August 2013

- Synthesized silver and organic superconducting crystals with hydrothermal deposition and electrochemical crystallization techniques.
- Analyzed these crystals with single crystal x-ray diffraction and the x-ray diffraction using Beamline 15 at the Advanced Photon Source. This work was focusing on studying novel crystal structures and developing a new class of spin liquid crystals.

PUBLICATIONS

13. **Carey, S. J.**; Mao, Z.; Zhao, W.; Campbell, C. T. Energetics of adsorbed phenol on Ni(111) and Pt(111). (Accepted at *Journal of Physical Chemistry C*).
12. **Carey, S. J.**; Zhao, W.; Campbell, C. T. Energetics of adsorbed benzene on Ni(111) and Pt(111) by calorimetry. *Surface Science* (2018) Ahead of Print.
11. Zaki, E.; Mirabella; F., Ivars, F.; Seifert, J.; **Carey, S. J.**; Li, X.; Paier, J.; Sauer, J., Shaikhutdinov, S.; Freund, H.-J.; Water adsorption on Fe_3O_4(111): dissociation and network formation (Accepted to *Physical Chemistry Chemical Physics*).
10. Zhao, W.; **Carey, S. J.**; Mao, Z.; Campbell, C. T. Adsorbed hydroxyl and water on Ni(111): heats of formation by calorimetry. *ACS Catalysis* (2018), 8(2), 1485-1489.
9. Zhao, W.; **Carey, S. J.**; Morgan, S. E.; Campbell, C. T. Energetics of adsorbed formate and formic acid on Ni(111) by calorimetry, *Journal of Catalysis* (2017), 352, 300-304.
8. **Carey, S. J.**; Zhao, W.; Campbell, C. T. Energetics of adsorbed methyl and methyl iodide on Ni(111) by calorimetry: comparison to Pt(111) and implications for catalysis, *ACS Catalysis* (2017), 7(2), 1286-1294.
7. Zhao, W.; Bajdich, M.; **Carey, S. J.**; Vojvodic, A.; Noerskov, J. K.; Campbell, C. T. Water dissociative adsorption on NiO(111): energetics and structure of the hydroxylated surface, *ACS Catalysis* (2016) 6(11), 7377-7384.
6. Daly, A. M.; **Carey, S. J**; Pejlovas, A. M.; Li, K.; Kukolich, S. G.; Kang, L. Gas phase measurements of mono-fluoro-benzoic acids and the dimer of 3-fluoro-benzoic acid. *Journal of Chemical Physics* (2015), 142(14), 144303.
5. Sun, M.; Sargus, B. A.; **Carey, S. J.**; Kukolich, S. G. Measurements of deuterium quadrupole coupling in propiolic acid and fluorobenzenes using pulsed-beam Fourier transform microwave spectrometers. *Journal of Chemical Physics* (2015), 142(15), 154306/1-154306/7.
4. **Carey, S. J.**; Sun, M.; Kukolich, S. G. Microwave Spectrum of 1-Fluoronaphthalene and 2-Fluoronaphthalene. *Journal of Molecular Spectroscopy* (2014**)**, 304, 25-27.
3. Sun, M.; Wang, Y.; **Carey, S. J.**; Mitchell, E. G.; Bowman, J.; Kukolich, S. G. Calculations and measurements of the deuterium tunneling frequency in the propiolic

acid-formic acid dimer and description of a newly constructed Fourier transform microwave spectrometer. *Journal of Chemical Physics* (2013), 139, 084316/1-084316/7.

2. Kukolich, S. G.; Mitchell, E. G.; **Carey, S. J.**; Sun, M.; Sargus, B. M. Microwave Structure for the Propiolic Acid – Formic Acid complex. *Journal of Physical Chemistry A* (2013), 117, 9525-9530.
1. Daly, A. M.; Cossairt, B. M.; Southwood, G.; **Carey, Spencer J.**; Cummins, C. C.; Kukolich, S.G. Microwave spectrum of arsenic triphosphide. *Journal of Molecular Spectroscopy* (2012), 278, 68-71.

PRESENTATIONS (Presenting author underlined)

1. **Carey, S. J.**; Frehner, A.; Campbell, C.T. "Energetics of adsorption of methanol and methoxy on Nickel (111) studied by microcalorimetry". Poster Presentation. Gordon Research Seminar: Chemical Reactions at Surfaces, Ventura, CA, February 2015
2. **Carey, S. J.**; Frehner, A.; Campbell, C.T. "Energetics of adsorption of methanol and methoxy on Nickel (111) studied by microcalorimetry". Poster Presentation. Gordon Research Conference: Chemical Reactions at Surfaces, Ventura, CA, February 2015
3. **Carey, S. J.**; Zhao, W.; Zhang, W.; Frehner, A.; Campbell, C. T.; "Adsorption energies of methanol, methyl iodide, and methyl on nickel(111) studied by microcalorimetry". Poster Presentation. Molecular Engineering Showcase, Seattle, WA, May 2015
4. **Carey, S. J.**; Zhao, W.; Zhang, W.; Frehner, A.; Campbell, C. T.; "Adsorption energies of methanol, methyl iodide, and methyl on nickel(111) studied by microcalorimetry". Poster Presentation. Pacific Coast Catalysis Society, Richland, WA, September 2015
5. **Carey, S. J.**; Zhao, W.; Campbell, C. T.; "Energetics of adsorbed methyl and formate on Nickel(111) by microcalorimetry: dissociative adsorption of methyl iodide and formic acid". Poster Presentation. Gordon Research Conference: Catalysis, New London, NH, June 2016
6. **Carey, S. J.**; Zhao, W.; Mao, Z.; Campbell, C. T.; "Energetics of adsorbed molecules and molecular fragments on Nickel (111) by microcalorimetry". Oral Presentation. European Conference on Surface Science, Szeged, Hungary, August 2017

AWARDS

- 2017, IUVSTA-Elsevier Student Award: €430
- 2017, University of Washington Department of Chemistry Travel Grant: $500
- 2016, Graduate Student Poster Award, Gordon Research Conference: Catalysis
- 2015, Molecular Engineering Showcase Poster Travel Award: $500
- 2015, Outstanding Graduate Student Poster, Pacific Coast Catalysis Society, $100
- University of Arizona Excellence in Undergraduate Research Award for outstanding achievement in independent, undergraduate research